General Relativistic Radiative Transfer

Dissertation
zur Erlangung des Doktorgrades
des Fachbereichs Physik
der Universität Hamburg

vorgelegt von

Sebastian Knop

aus Hamburg

Hamburg
2007

Dissertationsgutachter:	Prof. Dr. P. Hauschildt Prof. Dr. E. Baron Prof. Dr. K. Werner
Disputationsgutachter:	Prof. Dr. P. Hauschildt Prof. Dr. J. Schmitt
Datum der Disputation:	13. April 2007
Vorsitzender des Prüfungsausschusses:	Prof. Dr. G. Wiedemann
Vorsitzender des Promotionsausschusses:	Prof. Dr. G. Huber
Dekan der MIN-Fakultät:	Prof. Dr. A. Frühwald
Leiter des Departments:	Prof. Dr. R. Klanner

Zusammenfassung

Die Modellierung von astrophysikalischen Atmosphären mittels der Theorie des Strahlungstransports spielt eine zentrale Rolle bei dem Verständnis und der Untersuchung derselbigen. Die vorliegende Arbeit beschäftigt sich speziell mit relativistischen Atmosphären kompakter Objekte. Photonen innerhalb dieser Atmosphären erleiden eine gravitative Verschiebung ihrer Wellenlänge und bewegen sich auf gekrümmten Bahnen. Der Strahlungstransport wird dadurch direkt beeinflusst und daher ist in dieser Arbeit die allgemein relativistische Theorie des Strahlungstransports verwendet worden. Die Gleichung des Strahlungstransports wurde dabei so formuliert, dass die Lösung mittels einer »accelerated Λ-iteration« möglich ist.
Die Berechnungen sind auf räumlich eindimensionale Probleme beschränkt, wodurch sich die Anwendung auf sphärisch symmetrische Metriken reduziert. Der gewählte Ansatz ist jedoch auch für mehrdimensionale Anwendungen geeignet, was in der Herleitung der Strahlungstransportgleichung für die Kerr-Metrik gezeigt wird. Des Weiteren wird ein Ansatz formuliert, der es erlaubt den Strahlungstransport in bewegten Medien vor dem Hintergrund einer statischen gekrümmten Raumzeit zu beschreiben.
In einer ersten Anwendung ist der Strahlungstransport für ein Gas bestehend aus Modellatomen mit zwei Niveaus berechnet worden. Die resultierenden Linienspektren hängen dabei sowohl stark von der zugrundeliegenden Atmosphärenstruktur, als auch im besonderen von der Streualbedo des Kontinuums ab.
Außerdem ist Kontinuumsstrahlungstransport für eine als grau angenommene kontinuierliche Opazität berechnet worden. Die scheinbare Temperatur ist von der Stärke der Streuung abhängig und kann deutlich heißer erscheinen als die effektive Temperatur der Modellatmosphäre nahelegt.
Für die Erstellung realistischer Modelle ist die Integration des Strahlungstransports in ein Modellatmosphärenprogramm notwendig. Daher ist der allgemein relativistische Strahlungstransport in den Atmosphären Code `PHOENIX` integriert worden. Um die vergleichsweise hohe Rechenzeit des relativistischen Transports auszugleichen, ist die Implementation in Bezug auf Geschwindigkeit optimiert worden. Dies ist in erster Linie mit der Einführung einer sowohl schnellen, als auch robusten, Gauss-Seidel basierten iterativen Lösung gelungen. Die Ergebnisse für speziell relativistische NLTE Berechnungen der etablierten Strahlungstransportlösung wurden mit der neuen Lösung erfolgreich reproduziert.
Die vorliegende Arbeit beschreibt allgemein relativistischen Strahlungstransport in geeigneter Form für die Anwendung einer »accelerated Λ-iteration« als formale Lösung und stellt eine Implementation innerhalb von `PHOENIX` bereit, die als Startpunkt für die Konstruktion realistischer Modelle von kompakten Objekten dient.

Abstract

The modeling of the radiative transfer is important for the investigation and the understanding of astrophysical atmospheres. This work specializes on the atmospheres of compact objects. The photons within these atmospheres are subject to a gravitational shift of the wavelength and propagate along curved orbits. These relativistic effects influence directly the radiative transfer. Hence, the theory of general relativistic radiative transfer has been used in this work. The equation of radiation transport has been formulated in such a way, that the transfer problem can be solved by an accelerated Λ-iteration.
The calculations are restricted to one spatial dimension and require effectively the spacetime to be spherically symmetric. In formal developments within the Kerr metric it has been shown, that the chosen ansatz for describing the radiative transfer is also working in multidimensional applications. Furthermore, a formulation of radiative transfer in flows within static background spacetimes has been developed.
The radiative transfer for a two-level atom gas has been calculated as a first application. It has been found that the emerging line profiles not only depend sensitively on the physical structure, but also especially on the scattering albedo of the continuum.
Furthermore, gray continuum transfer has been calculated. Depending on the magnitude of the scattering, the apparent observed temperature may appear significantly higher than the effective temperature of the model atmospheres.
In order to construct a working code base for the construction of realistic atmosphere models, the general relativistic radiative transfer has been implemented in the atmosphere modeling code `PHOENIX`. Since the general relativistic radiative transfer is more computationally costly than the standard radiative transfer solvers, the implementation has been optimized for speed. A robust and very fast solver for the formal solution of the radiative transfer has been implemented. It is a Gauss-Seidel type iterative solver that uses improved initial guesses to minimizes the iterations needed. Finally, the new radiative transfer framework has been tested in special relativistic NLTE calculations and has identically reproduced the results of the standard radiative transfer.
In conclusion, this work describes the general radiative transfer equation in a form suitable for the use for an accelerated Λ-iteration and provides an implementation within the framework of `PHOENIX`, which does serve as a starting point for the construction of realistic models of relativistic atmospheres.

Contents

Chapter 1

Introduction

Astronomy is mostly based on the observation of objects and phenomena outside of the atmosphere of the Earth. The observations are complemented by both analytic and numerical theoretical models. The physics and the physical parameters used as an input for these models allow the interpretation of the observations by matching the observational data with the theoretical predictions.

Most astrophysical objects are observed via the electromagnetic radiation they emit. Therefore, the theory of radiative transfer is a key element for the understanding of the radiation and physical structure of these objects. In [Mihalas, D., 2003] a summary of the progress made within this field in the 20th century is given.

The classical equation of transfer first described by Schuster [Schuster, 1905] has been extensively used to describe the radiative transfer for astrophysical atmospheres, mostly stars. The theory needed for the description of radiation transport in moving media was first given by Thomas [Thomas, 1930], but was effectively introduced to the scientific community in a comoving formulation in [Mihalas, 1980]. An inherently covariant formulation for the description of general relativistic radiative transfer was found by Lindquist [Lindquist, 1966] with the aid of the Boltzmann equation.

Through the advent of modern computers the radiative transfer has been calculated with a level of physical realism unmatched before, including vast databases for opacities and NLTE[1] treatment. One of the main obstacles in the radiative transfer modeling has been the inclusion of scattering into the calculations. An efficient solution has been found in an operator splitting method called accelerated Λ-iteration. This powerful tool has been established as a de facto standard in the modeling of static and special relativistically expanding atmospheres (see [Hubeny, 2003] for a review), but has not been applied to the general relativistic radiative transfer problem before.

Nonetheless the covariant formulation of Lindquist provided a base for numerous applications. However, the applications have been geared more towards radiation hydrodynamics utilizing moment equations and the inclusion of fluid motion [Anderson and Spiegel, 1972, Castor, 1972, Schmid-Burgk, 1978, Shapiro, 1996]. With the work of [Schinder, 1988, Schinder and Bludman, 1989] the ansatz of a tangent ray solution in the comoving frame

[1] Abbr.: non local thermodynamical equilibrium. See Section 2.3.1

[Mihalas *et al.*, 1975, Mihalas, 1978] has been adopted in general relativistic transfer from special relativistic modeling. The use of a solution that solves the transfer along characteristics is well suited for curved spacetimes, because the bending of the photon paths and the subsequent imaging within the spacetime can be fully accounted for. The transfer has only been formulated for static spacetimes at that point, but the work of [Zane *et al.*, 1996] has generalized the ansatz further to include the treatment of relativistic flows in background spacetimes. The radiative transfer in these developments have been geared towards the sole use of continuous opacities. The present work includes radiative line transfer, which requires a different ansatz in the formulation of the equation of transfer.

Schinder and Bludman [Schinder and Bludman, 1989] realized that the presence of Killing vectors in the spacetime can be exploited to express the components of the photon momenta in terms of constants of motion. Therefore, the energy of the photons and the direction within the local comoving frames can be expressed by the radial coordinate alone for spherical symmetric metrics. The reduction of the independent variables to only one simplifies the problem enormously. As the energy of a photon depends on the position within the atmosphere, a comoving wavelength parameterization will constantly change along the characteristic. This is of little relevance as long as no spectral lines are to be resolved throughout the atmosphere. Otherwise a prohibitively large number of additional wavelength points must be inserted into the wavelength parameterization. The treatment of spectral lines in the radiative transfer calculations is desirable, however, and is included in this work. Therefore, this work avoids the use of the constants of motion and instead uses a comoving description of the photon momenta, which can be described with a fixed comoving wavelength grid throughout the atmosphere. This ansatz requires an explicit coupling of the wavelengths within the equation of transfer. The coupling of wavelengths is also present in special relativistic cases and is compatible with the established accelerated Λ-iteration methods and NLTE solving frameworks [Hauschildt and Baron, 1999]. Therefore, these established methods are applicable to the general relativistic problem. The aim of this work is to solve the equation of general relativistic radiative transfer via a characteristic method with the aid of an accelerated Λ-iteration. This allows for the solution of the radiative transfer problem throughout the atmosphere and is not limited to the imaging of classically calculated spectra in curved spacetime with radiative transfer functions [Cunningham, 1975]. For the first time the effect of general relativity on the NLTE line transfer itself can be investigated. The calculations in this work are restricted to spherical symmetric calculations, but due to the generality of the characteristic method the radiative transfer can be generalized to multiple dimensions. In addition, an ansatz is developed to describe the general radiative transfer in flows in static background spacetimes in order to provide a broadly applicable solution for the general relativistic transfer problem.

In order to be able to construct physical models, a sophisticated atmosphere modeling code is required. The `PHOENIX` package was chosen in this work and the implementation is compatible with the use within its framework.

A possible application is the modeling of the atmospheres of neutron stars. The state of the art model atmospheres are already very sophisticated, since for instance the treatment of strong magnetic fields and relativistic imaging is included. See [Zavlin and Pavlov, 2002]

for a summary. However, none of these models utilizes general relativistic radiative transfer within the atmosphere. The magnitude of the general relativistic effects are a priori unknown, it is thus desirable to use as sophisticated models as possible to better determine the properties of neutron stars in order to constrain the realized equation of state and the interior structure of neutron stars [Yakovlev *et al.*, 2002].
[Broderick, 2006] also realized the importance of general relativistic transfer in compact objects and devised a new method of solving the radiative transfer along photon orbits. However, the solution is not capable of treating scattering, what is a very important ingredient for astrophysical modeling and especially in neutron star atmospheres [Madej, 1974].
Another possible application is the neutrino transport in stellar core collapse and neutron star formation calculations [Wilson, 1971, Bruenn, 1985]. It has been found that the inclusion of general relativity is important in this context and the neutrino transport should also be calculated within the framework of general relativity accordingly. The results of fully general relativistic radiative hydrodynamical calculations [Baron *et al.*, 1989, Bruenn *et al.*, 2001] could be improved with the more sophisticated method of solution for the transfer.
Furthermore, the theory of relativistic radiative transfer applies to all scenarios where compact objects are involved, such as black hole accretion, AGN, or gamma ray bursts. These systems should be described in multiple dimensions using radiation hydrodynamics. More immediate one-dimensional applications based on this work include the calculations of the radiative transfer across shock fronts or spectra from line forming regions that are restricted to an one-dimensional description.
This work is organized as follows. Chapter 2 gives an overview over the physical quantities needed to describe the radiative transfer. These include the radiation field itself as well as the coefficients describing the interactions of radiation with matter. The equation of radiative transfer is discussed in detail in Chapter 3. At first, it is formulated for general base coordinate systems and locally spherical polar coordinates in the description of the photon momentum. The equation of transfer is then explicitly given for comoving spherical symmetric metrics, reproducing the result of Lindquist, but formulated in terms of specific intensities. Furthermore, the equation of transfer is developed for the Kerr metric and an ansatz for the inclusion of flows in the equation of radiative transfer in static background spacetimes is developed and explicitly calculated for a purely radial flow in Chapter 3. In Chapter 4 the description and calculation of the photon orbits needed for the solution of the radiative transfer are discussed. Details on the formal solution of the radiative transfer and the operator splitting technique used in this work are given in Chapter 5. The results of test calculations of the new general relativistic transfer in a testing environment are presented in Chapter 6, while the integration into an existing atmosphere modeling code and large scale tests are discussed in Chapter 7. Finally in Chapter 8, the results are summarized, put into perspective and an outlook is given.

Chapter 2

Radiation Fields

The aim of the theory of radiative transfer in the context of astrophysics is the understanding of the energy which is transported by radiation within astrophysical objects. The radiative energy emitted by these objects is of special interest because it can be observed directly.
Hence it is natural that the main quantity of radiation transport describes an energy. It is the energy that is emitted in the from of photons into a solid angle at a given spatial point from a surface element per second and per wavelength of the photons. This quantity is called the specific intensity. If it is known at every point of an astrophysical object the energy which an observer[1] will receive can be calculated in general[2].
Therefore, the specific intensity is the quantity which is computed in the theory of radiative transfer. It should be pointed out that the knowledge of the specific intensity is a sufficient condition in order to describe the emitted energy. The specific intensity can be calculated if the emitting and absorbing properties of the atmosphere are known. It is also commonly said that these properties – or their ratio – are the quantities of the theory of radiative transfer which must be computed.
In order to be able to formulate a mathematical theory of radiation transport additional quantities and their relations to physics must be known. In the following sections these relations will be briefly introduced.

In Section 2.1 a mathematical introduction to the specific intensity and its related quantities is given, as well as an overview of the treatment within the framework of an energy momentum tensor. The implications of spherical topology, spherical symmetry, and the corresponding coordinate systems for the description of the specific intensity are introduced in Section 2.2. Section 2.3 gives an overview over the interaction of radiation with matter and the associated quantities. The rate equations which describe the state of the matter are discussed in Section 2.4 and useful definitions for radiative transfer are made in Section 2.5.

[1] The position relative to the source must be known, however. Often it is assumed that the observer is at infinity.

[2] In spherical symmetry less information is needed and the observable energy is described by the Eddington flux (see Section 2.2).

2.1 The Mathematical Description of Radiation Fields

Radiation consists of photons and the radiation field can be described as a gas of photons. Such an ensemble of photons is physically described by a distribution function $f(t, \vec{x}, \vec{p})$ [Landau and Lifschitz, 1987]. With $f(t, \vec{x}, \vec{p})\mathrm{d}^3\vec{p}$ being the number of photons at the time t, at the point $\vec{x}$, and with a momentum within $(\vec{p}, \vec{p} + \mathrm{d}\vec{p})$.
Since, except for their energy, the properties of the photons are not directly observable, another way to describe the radiation field is frequently used. The specific intensity $I(t, \vec{x}, \lambda, \vec{n})$ is the energy that is transported by radiation in the wavelength interval $(\lambda, \lambda + \mathrm{d}\lambda)$ across a surface $\mathrm{d}\vec{S}$ during a time interval $\mathrm{d}t$ into a solid angle $\mathrm{d}\Omega$ around the direction $\vec{n}$. The differential expression for the energy is [Mihalas, 1970]

$$\mathrm{d}E = I(t, \vec{x}, \lambda, \vec{n})\ (\mathrm{d}\vec{S} \cdot \vec{n})\ \mathrm{d}\Omega\ \mathrm{d}\lambda\ \mathrm{d}t \tag{2.1}$$

Due to the macroscopic equivalence of the distribution function and the specific intensity, there has to exist a relation between these quantities. The energy of photons is determined by their momentum and thus the distribution function can be used to describe the transported energy. Since photons move with the speed of light – c – it follows that $c\mathrm{d}t$ photons cross a surface element in the time $\mathrm{d}t$ carrying the energy $\frac{hc}{\lambda}$ with them and h being Planck's constant. Using the relation $\mathrm{d}^3\vec{p} = -\frac{h^3}{\lambda^4}\mathrm{d}\lambda\mathrm{d}\Omega$, it follows [Ehlers, 1971, Mihalas and Weibel-Mihalas, 1984]

$$\mathrm{d}E = \frac{c^2 h}{\lambda} f(t, \vec{x}, \vec{p})\mathrm{d}^3\vec{p}\ (\mathrm{d}\vec{S} \cdot \vec{n})\ \mathrm{d}t \tag{2.2}$$

$$\mathrm{d}E = -\frac{c^2 h^4}{\lambda^5} f(t, \vec{x}, \lambda, \vec{n})\ (\mathrm{d}\vec{S} \cdot \vec{n})\ \mathrm{d}\Omega\ \mathrm{d}\lambda\ \mathrm{d}t \tag{2.3}$$

$$\rightarrow \quad I_\lambda(t, \vec{x}, \vec{n}) = \frac{c^2}{h}\frac{h^5}{\lambda^5} f(t, \vec{x}, \lambda, \vec{n}) \tag{2.4}$$

Due to the change of the differential the arguments of the distribution function in (2.3) formally changed. The minus signs originates from the fact that the momentum decreases for increasing wavelength.
The equivalent formulation of Equation (2.4) with frequency instead of wavelength reads

$$I_\nu(t, \vec{x}, \vec{n}) = \frac{h^4\nu^3}{c^2} f(t, \vec{x}, \nu, \vec{n}) \tag{2.5}$$

The distribution function $f(t, \vec{x}, \vec{p})$ is a Lorentz invariant and can be generalized to a covariant form $f(x^\mu, p^\mu)$ [van Kampen, 1969, Misner *et al.*, 1973] with

$$x^\mu = (\tau, \vec{x}) \quad \text{, and} \qquad p^\mu = \frac{h}{\lambda}(1, \vec{n})$$

and in the following this new form will be used[3].

[3] If interactions of the particles described with the distribution function with the matter of the atmosphere

The distribution function and the specific intensity respectively contain the complete information of the radiation field. As long as only the transport of energy is of interest, the radiation can be considered a classical field and the theory of the energy momentum tensor is applicable [Landau and Lifschitz, 1997]. The radiation energy momentum tensor of the photon gas [Landau and Lifschitz, 1997, Mihalas and Weibel-Mihalas, 1984] can be defined as

$$T^{\alpha\beta} = c \int \frac{f(x^\mu, p^\mu)}{p^0} p^\alpha p^\beta \mathrm{d}^3\vec{p}$$

Formulated in terms of the specific intensity it reads

$$\begin{aligned} T^{\alpha\beta} &= \frac{1}{c}\int \mathrm{d}\lambda \int \mathrm{d}\Omega I_\lambda(\vec{x},\vec{n},t)\frac{\lambda^2}{h^2}p^\alpha p^\beta && (2.6)\\ &= \frac{1}{c}\int \mathrm{d}\lambda \int \mathrm{d}\Omega I_\lambda(\vec{x},\vec{n},t) \begin{pmatrix} 1 & n_x & n_y & n_z \\ n_x & n_x^2 & n_x n_y & n_x n_z \\ n_y & n_y n_x & n_y^2 & n_y n_z \\ n_z & n_z n_x & n_z n_y & n_z^2 \end{pmatrix} && (2.7)\\ &= \begin{pmatrix} E & \frac{\vec{F}}{c} \\ \frac{\vec{F}}{c} & P^{ij} \end{pmatrix} && (2.8) \end{aligned}$$

The energy momentum tensor describes the density and the flux of energy and momentum. Hence its components play an important role in the theory of radiation transport. Their fundamental definitions are:

E is the total radiation energy density. It can be expressed as an integral over wavelength

$$E = \int E_\lambda \mathrm{d}\lambda$$

where E_λ is the monochromatic radiation energy density.

$$\begin{aligned} E_\lambda &= \frac{1}{c}\oint I_\lambda(\vec{x},\vec{n},t)\mathrm{d}\Omega \\ E_\lambda &= \oint \frac{ch^4}{\lambda^5}\left(-\frac{\mathrm{d}p}{\mathrm{d}\lambda}\right) f(x^\mu, p^\mu)\mathrm{d}\Omega \end{aligned}$$

The quantity $\vec{F}$ is the integrated radiation flux. It can be expressed as the integral

$$\vec{F} = \int \vec{F}_\lambda \mathrm{d}\lambda$$

with $\vec{F}_\lambda$ being the monochromatic radiation flux. $\vec{F}_\lambda$ can be expressed in terms of the

are included, the strict Lorentz invariance breaks down. See Section 3.1 and [Oxenius, 1986].

distribution function and specific intensity

$$\begin{aligned}\vec{F_\lambda} &= \oint I_\lambda(\vec{x},\vec{n},t)\vec{n}\mathrm{d}\Omega \\ \vec{F_\lambda} &= \oint \frac{h^4}{\lambda^5}\left(-\frac{\mathrm{d}p}{\mathrm{d}\lambda}\right) f(x^\mu,p^\mu)\vec{n}\mathrm{d}\Omega\end{aligned}$$

Note that in the definition of $\vec{F_\lambda}$ a factor of $\frac{1}{c}$ was omitted and instead has been included in the definition of $T^{\alpha\beta}$. With this definition $\vec{F_\lambda}$ is a vector which integrated over an area gives the energy flux through this given area and $\vec{F_\lambda}$ is strongly related to the energy received by an observer.
P^{ij} is the total radiation pressure tensor. Its integral description reads

$$P^{ij} = \int P^{ij}_\lambda \mathrm{d}\lambda$$

P^{ij}_λ is called the monochromatic radiation pressure tensor. It describes the number of photons of the given wavelength which cross unit areas perpendicular to the jth coordinate of the ith momentum variable.

$$\begin{aligned}P^{ij}_\lambda &= \frac{1}{c}\oint I_\lambda(\vec{x},\vec{n},t)\,\vec{n}\otimes\vec{n}\,\mathrm{d}\Omega \\ P^{ij}_\lambda &= \oint \frac{ch^4}{\lambda^5}\left(-\frac{\mathrm{d}p}{\mathrm{d}\lambda}\right) f(x^\mu,p^\mu)\vec{n}\otimes\vec{n}\,\mathrm{d}\Omega\end{aligned}$$

2.2 Radiation Fields in Spherical Topology

Many astrophysical object – such as stars for instance – have a spherical shape. Therefore, spherical polar coordinates are often the best suited coordinate system in radiative transfer. In the theory of general relativity, coordinates must be interpreted as coordinates on a manifold. Additional mathematical structures, such as fundamental forms, prohibit identifications with coordinates known in Euclidean space. However, the concept of symmetries does carry over into coordinates of manifolds. Hence the formal notation that is used in the following can be retained for descriptions of radiative transfer in curved spacetimes.
Therefore, coordinate systems in flat and curved spacetime may resemble each other. But it should always be kept in mind that they can not be identified as one coordinate system.

In spherical coordinates, a spatial point is described by three coordinates

$$P = (x_1, x_2, x_3) = (r, \Theta, \Phi)$$

with r as the radius, Θ as the polar angle, and Φ as the azimuth. At the given point P a

local orthonormal coordinate system can be simply constructed[4]

$$\vec{e}_i = \left.\frac{\vec{\partial}}{\partial x_i}\right|_P$$

Instead of describing local vectors at the point P in these Cartesian coordinates, another set of spherical polar coordinates is introduced

$$P' = (y_1, y_2, y_3) = (r', \theta, \varphi)$$

An important vector in this coordinate system that is used in the radiative transfer theory is the direction of propagation of the specific intensity $\vec{n}$. Only the direction is important so the radial coordinate is dropped

$$\vec{n} = (\theta, \varphi)$$

From this it follows that the specific intensity $I_\lambda(t, \vec{x}, \vec{n})$ in spherical topology is written as

$$I_\lambda(t, r, \Theta, \Phi, \theta, \varphi)$$

Often spherical symmetry is assumed and this results in a simplified description of the specific intensity. The physical conditions will only depend on the radial coordinate r and the dependence on (Θ, Φ) can be dropped. A change of the local φ component is equivalent to a change of the local basis vectors $\frac{\vec{\partial}}{\partial\Theta}$ and $\frac{\vec{\partial}}{\partial\Phi}$ and thus a variation of φ just means a combination of vanishing variations of Θ and Φ [Chandrasekhar, 1950].
Therefore, the radiation field becomes independent from φ. The remaining local coordinate θ is usually replaced by its cosine

$$\mu = \cos\theta \tag{2.9}$$

When assuming spherical symmetry the integration over solid angle is possible for the partial integration over $\mathrm{d}\varphi$. The remaining integrals of the specific intensities over $\mathrm{d}\mu$ are called the moments of the radiation field [Chandrasekhar, 1950, Mihalas, 1970].

$$[J_\lambda(r), H_\lambda(r), K_\lambda(r)] = \frac{1}{2}\int_{-1}^{1} I_\lambda(r,\mu)[1, \mu, \mu^2]\mathrm{d}\mu \tag{2.10}$$

$$[J(r), H(r), K(r)] = \frac{1}{2}\int_0^\infty \left(\int_{-1}^{1} I_\lambda(r,\mu)[1, \mu, \mu^2]\mathrm{d}\mu\right)\mathrm{d}\lambda \tag{2.11}$$

The exponent of μ in the integral determines the name of the moment. Accordingly J_λ is the zeroth moment of the radiation field. It is closely related to the monochromatic energy density E_λ

$$J_\lambda = \frac{c}{4\pi}E_\lambda$$

[4]This coordinate system is called natural or induced basis and its concept is also applicable for coordinates of manifolds.

The first moment is also called Eddington flux and is related to the monochromatic radiation flux.

$$H_\lambda(r) = \frac{1}{4\pi} F_{z,\lambda}(r)$$

The moment of order two is also known as the K-integral. The spherically symmetric radiation pressure tensor is related to the zeroth and second moment

$$P_\lambda^{ij} = \frac{4\pi}{c} \begin{pmatrix} \frac{1}{2}(J_\lambda - K_\lambda) & 0 & 0 \\ 0 & \frac{1}{2}(J_\lambda - K_\lambda) & 0 \\ 0 & 0 & K_\lambda \end{pmatrix} \tag{2.12}$$

From Equation (2.12) it is obvious that the radiation field will be isotropic when $K_\lambda = 1/3 J_\lambda$ and K_λ can be interpreted as the radial radiation pressure.
In spherical symmetry the radiation energy momentum tensor can then be expressed through the various moments and reads in a Cartesian base coordinate system

$$T^{\alpha\beta} = \frac{4\pi}{c} \begin{pmatrix} J & 0 & 0 & H \\ 0 & \frac{1}{2}(J-K) & 0 & 0 \\ 0 & 0 & \frac{1}{2}(J-K) & 0 \\ H & 0 & 0 & K \end{pmatrix} \tag{2.13}$$

For expression in spherical coordinates the tensor has to be transformed with the metric of spherical coordinates. The radiation energy momentum tensor reads then

$$T^{\alpha\beta} = \frac{4\pi}{c} \begin{pmatrix} J & H & 0 & 0 \\ H & K & 0 & 0 \\ 0 & 0 & \frac{1}{2}\frac{(J-K)}{r^2} & 0 \\ 0 & 0 & 0 & \frac{1}{2}\frac{(J-K)}{r^2 \sin^2\Theta} \end{pmatrix} \tag{2.14}$$

2.3 Interaction of Radiation with Matter

If matter is present within a radiation field the radiation will interact with the matter. The interaction of photons with atoms (or molecules) and electrons are of quantum mechanical nature and the theory of quantum mechanics must be used to describe the physics. However, the macroscopic results of the interaction can still be described by the specific intensity and macroscopic coefficients.
The processes between matter and radiation are manifold but can be separated into two basic cases. If we adopt the description by the specific intensity the relevant quantity is the energy in a given beam of radiation. An interaction can be classified whether it removes or adds energy to the beam. The interactions that remove energy from the beam are called extinction processes and the interactions which add energy are referred to as emission processes.
An extinction process can be distinguished further: Either there is another photon present after the interaction or the photon is destroyed.

The processes which retain a photon are called scattering. A scattering process is still an extinction since the direction of propagation of the two photons may be different and hence energy is removed from the beam.
Processes that destroy the photon are called absorption, the photon increases the internal energy of the absorber. Since the atoms and electrons also interact among themselves, the energy is statistically distributed over all atoms and electrons via collisions. The energy of the absorbed photon is said to be added to the thermal pool of the gas.
All extinction processes at a given wavelength are described by a macroscopic extinction coefficient χ_λ which is also called the opacity. The energy removed from a beam of radiation along the distance $\mathrm{d}s$ reads

$$\mathrm{d}E^- = \chi_\lambda(\vec{x},\vec{n})\, I_\lambda(\vec{x},\vec{n})\, (\mathrm{d}\vec{S}\cdot\vec{n})\, \mathrm{d}\Omega\, \mathrm{d}\lambda\, \mathrm{d}s \tag{2.15}$$

The opacity is further divided into a scattering part σ_λ and an absorption part κ_λ.

$$\chi_\lambda(\vec{x},\vec{n}) = \sigma_\lambda(\vec{x},\vec{n}) + \kappa_\lambda(\vec{x},\vec{n}) \tag{2.16}$$

The emission processes can also be divided into several parts: Thermal emission, scattering emission and stimulated emission. Thermal emission is independent of the radiation field present. The gas of atoms has a thermal pool of kinetic energy and individual atoms are in excited states that may emit photons. This process is the inverse of the absorption described above.
Photons of other beams can be scattered into a given beam and produce scattering emission. The radiation field can also perturb the exited states of atoms and cause the emission of photons. In this case, the energy and direction of the photons are correlated and the rate of this stimulated emission is proportional to the radiation field. Therefore, it can be described as negative absorption and is typically included in the extinction coefficient.
The macroscopic coefficient of the emission – η_λ – is also called the emissivity. The energy added to a beam is then given by

$$\mathrm{d}E^+ = \eta_\lambda(\vec{x},\vec{n})\, (\mathrm{d}\vec{S}\cdot\vec{n})\, \mathrm{d}\Omega\, \mathrm{d}\lambda\, \mathrm{d}s \tag{2.17}$$

The emissivity is further divided into a scattering part η_λ^σ and a thermal part η_λ^κ.

$$\eta_\lambda(\vec{x},\vec{n}) = \eta_\lambda^\sigma(\vec{x},\vec{n}) + \eta_\lambda^\kappa(\vec{x},\vec{n}) \tag{2.18}$$

The coefficients in the relations (2.16) and (2.18) include contributions from transitions of all bound and continuum states of the different atoms and molecules in the gas.
In order to calculate these wavelength dependent coefficients all transitions which encompass the energy at the given wavelength have to be considered. The cross sections of the transitions are either known from theory or from experiments. However, the possibility for a transitions to occur is only known when the occupation numbers of the various states of the atoms are known.
In some cases the occupation numbers can be derived from statistical mechanics (see Section 2.3.1) but must in general be determined by solving the rate equations for the given species (see Section 2.4).

2.3.1 Applicability of Statistical Mechanics

The Boltzmann distribution describes the probability of an atom or molecule to be in a certain state $|n\rangle$ and can be used to describe the probability for the according occupation number with degenerate states taken into account [Landau and Lifschitz, 1987]. The application of Boltzmann statistics demands that the gas can be treated as an ideal gas and is in thermal equilibrium. That means that there are no mutual interactions of the constituents other than elastic collisions.
Since in astrophysical atmospheres besides the interaction with the radiation field inelastic collisions occur frequently and the statistic is not applicable in general. The radiation field and the collisions cause different transitions within an atom or molecule and influences the occupation numbers of the participating states. Since the different level populations change the emissivity and opacity, the radiation field changes through the interactions. The coupling of radiation and matter is a nonlinear process. Hence the radiative transfer can in generally only be solved if it is coupled to the rate equations (see Section 2.4) which explicitly describe the population and depopulation of states in the atoms and molecules.

In some situations the Boltzmann statistic is still applicable. If the rates of the population and depopulation are equal to their thermal equilibrium rates, then also the population numbers will have their thermal equilibrium values. In thermal equilibrium every transition is exactly canceled by its inverse process. This situation is known as detailed balance.
Due to the different mechanisms which cause transitions, the rates consist of two parts. On the one hand there are collisional rates and on the other there are radiative rates. The collisional rates occur at their equilibrium values as long as the gas of the colliders is described by a Maxwellian distribution. Since this is typically true for astrophysical gases considered here the collisional rates drive the level population toward their equilibrium values.
The radiative rates depend directly on the radiation field and will be different from their equilibrium values as long as the radiation field is not Planckian. If now the collisional rates dominate the radiative rates the occupation numbers will have their equilibrium values and the Boltzmann formula can be used to determine the level populations.
If detailed balance holds for all transitions or the collisional rates dominate the situation is called *local thermodynamic equilibrium* (LTE) whereas the general case is termed as *non-local thermodynamic equilibrium* (NLTE). Note that the rates are different from species to species and the approximation of LTE may be valid for only some of the species. Therefore, there may be a mixed treatment of species in regard of the use of LTE[5].

For LTE analytic relations between the emissivity and opacity can be found. Since in thermal equilibrium the Kirchoff-Planck relation is valid, which states that the absorbed energy equals the emitted energy, the thermal emissivity and the absorption are simply related by

$$\eta_\lambda^\kappa(\vec{x},\vec{n}) = \kappa_\lambda(\vec{x},\vec{n})B_\lambda(\vec{x}) \tag{2.19}$$

[5]This may also apply for species which do not have a large opacity that depends strongly on the microphysical state. In these cases the treatment in LTE is justified to reduce the computational time.

In the following "starred" versions of occupation numbers (see for instance relation (2.34)) are calculated with the Boltzmann or Saha-Boltzmann formula but use actual (NLTE) numbers of electron density and occupation number of the continuum.

2.3.2 The Redistribution Function

A similar relation to expression (2.19) for the thermal emissivity holds for the coefficients of the scattering emissivity and opacity. However, in order to formulate the relation the scattering process itself must be described in detail.
The scattering of a photon with the basic properties $(\vec{n}', \lambda')$ into a photon with $(\vec{n}, \lambda)$ is described by a normalized redistribution function [Mihalas, 1970] $R(\lambda', \lambda, \vec{n}', \vec{n})$ with the basic property

$$\oint \oint \int \int R(\lambda', \lambda, \vec{n}', \vec{n}) \mathrm{d}\lambda' \mathrm{d}\lambda \frac{\mathrm{d}\Omega'}{4\pi} \frac{\mathrm{d}\Omega}{4\pi} = 1 \tag{2.20}$$

The energy of a bound-bound transition is not sharp and is instead described by profile functions with finite width. In general, the profiles for emission and absorption may be different. Theses profiles are contained within R. The profile for absorption Φ is obtained by integration of R over the outgoing wavelengths and solid angle, whereas the emission profile Ψ is obtained by integration over incoming wavelengths and solid angle.

$$\Phi(\vec{n}', \lambda') = \oint \int R(\lambda', \lambda, \vec{n}', \vec{n}) \mathrm{d}\lambda \frac{\mathrm{d}\Omega}{4\pi} \tag{2.21}$$

$$\Psi(\vec{n}, \lambda) = \oint \int R(\lambda', \lambda, \vec{n}', \vec{n}) \mathrm{d}\lambda' \frac{\mathrm{d}\Omega'}{4\pi} \tag{2.22}$$

If the scattering opacity $\sigma_\lambda(\vec{x}', \vec{n}')$ is known the scattering emissivity $\eta^\sigma_\lambda(\vec{x}, \vec{n})$ is given by

$$\eta^\sigma_\lambda(\vec{x}, \vec{n}) \mathrm{d}\lambda \mathrm{d}\Omega = \mathrm{d}\lambda \mathrm{d}\Omega \oint \int \sigma_\lambda(\vec{x}', \vec{n}') I(\vec{x}, \lambda', \vec{n}) R(\lambda', \lambda, \vec{n}', \vec{n}) \mathrm{d}\lambda' \frac{\mathrm{d}\Omega'}{4\pi} \tag{2.23}$$

In practice, the redistribution function $R(\lambda', \lambda)$ is frequently averaged over solid angle since the main interest lies in the wavelength distribution. The integration over solid angle then only applies to the specific intensity

$$\eta^\sigma_\lambda(\vec{x}, \vec{n}) \mathrm{d}\lambda \mathrm{d}\Omega = \mathrm{d}\lambda \mathrm{d}\Omega \int \sigma_\lambda(\vec{x}') J(\vec{x}, \lambda') R(\lambda', \lambda) \mathrm{d}\lambda' \tag{2.24}$$

With the properties (2.21) and (2.22) the averaged redistribution function can be written in case of no correlation of the absorbed and emitted photons as

$$R(\lambda', \lambda) = \Phi(\lambda') \Psi(\lambda)$$

This case is called complete redistribution if $\Phi(\lambda) = \Psi(\lambda)$ holds. It is, for instance, a good assumption when the time of the interaction is long enough for collisions to occur, which redistribute the excited electron to the degenerate sub states of the upper level whereby any correlation is removed.

The opposite case of full correlation is called coherent scattering, it does not change the energy of the photons. Then the redistribution function is given as

$$R(\lambda', \lambda) = \Phi(\lambda')\delta(\lambda - \lambda')$$

where $\delta(\lambda - \lambda')$ is Dirac's delta-distribution.
In general, the redistribution function not only depends on the transition but also on the physical conditions and possible perturbers. So the best physical description of R will depend on the situation and will be a mix of the aforementioned redistributions.

2.4 Rate Equations

The assumption of LTE is not valid if the influence of the radiation field is a too large perturbation and the radiative transitions are not in detailed balance ($J_\lambda \neq B_\lambda$). Then the occupation numbers of the different states of the atoms (or molecules) must be determined through the solution of the rate equations. This is customarily referred to as NLTE calculations.
In order to describe the rate of a process, the cross section for the process must be known. The cross sections are given by quantum mechanical calculations or by experiment. In general the cross section may depend on solid angle, but here and in the following we assume isotropy.

Einstein introduced three coefficients A_{ji}, B_{ji}, and B_{ij} for transitions between two bound states $|i\rangle$ and $|i\rangle$. The coefficients are simply related to the cross section for the given transition and process.
A_{ji} describes the spontaneous emission probability, B_{ji} the stimulated emission probability, and B_{ij} the absorption probability [Mihalas and Weibel-Mihalas, 1984]. Following detailed balance arguments [Mihalas, 1970], the following relations between the coefficients can be found

$$A_{ji} = \frac{2h\nu_{ij}^3}{c^2} B_{ji} \tag{2.25}$$

$$\frac{B_{ij}}{B_{ji}} = \frac{g_j}{g_i} \iff B_{ij} g_i = B_{ji} g_j \tag{2.26}$$

where h is Planck's constant, $h\nu_{ij}$ the energy difference between the states $|i\rangle$ and $|i\rangle$, and g the statistical weight of the given state.
The Einstein relation has been generalized by Milne [Mihalas, 1970] to transitions between bound $|i\rangle$ and continuum states $|\kappa\rangle$. The velocity of the free electrons is chosen to describe the continuous energies of the unbound states. The probability for a photoionization by a photon with energy $h\nu = \frac{hc}{\lambda}$ is called p_λ.
Transitions between unbound states – for instance free-free transitions – are possible but do not effect the occupation numbers and the according rates are not included in the rate equations.

With a symbolical description of transition probabilities the rates of the different transitions can be specified as following

$$R_{ij} = B_{ij} \int \left(\int R(\lambda, \lambda') \mathrm{d}\lambda' \right) I_\lambda \mathrm{d}\lambda \tag{2.27}$$

$$R_{ji} = A_{ji} + B_{ji} \int \left(\int R(\lambda, \lambda') \mathrm{d}\lambda' \right) I_\lambda \mathrm{d}\lambda \tag{2.28}$$

$$R_{i\kappa} = 4\pi \int p_\lambda J_\lambda \mathrm{d}\lambda \tag{2.29}$$

$$R_{\kappa i} = 4\pi \int p_\lambda \left(J_\lambda + \frac{2hc^2}{\lambda^5} \right) \exp\left(-hc/kT\lambda\right) \mathrm{d}\lambda \tag{2.30}$$

Whereas the collisional rates read

$$C_{ij(\kappa)} = n_e \int_{v_0}^{\infty} \sigma_{ij(\kappa)} f(v) v \mathrm{d}v \equiv n_e q_{ij(\kappa)}(T) \tag{2.31}$$

$$C_{j(\kappa)i} = \left(\frac{n_i}{n_{j(\kappa)}} \right)^* n_e q_{ij(\kappa)}(T) \tag{2.32}$$

with σ being the cross section and $f(v)$ the velocity distribution of the colliders. From Equation (2.31) it can be seen that the flux of the colliders $vf(v)$ determines the collisional rate.

The rate equations can be derived as follows. For a given state all the rates of transitions that depopulate the state are subtracted from the rate of transitions that populate the state. The result is the change of the occupation number with time. The rate of actual transitions is the product of the radiative of collisional rate with the according occupation number of the initial state of the transition.

The rate equations read then

$$-\frac{\mathrm{d}n_i}{\mathrm{d}t} = \sum_{i \neq j} \mathfrak{R}_{ij} - \sum_{i \neq j} \mathfrak{C}_{ij} + \mathfrak{R}_{i\kappa} + \mathfrak{C}_{i\kappa} \tag{2.33}$$

where the following definitions are used

$$\begin{aligned} \mathfrak{R}_{ij} &= n_i R_{ij} - n_j R_{ji} \\ \mathfrak{C}_{ij} &= n_i C_{ij} - n_j C_{ji} \\ \mathfrak{R}_{i\kappa} &= n_i R_{i\kappa} - n_\kappa R_{\kappa i} \\ \mathfrak{C}_{i\kappa} &= n_i C_{i\kappa} - n_\kappa C_{\kappa i} \end{aligned}$$

The rate equations are balancing equations for the occupation numbers for the different states of the ion. Typically the balance is assumed to be stationary so that $\frac{\mathrm{d}n_i}{\mathrm{d}t} = 0$.

The influence of the NLTE calculations on a given level in an atom is described by the departure coefficient b_i. The b_i is defined as the ratio of the actual occupation number and

the starred occupation number[6]

$$b_i = \frac{n_i}{n_i^*} \tag{2.34}$$

The index i refers to the level of the ion at hand. If the b_i deviate from one the approximation of LTE is not valid and the solution of the rate equation is a necessary to determine the opacities correctly.

2.5 Optical Depth and Source Function

The use of purely spatial variables is not well suited for the description of lengths in atmosphere. This is due to the fact that no information about the interaction with the matter is included in the description. Therefore, the concept of optical depth is introduced in the context of radiative transfer.
The optical depth τ is defined as the path integral of the opacity χ along some path γ through the atmosphere.

$$\tau_\lambda = \int_\gamma \chi_\lambda(s)\mathrm{d}s \tag{2.35}$$

Since the opacity is wavelength dependent the optical depth is wavelength dependent as well. As the inverse of the opacity can be interpreted as the mean free path of a photon with the given wavelength the optical depth equals the number of mean free paths along the path γ.
For the construction of numerical atmosphere models one needs a coordinate grid on which the physical quantities are discretized. In spherical symmetry only a radial grid is needed. This grid is most conveniently constructed with the use of the optical depth as a radial coordinate. In this case the path γ is just the depth in the atmosphere. It is customary to define the start point of the path at the outermost point of the atmosphere. Since the spatial radial coordinate increases outwards the definition for a radial optical depth grid reads

$$\tau_\lambda^{\mathrm{rad.}} = -\int_0^r \chi_\lambda(s)\mathrm{d}s \tag{2.36}$$

The equation of radiative transfer (see Chapter 3) is in general parameterized with an affine parameter that can be related to the optical depth.

A useful definition in the theory of radiative transfer is the source function. It is defined as the ratio of emissivity and opacity at a given wavelength.

$$S_\lambda \stackrel{!}{=} \frac{\eta_\lambda}{\chi_\lambda} \tag{2.37}$$

Hence the source function describes whether energy is added to or removed from the radiation field.

[6] See Section 2.3.1. Note that in the literature the starred occupation numbers are sometimes also defined as occupation numbers derived within a purely LTE framework.

For the case of coherent scattering the source function can explicitly be written as

$$S_\lambda = \frac{\kappa_\lambda}{\kappa_\lambda + \sigma_\lambda} B_\lambda + \frac{\sigma_\lambda}{\kappa_\lambda + \sigma_\lambda} J_\lambda \tag{2.38}$$

$$S_\lambda = \epsilon B_\lambda + (1 - \epsilon) J_\lambda \tag{2.39}$$

The parameter ϵ is called the thermal coupling parameter and determines the percentage of photons which are not scattered but absorbed. In the case where no scattering is present – $\epsilon = 1$ – the LTE approximation is sufficiently valid and it holds

$$S_\lambda = B_\lambda \tag{2.40}$$

The form of Equation (2.39) is of special importance as it represents a general form of the source function. If an additional opacity in form of a non-coherently scattering line is introduced in the given wavelength range and it is assumed that a fraction $(1 - \epsilon'')$ of the photons are scattered in the line then the source function can be written

$$\chi_\lambda = \kappa_\lambda + \sigma_\lambda + \chi_{\text{line}} \Phi_\lambda \tag{2.41}$$

$$\eta_\lambda = \kappa_\lambda B_\lambda + \sigma_\lambda J_\lambda + \epsilon'' \chi_{\text{line}} \Phi_\lambda B_\lambda + (1 - \epsilon'') \Phi_\lambda \int \chi_{\text{line}} \Psi_\lambda J_\lambda \mathrm{d}\lambda \tag{2.42}$$

$$\Rightarrow S_\lambda = \epsilon' B_\lambda + (1 - \epsilon') \bar{J}_\lambda \tag{2.43}$$

The form of Equation (2.39) is retained. However, the definition of the thermal coupling parameter has gotten more complicated. In order to achieve this compactified form the mean intensity had to be averaged over the absorption profile of the line and the continuous scattering. For the rest of this work and the further treatment of radiative transfer the source function can always be assumed to be of the form (2.43).

Chapter 3

Theory of Radiation Transport

The theory of radiative transfer for atmospheres in flat spacetime is customarily derived in a heuristic manner using the definitions from Chapter 2. The change of the energy of a beam of radiation in an infinitesimal element of matter is balanced by the emissivity and opacity within the element. The unbalanced rest of the energy is interpreted as the infinitesimal change of the specific intensity along its infinitesimal path through the element.

The resulting differential equation is extended to all spatial points and holds for a given moment in time. This form of the equation of radiative transfer is thus not suited for use in the framework of general relativity. The lack of a covariant formulation and the assumption of an absolute time are contradicting the principles of general relativity.

A description of the transfer of radiation in general relativity must use an ansatz which includes more information about the physics at hand. The foundation of general relativistic radiation transport was laid down by [Lindquist, 1966]. He used kinetic theory to describe the radiation field as a gas of photons and used the Boltzmann equation to describe the dynamics of the system.

Classical radiative transfer is formulated in local coordinate systems in which spherical polar coordinates are introduced to describe the local radiation field. In order to follow this route, Lindquist utilized the tetrad formalism which allows one to pick an orthonormal coordinate system at every point in the tangent space of the base manifold. In this coordinate system one can introduce the spherical polar coordinates as usual.

In this chapter the fundamental equations for the transport of radiation will be presented. The equation of radiative transfer will be motivated as the Boltzmann-equation with collisions for the distribution function in Section 3.1.

After changing to the specific intensity picture the general form of the equation of radiative transfer for a comoving wavelength description and explicitly constructed local coordinates is introduced in Section 3.2.

Section 3.3 gives an overview over the explicit equations of radiative transfer for flat, Schwarzschild, and Kerr spacetimes.

The radiative transfer is extended to relativistic flows in Section 3.4 and in Section 3.5 an overview over the influence of the presence of a magnetic field to the radiative transfer is given.

Notation information In the following a semicolon ";" will denote a covariant derivative, Greek indices will run from 0 to 4 unless noted otherwise, and tetrad components indices will be enclosed in parentheses.

3.1 The Boltzmann Equation as the Equation of Radiative Transfer

The equation of radiative transfer must be written in a general way so that it can be formulated covariantly. The classic derivations of transfer equations for the specific intensity in static or moving media as for instance in [Mihalas, 1978] or [Chandrasekhar, 1950] rely on a heuristic derivation as just energy conservation is used to derive the equations. The time dependence is added as in Newtonian physics and is not suited for relativistic systems.
As demonstrated in Section 2.1, the picture of the specific intensity is equivalent to the description with a distribution function. The distribution function can be generalized into a covariant form. If at first the radiation field is assumed to consist of noninteracting photons then the basic equation of kinetic theory – the collision less Boltzmann equation – is applicable to the problem.
The Boltzmann equation is a consequence of Liouville's theorem. Since the phase space volume and the number of particles are constant along the phase space trajectory, the number density in phase space or the distribution function is constant.
This situation generalizes into spacetime where at a given event an observer can also measure the phase space volume and the number of photons in his own frame. This volume is also constant along any given geodesic [Misner *et al.*, 1973] and hence the Boltzmann equation also holds in spacetimes

$$\frac{\mathrm{d}f}{\mathrm{d}\xi}(x^\mu, p^\mu) = 0 \tag{3.1}$$

where ξ is an affine parameter[1]. Since the distribution function is a scalar there is no need to apply a covariant derivative in Equation (3.1).
However the case of a collision free photon gas is of no interest, because we want to calculate the variation of the distribution function through spacetime. In classic kinetic theory interactions are summarized in a collision term that will depend on the distribution function itself. Since several points of the phase space may contribute to the collisions the term is generally an integral. Therefore, the Boltzmann equation becomes an integro-differential equation. From considerations in Section 2.3 about the interaction of radiation with matter the general from of the collisional term for the radiative transfer can be deduced. There must be a term that is linear in the distribution function and a stand-alone term.

$$\left.\frac{\delta f}{\delta \xi}(x^\mu, p^\mu)\right|_{\mathrm{coll}} = g(f(x^\mu, p^\mu))f(x^\mu, p^\mu) + l(f(x^\mu, p^\mu)) \tag{3.2}$$

[1] It is customary to use λ as an affine parameter, but to avoid confusion with wavelength ξ is used here instead.

Correspondingly g represents the opacity and l the emissivity in the photon distribution function picture. They are related to the coefficients in the specific intensity picture via

$$\eta_\lambda = \frac{c^2}{h}\frac{h^4}{\lambda^4} l \quad \text{and} \quad \chi_\lambda = -\frac{\lambda}{h} g$$

The inclusion of the collisional term is not fully correct for the general case. At a given event the distribution function has to be the same for all observers and hence must be a Lorentz invariant. This is not possible for absorption and emission processes since the time intervals between interactions will generally differ for the different observers and the number of photons will differ as well. There cannot be an affine parameterization of the distribution function as long as the total number of photons changes [Oxenius, 1986]. The aim of radiative transfer is not to describe single photons but the total energy transported. Thus one can introduce distribution functions that are averaged over small portions of spacetime. This evens out the fluctuations of the number of photons in the given phase space element for the different observers. The averaged distribution function is then Lorentz invariant and the framework of the Boltzmann equation can still be applied to the radiative transfer problem [Ehlers, 1971].

$$\frac{\mathrm{d}f}{\mathrm{d}\xi}(x^\mu, p^\mu) = \left.\frac{\delta f}{\delta \xi}(x^\mu, p^\mu)\right|_{\text{coll}} = g(f(x^\mu, p^\mu)) f(x^\mu, p^\mu) + l(f(x^\mu, p^\mu)) \tag{3.3}$$

For a given set of coordinates x^μ and p^μ the differential in Equation (3.3) can be explicitly written as

$$\begin{aligned}
\frac{\mathrm{d}f}{\mathrm{d}\xi} &= \underbrace{\frac{\mathrm{d}x^\alpha}{\mathrm{d}\xi}}_{p^\alpha} \frac{\partial f}{\partial x^\alpha}(x^\mu, p^\mu) + \underbrace{\frac{\mathrm{d}p^\alpha}{\mathrm{d}\xi}}_{-\Gamma^\alpha{}_{\beta\gamma} p^\beta p^\gamma} \frac{\partial f}{\partial p^\alpha}(x^\mu, p^\mu) && (3.4)\\
&= p^\alpha \frac{\partial f}{\partial x^\alpha}(x^\mu, p^\mu) - \Gamma^\alpha{}_{\beta\gamma} p^\beta p^\gamma \frac{\partial f}{\partial p^\alpha}(x^\mu, p^\mu) && (3.5)\\
&= g f(x^\mu, p^\mu) + l && (3.6)
\end{aligned}$$

where the normal derivative $\frac{\mathrm{d}p^\alpha}{\mathrm{d}\xi}$ has been substituted via the geodesic equation (see Equation (4.1)).

With relation (2.4) it is straightforward to switch to the specific intensity and the covariant equation of radiative transfer becomes [Mihalas and Weibel-Mihalas, 1984]:

$$\begin{aligned}
p^\alpha \left[\frac{\partial}{\partial x^\alpha} - \Gamma^\gamma{}_{\alpha\beta} p^\beta \frac{\partial}{\partial p^\gamma}\right] \frac{h}{c^2}\frac{\lambda^5}{h^5} I_\lambda &= \frac{h}{c^2}\frac{\lambda^4}{h^4}\eta_\lambda - \frac{h}{\lambda}\chi_\lambda \frac{h}{c^2}\frac{\lambda^5}{h^5} I_\lambda && (3.7)\\
p^\alpha \left[\frac{\partial}{\partial x^\alpha} - \Gamma^\gamma{}_{\alpha\beta} p^\beta \frac{\partial}{\partial p^\gamma}\right] \lambda^5 I_\lambda &= h\lambda^4 \eta_\lambda - h\chi_\lambda \lambda^4 I_\lambda && (3.8)
\end{aligned}$$

This equation is not in the most general form since it has been assumed that the momentum in the frame of the observer with the four velocity $u(x^\mu)$ is $p = (u^\mu \cdot p^\mu) = \frac{h}{\lambda}$.

3.2 General Relativistic Radiation Transport

Equation (3.8) holds for an observer who uses the coordinate systems x^μ and p^μ. Classical radiative transfer uses local coordinate systems for the momentum to describe the specific intensities (see Section 2.2), however.

The Equation (3.8) holds for all coordinate systems. But normally the momentum and the connection coefficients are formulated in the induced basis of the coordinates x^μ. This is due to the analytical connection between the metric and the connection coefficients. Consequently, the momentum and the connection coefficients must be projected into local coordinate frames in order to achieve a description analogous to classical radiative transfer.

Since the momentum variables in (3.8) are formulated in the tangent space of the base manifold that is covered by the coordinate system x^μ, a new orthonormal coordinate system has to be introduced in the tangent space for a local description of the radiation field.

This is achieved by the use of the tetrad formalism. This technique introduces locally Lorentzian coordinate systems in the tangent space[2]. Every base vector of these coordinate systems will depend on the event in spacetime at which it is constructed. Therefore, four covariant vector fields describe the construction of the local system. The set of four vectors at a given event is referred to as a tetrad.

The tetrad at a given event can be written as a basis of four contravariant vectors

$$e_{(a)}{}^{\alpha} \tag{3.9}$$

which are related to a set of covariant vectors via the metric tensor of the base manifold

$$e_{(a)\alpha} = g_{\alpha\beta} e_{(a)}{}^{\beta} \tag{3.10}$$

An inverse tetrad vector $e^{(a)\alpha}$ can be defined via

$$e^{(a)\alpha} e_{(b)\alpha} = e^{(a)}{}_{\alpha} e_{(b)}{}^{\alpha} = \delta^{(a)}_{(b)}$$

Hence, the tetrad indices are transformed with the Minkowski-metric $\eta_{(a)(b)}$ and it further holds

$$e_{(a)}{}^{\alpha} e_{(b)\alpha} = \eta_{(a)(b)} \tag{3.11}$$

$$\eta_{(a)(b)} e^{(a)}{}_{\alpha} = e_{(b)\alpha} \tag{3.12}$$

$$e_{(a)}{}^{\alpha} e^{(a)}{}_{\beta} = \delta^{\alpha}_{\beta} \tag{3.13}$$

With these definitions every tensor field can be projected into the tetrad and the physics is described by the equations of the projected quantities. Tensors can be expressed by their

[2] In variations of the formalism the local coordinate systems do not have to be orthonormal.

corresponding tetrad components and tetrad vectors:

$$A_{(a)(b)} = e_{(a)}{}^{\alpha} e_{(b)}{}^{\beta} A_{\alpha\beta} \tag{3.14}$$

$$A^{(a)(b)} = e^{(a)}{}_{\alpha} e^{(b)}{}_{\beta} A^{\alpha\beta} \tag{3.15}$$

$$A_{\alpha\beta} = e^{(a)}{}_{\alpha} e^{(b)}{}_{\beta} A_{(a)(b)} \tag{3.16}$$

$$A^{\alpha\beta} = e_{(a)}{}^{\alpha} e_{(b)}{}^{\beta} A^{(a)(b)} \tag{3.17}$$

The equation of radiative transfer in the tetrad then reads

$$\begin{aligned} h\lambda^4\eta_\lambda - h\chi_\lambda\lambda^4 I_\lambda &= p^\alpha \frac{\partial}{\partial x^\alpha}\lambda^5 I_\lambda + \frac{\partial p^\alpha}{\partial \xi}\frac{\partial}{\partial p^\alpha}\lambda^5 I_\lambda \\ &= e^\alpha{}_{(a)} p^{(a)} \frac{\partial}{\partial x^\alpha}\lambda^5 I_\lambda + \frac{\partial p^{(a)}}{\partial \xi}\frac{\partial}{\partial p^{(a)}}\lambda^5 I_\lambda \end{aligned} \tag{3.18}$$

As in Equation (3.8) λ is not an affine parameter, but the wavelength of the photon measured in the frame of the local observer.
In order to calculate $\frac{\partial p^{(a)}}{\partial \xi}$ in the tetrad the following relation [Lindquist, 1966, Mihalas and Weibel-Mihalas, 1984] is used (see Appendix A)

$$\frac{\partial p^{(a)}}{\partial \xi} = -\gamma^{(a)}{}_{(d)(c)} p^{(d)} p^{(c)}$$

The $\gamma^{(a)}{}_{(d)(c)}$ are called Ricci-rotation coefficients and they are defined[3] as

$$\gamma^{(a)}{}_{(d)(c)} = e^{(a)}{}_{\alpha} e_{(d)}{}^{\beta} e_{(c)}{}^{\alpha}{}_{;\beta} \tag{3.19}$$

Hence the equation of transfer formulated in a tetrad reads

$$e^\alpha{}_{(a)} p^{(a)} \frac{\partial}{\partial x^\alpha}\lambda^5 I_\lambda - \gamma^{(a)}{}_{(d)(c)} p^{(d)} p^{(c)} \frac{\partial}{\partial p^{(a)}}\lambda^5 I_\lambda = h\lambda^4\eta_\lambda - h\chi_\lambda\lambda^4 I_\lambda \tag{3.20}$$

One of the aspects of using the tetrad formalism is the ability to introduce curvilinear coordinate systems in the tangent space at every point of the base manifold. Since it is customary in radiative transfer to describe the local radiation field in spherical polar coordinates the equation of radiative transfer (3.20) is still subject to a coordinate transformation of the momentum coordinates.

[3]Note that this given form of the Ricci-rotation coefficients deviates in its definition from most standard textbooks. The coefficients are normally defined with purely lower tetrad indices and the order of the indices is different. Following for instance [Landau and Lifschitz, 1997] the definitions would be simply related

$$\gamma'_{(a)(b)(c)} = \eta_{(b)(d)} \gamma^{(d)}{}_{(c)(a)}$$

However, our form is more suited here as we have to sum over the upper tetrad index and the total sum is more conveniently ordered in our form.

It is noteworthy at this point that in the works of [Schinder and Bludman, 1989, Zane *et al.*, 1996] the explicit construction of the local frames is avoided. In the presence of Killing vector fields the spacetime exhibits symmetries. The resulting constants of motion can be used to express the photon momentum in dependence of the coordinates of spacetime. In spherical symmetry the parameterization of f with ξ in Equation (3.3) is reduced to $\frac{\mathrm{d}f}{\mathrm{d}r}$ with r being the radial coordinate of the spacetime. This avoids the occurrence of the connection coefficients in relation (3.8) altogether, but prohibits the explicit construction of the local frames and utilizes an unwanted coordinate dependent parameterization of the wavelength. Since a wavelength parameterization that is constant throughout the atmosphere is used in this work, this ansatz is not used and the tetrad fields are explicitly constructed and local spherical polar coordinates are used.

However, before the new coordinates can be introduced, it has to be noted that because photons move with the speed of light the locus of possible momenta is a submanifold of the tangent space with the constraint condition $p^\mu p_\mu = 0$. Hence only three components of the momentum are independent and it must only be differentiated in respect to three of them. The choice of the component which is neglected is arbitrary. In the following only the components $p^{(a)}, ((a) = 1, 2, 3)$ will be used. The quantities that are to be transformed are the differential operators of the momentum coordinates $\frac{\partial}{\partial p^{(a)}}$. The $\frac{\partial}{\partial p^{(a)}}$ are covectors and their transformation under a mapping $y = f(x)$ between two manifolds is governed by the Jacobian matrix $\mathbf{J}_{ij} = \frac{\partial f^i}{\partial x^j}$ of the map [Frankel, 2004].

$$\mathrm{d}y^i = \sum_j \mathbf{J}_{ij} \mathrm{d}x^j \tag{3.21}$$

However, there is a complication because of the new coordinates $(\lambda, \theta, \varphi)$ that were introduced in Section 2.2. Due to the spatially independent characterization of the energy of the photon with the wavelength λ only two spatial coordinates remain. There is no simple way to explicitly give the mapping into these new coordinates. But the inverse map can be simply expressed as

$$p^{(a)} = \frac{h}{\lambda} \left(1, \cos\theta, \sin\theta\cos\varphi, \sin\theta\sin\varphi\right) \tag{3.22}$$

So the desired Jacobian matrix for the transformation of the differential operators is given as the inverse of the Jacobian matrix of the mapping in Equation (3.22) which is restricted to the three spatial coordinates. For the matrix from Equation (3.21) it holds

$$\begin{aligned} {}^T\mathbf{J}^{-1} &= \frac{\partial(p^1, p^2, p^3)}{\partial(\lambda, \theta, \varphi)} \\ &= \frac{h}{\lambda} \begin{pmatrix} -\frac{1}{\lambda}\sin\theta\cos\varphi & \cos\theta\cos\varphi & -\sin\theta\sin\varphi \\ -\frac{1}{\lambda}\sin\theta\sin\varphi & \cos\theta\sin\varphi & \sin\theta\cos\varphi \\ -\frac{1}{\lambda}\cos\theta & -\sin\theta & 0 \end{pmatrix} \\ \rightarrow \mathbf{J} &= \frac{\partial(\lambda, \theta, \varphi)}{\partial(p^1, p^2, p^3)} \end{aligned} \tag{3.23}$$

$$= \frac{\lambda}{h}\begin{pmatrix} -\lambda\cos\theta & -\sin\theta & 0 \\ -\lambda\sin\theta\cos\varphi & \cos\theta\cos\varphi & -\frac{\sin\varphi}{\sin\theta} \\ -\lambda\sin\theta\sin\varphi & \cos\theta\sin\varphi & \frac{\cos\varphi}{\sin\theta} \end{pmatrix} \tag{3.24}$$

With Equation (3.21) we obtain the differential operators

$$\frac{\partial}{\partial p^1} = \frac{\lambda}{h}\left(-\lambda\cos\theta\frac{\partial}{\partial\lambda} - \sin\theta\frac{\partial}{\partial\theta}\right) \tag{3.25}$$

$$\frac{\partial}{\partial p^2} = \frac{\lambda}{h}\left(-\lambda\sin\theta\cos\varphi\frac{\partial}{\partial\lambda} + \cos\theta\cos\varphi\frac{\partial}{\partial\theta} - \frac{\sin\varphi}{\sin\theta}\frac{\partial}{\partial\varphi}\right) \tag{3.26}$$

$$\frac{\partial}{\partial p^3} = \frac{\lambda}{h}\left(-\lambda\sin\theta\sin\varphi\frac{\partial}{\partial\lambda} + \cos\theta\sin\varphi\frac{\partial}{\partial\theta} + \frac{\cos\varphi}{\sin\theta}\frac{\partial}{\partial\varphi}\right) \tag{3.27}$$

The general equation of radiative transfer in the tetrad formalism with the customary definition of the photon momentum then reads

$$\begin{aligned} & e^{\alpha}{}_{(a)}p^{(a)}\frac{\partial}{\partial x^{\alpha}}\lambda^5 I_\lambda - \gamma^{(a)}{}_{(d)(c)}p^{(d)}p^{(c)}\frac{\partial}{\partial p^{(a)}}\lambda^5 I_\lambda \\ = \; & e^{\alpha}{}_{(a)}p^{(a)}\frac{\partial}{\partial x^{\alpha}}\lambda^5 I_\lambda \\ & -\frac{\lambda}{h}\left\{\gamma^{(1)}{}_{(d)(c)}p^{(d)}p^{(c)}\left(-\lambda\cos\theta\frac{\partial}{\partial\lambda} - \sin\theta\frac{\partial}{\partial\theta}\right)\right. \\ & +\gamma^{(2)}{}_{(d)(c)}p^{(d)}p^{(c)}\left(-\lambda\sin\theta\cos\varphi\frac{\partial}{\partial\lambda} + \cos\theta\cos\varphi\frac{\partial}{\partial\theta} - \frac{\sin\varphi}{\sin\theta}\frac{\partial}{\partial\varphi}\right) \\ & \left.+\gamma^{(3)}{}_{(d)(c)}p^{(d)}p^{(c)}\left(-\lambda\sin\theta\sin\varphi\frac{\partial}{\partial\lambda} + \cos\theta\sin\varphi\frac{\partial}{\partial\theta} + \frac{\cos\varphi}{\sin\theta}\frac{\partial}{\partial\varphi}\right)\right\}\lambda^5 I_\lambda \\ = \; & h\lambda^4\eta_\lambda - h\chi_\lambda\lambda^4 I_\lambda \end{aligned} \tag{3.28}$$

3.3 Different Equations of Radiative Transfer

The Equation (3.28) is the general equation of radiative transfer with the customary description of the local radiation field in spherical polar coordinates. The equation does not require any special coordinates of the spacetime and any orthonormal frame of a local observer can be used as a tetrad frame.

The equation can only be specialized if the metric of the underlying spacetime is specified. The metric not only determines the coordinates of the spacetime and the differential operators but also determines the relation to the four tetrad fields.

The tetrad fields describe the construction of the locally Lorentzian frames and as the metric coefficients vary along the geodesics the basis vectors of these frames change constantly. The description of the local momentum components is therefore complicated along the geodesic and is determined by the Ricci-rotation coefficients. In the natural basis of the tangent space the connection coefficients exactly describe this change of the momentum

coordinates. Thus the Ricci-rotation coefficients are the equivalent of the connection coefficients in the tetrad frame. They do not depend on the tetrad fields alone but also on the metric of the spacetime.

Therefore, it is sufficient to provide the appropriate metric for the system at hand and apply it to Equation (3.28) to find the equation of the given system.

In the following the equations of radiative transfer for different physical systems are introduced.

3.3.1 Flat spacetime

Physically a flat spacetime for comoving observers means the neglection of general relativity and results in a Newtonian[4] description of the physics.

It is customary to use spherical polar coordinates (τ, r, Θ, Φ) to describe the atmosphere. The metric then reads

$$g_{\alpha\beta} = \begin{pmatrix} 1 & 0 & 0 & 0 \\ 0 & -1 & 0 & 0 \\ 0 & 0 & -r^2 & 0 \\ 0 & 0 & 0 & -r^2 \sin^2\Theta \end{pmatrix} \tag{3.29}$$

With only two components of the metric tensor not being constant, only few connection coefficients do not vanish. Just ${\Gamma^1}_{22}$, ${\Gamma^1}_{33}$, ${\Gamma^2}_{12} = {\Gamma^2}_{21}$, ${\Gamma^2}_{33}$, ${\Gamma^3}_{13} = {\Gamma^3}_{31}$, and ${\Gamma^3}_{23} = {\Gamma^3}_{32}$ are non-zero:

$$\begin{aligned} &{\Gamma^1}_{22} = -r && {\Gamma^1}_{33} = -r\sin^2\Theta && {\Gamma^2}_{12} = {\Gamma^2}_{21} = \frac{1}{r} \\ &{\Gamma^2}_{33} = -\sin\Theta\cos\Theta && {\Gamma^3}_{13} = {\Gamma^3}_{31} = \frac{1}{r} && {\Gamma^3}_{23} = {\Gamma^3}_{32} = \cot\Theta \end{aligned} \tag{3.30}$$

The tetrad frame is chosen as the normalized natural basis in the tangent space. To satisfy the relations (3.11) to (3.13) the tetrad basis (3.9) and the dual basis (3.10) are given as

$${e_{(a)}}^{\alpha} = \left(\frac{\vec{\partial}}{\partial\tau}, \frac{\vec{\partial}}{\partial r}, \frac{1}{r}\frac{\vec{\partial}}{\partial\Theta}, \frac{1}{r\sin\Theta}\frac{\vec{\partial}}{\partial\Phi} \right) \tag{3.31}$$

$$= \begin{pmatrix} 1 & 0 & 0 & 0 \\ 0 & 1 & 0 & 0 \\ 0 & 0 & \frac{1}{r} & 0 \\ 0 & 0 & 0 & \frac{1}{r\sin\Theta} \end{pmatrix} \tag{3.32}$$

$${e^{(a)}}_{\alpha} = \left({e_{(a)}}^{\alpha} \right)^{-1} \tag{3.33}$$

[4] A special relativistic description of the physics would only apply if observers are introduced which are moving within the spacetime.

$$= \begin{pmatrix} 1 & 0 & 0 & 0 \\ 0 & 1 & 0 & 0 \\ 0 & 0 & r & 0 \\ 0 & 0 & 0 & r\sin\Theta \end{pmatrix} \tag{3.34}$$

With relation (A.10) the non-vanishing Ricci-rotation coefficients are then

$$\begin{aligned} \gamma^{(1)}{}_{(2)(2)} &= -\frac{1}{r} & \gamma^{(1)}{}_{(3)(3)} &= -\frac{1}{r} & \gamma^{(2)}{}_{(2)(1)} &= \frac{1}{r} \\ \gamma^{(2)}{}_{(3)(3)} &= -\frac{\cot\Theta}{r} & \gamma^{(3)}{}_{(3)(1)} &= \frac{1}{r} & \gamma^{(3)}{}_{(3)(2)} &= \frac{\cot\Theta}{r} \end{aligned} \tag{3.35}$$

Using the relations (3.22), (3.32), and (3.35), every quantity in Equation (3.28) is known and with the relation

$$e_{(a)}{}^{\alpha}\partial_{\alpha} = \partial_{(a)} = \frac{h}{\lambda}\left(\frac{\partial}{\partial\tau}, \frac{\partial}{\partial r}, \frac{1}{r}\frac{\partial}{\partial\Theta}, \frac{1}{\sin\Theta}\frac{\partial}{\partial\Phi}\right)$$

it follows for the equation of transfer in flat space after some straight forward algebra

$$\begin{aligned} &\left[\frac{\partial}{\partial\tau} + \mu\frac{\partial}{\partial r} + \frac{\sin\theta\cos\varphi}{r}\frac{\partial}{\partial\Theta} + \frac{\sin\theta\sin\varphi}{r\sin\Theta}\frac{\partial}{\partial\Phi}\right. \\ &\quad \left. + \frac{1-\mu^2}{r}\frac{\partial}{\partial\mu} - \frac{\sin\theta\sin\varphi\cos\Theta}{r\sin\Theta}\frac{\partial}{\partial\varphi}\right] I_{\lambda} \\ = \;& \eta_{\lambda} - \chi_{\lambda} I_{\lambda} \end{aligned} \tag{3.36}$$

This equation is indeed identical to the equation heuristically derived in [Mihalas, 1978].

3.3.2 Spherically Symmetric Spacetime

The equation of radiative transfer for spherically symmetric spacetimes was first described by Lindquist [Lindquist, 1966] and is a simple application of the general Equation (3.28). The spherically symmetric spacetime is described by the spherical polar coordinates (τ, r, Θ, Φ) and the comoving metric reads

$$g_{\alpha\beta} = \begin{pmatrix} \exp(2\Psi) & 0 & 0 & 0 \\ 0 & -\exp(2\Lambda) & 0 & 0 \\ 0 & 0 & -R^2 & 0 \\ 0 & 0 & 0 & -R^2\sin^2\Theta \end{pmatrix} \tag{3.37}$$

with Ψ, Λ, and R being functions depending only on the two coordinates (τ, r). The connection coefficients of the metric (3.37) which do not vanish are given in Appendix B.1. The tetrad frame is again chosen as the normalized natural basis in the tangent space. The

relations (3.11) to (3.13) demand that the tetrad basis (3.9) and the dual basis (3.10) is given by

$$\begin{aligned} e_{(a)}{}^{\alpha} &= \left(\exp(-\Psi)\frac{\vec{\partial}}{\partial\tau}, \exp(-\Lambda)\frac{\vec{\partial}}{\partial r}, \frac{1}{R}\frac{\vec{\partial}}{\partial\Theta}, \frac{1}{R\sin\Theta}\frac{\vec{\partial}}{\partial\Phi}\right) \\ &= \begin{pmatrix} \exp(-\Psi) & 0 & 0 & 0 \\ 0 & \exp(-\Lambda) & 0 & 0 \\ 0 & 0 & \frac{1}{R} & 0 \\ 0 & 0 & 0 & \frac{1}{R\sin\Theta} \end{pmatrix} \end{aligned} \tag{3.38}$$

$$\begin{aligned} e^{(a)}{}_{\alpha} &= \left(e_{(a)}{}^{\alpha}\right)^{-1} \\ &= \begin{pmatrix} \exp(\Psi) & 0 & 0 & 0 \\ 0 & \exp(\Lambda) & 0 & 0 \\ 0 & 0 & R & 0 \\ 0 & 0 & 0 & R\sin\Theta \end{pmatrix} \end{aligned} \tag{3.39}$$

With the tetrads being completely specified the Ricci-rotation coefficients can be calculated. It must be noted that since in Equation (3.28) only differential operators of three momentum components are used, the calculation of $\gamma^{(0)}{}_{(d)(c)}$ can be omitted. Further, the Ricci-rotation coefficients are not symmetric in the lower indices. The only nonvanishing coefficients are

$$\begin{aligned} \gamma^{(1)}{}_{(0)(0)} &= \exp(-\Psi)\frac{\partial\Psi}{\partial r} & \gamma^{(1)}{}_{(1)(0)} &= \exp(-\Psi)\frac{\partial\Lambda}{\partial\tau} \\ \gamma^{(1)}{}_{(2)(2)} &= -\frac{\exp(-\Lambda)}{R}\frac{\partial R}{\partial r} & \gamma^{(1)}{}_{(3)(3)} &= -\frac{\exp(-\Lambda)}{R}\frac{\partial R}{\partial r} \\ \gamma^{(2)}{}_{(2)(0)} &= \frac{\exp(-\Psi)}{R}\frac{\partial R}{\partial\tau} & \gamma^{(2)}{}_{(2)(1)} &= \frac{\exp(-\Lambda)}{R}\frac{\partial R}{\partial r} \\ \gamma^{(2)}{}_{(3)(3)} &= -\frac{\cot\Theta}{R} & \gamma^{(3)}{}_{(3)(0)} &= \frac{\exp(-\Psi)}{R}\frac{\partial R}{\partial\tau} \\ \gamma^{(3)}{}_{(3)(1)} &= \frac{\exp(-\Lambda)}{R}\frac{\partial R}{\partial r} & \gamma^{(3)}{}_{(3)(2)} &= \frac{\cot\Theta}{R} \end{aligned} \tag{3.40}$$

With the relations (3.22), (3.38), and (3.40), every quantity in Equation (3.28) is known. After some straightforward algebra that mostly reorders the summands, simplifies, and uses the relation

$$e_{(a)}{}^{\alpha}\partial_{\alpha} = \partial_{(a)} = \frac{h}{\lambda}\left(\exp(-\Psi)\frac{\partial}{\partial\tau}, \exp(-\Lambda)\frac{\partial}{\partial r}, 0, 0\right)$$

it follows for the equation of transfer in spherically symmetric spacetime

$$\begin{aligned}
&\Bigg[\exp(-\Psi)\frac{\partial}{\partial\tau}+\mu\exp(-\Lambda)\frac{\partial}{\partial r}\\
&\quad+(1-\mu^2)\left\{\mu\left(\frac{\exp(-\Psi)}{R}\frac{\partial R}{\partial\tau}-\exp(-\Psi)\frac{\partial\Lambda}{\partial\tau}\right)\right.\\
&\qquad\qquad\left.-\exp(-\Lambda)\frac{\partial\Psi}{\partial r}+\frac{\exp(-\Lambda)}{R}\frac{\partial R}{\partial r}\right\}\frac{\partial}{\partial\mu}\Bigg]I_\lambda\\
&\quad+\left\{\exp(-\Psi)\frac{\partial\Psi}{\partial r}\mu+\mu^2\exp(-\Psi)\frac{\partial\Lambda}{\partial\tau}+(1-\mu^2)\frac{\exp(-\Psi)}{R}\frac{\partial R}{\partial\tau}\right\}\left(\frac{\partial\lambda I_\lambda}{\partial\lambda}+4I_\lambda\right)\\
=\;&\eta_\lambda-\chi_\lambda I_\lambda
\end{aligned}\tag{3.41}$$

Equation (3.41) is identical with the equation found by Lindquist. The only difference is the use of the specific intensity in contrast to the distribution function used by Lindquist.

3.3.3 The Schwarzschild Spacetime

The Schwarzschild solution is a special case of the general spherically symmetric metric (3.37). As it is a vacuum solution of Einstein's field equations it ignores the contribution of the matter present to the metric of the system. Because the mass of the atmosphere is negligible in comparison with the mass of the Schwarzschild solution this approximation is justified.
The metric tensor for the coordinate system (τ, r, Θ, Φ) can be written as

$$g_{\alpha\beta}=\begin{pmatrix}1-\frac{2GM}{c^2r} & 0 & 0 & 0\\ 0 & -\frac{1}{1-\frac{2GM}{c^2r}} & 0 & 0\\ 0 & 0 & -r^2 & 0\\ 0 & 0 & 0 & -r^2\sin^2\Theta\end{pmatrix}\tag{3.42}$$

with G being the gravitational constant, c the speed of light, and M being the total mass of the gravitational field generating object. With Ψ, Λ, and R now only being functions of the radial coordinate r the equation of transfer (3.41) is greatly simplified.

$$\begin{aligned}
&\Bigg[\frac{1}{\sqrt{1-\frac{2GM}{c^2r}}}\frac{\partial}{\partial\tau}+\mu\sqrt{1-\frac{2GM}{c^2r}}\frac{\partial}{\partial r}\\
&\quad+\frac{1-\mu^2}{r}\left\{1-\frac{MG}{c^2r-2GM}\right\}\sqrt{1-\frac{2GM}{c^2r}}\frac{\partial}{\partial\mu}\Bigg]I_\lambda\\
&\quad+\frac{1}{\sqrt{1-\frac{2GM}{c^2r}}}\frac{GM}{c^2r}\mu\left(\frac{\partial\lambda I_\lambda}{\partial\lambda}+4I_\lambda\right)\\
=\;&\eta_\lambda-\chi_\lambda I_\lambda
\end{aligned}\tag{3.43}$$

If time independence of the intensity is assumed the time derivative can be dropped and the equation can be written in a characteristic form:

$$\frac{\partial I_\lambda}{\partial s} + a_\lambda \frac{\partial \lambda I_\lambda}{\partial \lambda} + 4 a_\lambda I_\lambda = \eta_\lambda - \chi_\lambda I_\lambda \tag{3.44}$$

with

$$\frac{\partial}{\partial s} = \frac{\partial r}{\partial s}\frac{\partial}{\partial r} + \frac{\partial \mu}{\partial s}\frac{\partial}{\partial \mu} \tag{3.45}$$

$$\frac{\partial r}{\partial s} = \sqrt{1 - \frac{2GM}{c^2 r}}\,\mu \tag{3.46}$$

$$\frac{\partial \mu}{\partial s} = \frac{1-\mu^2}{r}\left(1 - \frac{GM}{c^2 r - 2GM}\right)\sqrt{1 - \frac{2GM}{c^2 r}} \tag{3.47}$$

$$a_\lambda = \frac{1}{\sqrt{1 - \frac{2GM}{c^2 r}}}\frac{GM}{c^2 r^2}\mu \tag{3.48}$$

In Equation (3.44) the gravitational shift of wavelength is described by the two terms that contain the coefficient a_λ. They originate from an expansion of the term $\frac{a_\lambda}{\lambda^4}\frac{\partial \lambda^5 I_\lambda}{\partial \lambda}$. The expanded from is used, because it can be easily implemented numerically. The wavelength derivative term is discretized and the other is treated as an additional opacity. The sign of the coefficient a_λ determines the direction of the wavelength derivative and directly influences the numerical discretization. The details of the numerical solution are given in Chapter 5.
Equation (3.43) is of central importance to this work. Its numerical solution is the starting point for the testing of the general relativistic radiative transfer solver. The results of this application are given in Chapter 6.

3.3.4 The Kerr Spacetime

The Kerr solution is an axis symmetric solution to Einstein's field equations. It has the line element

$$\mathrm{d}s = \rho^2 \frac{\Delta}{\Sigma^2}\mathrm{d}\tau^2 - \frac{\Sigma^2}{\rho^2}\left(\mathrm{d}\Phi - \frac{2GMar}{c^2\Sigma^2}\mathrm{d}\tau\right)\sin^2\Theta - \frac{\rho^2}{\Delta}\mathrm{d}r^2 - \rho^2 \mathrm{d}\Theta^2 \tag{3.49}$$

that is formulated in Boyer-Lindquist coordinates (τ, r, Θ, Φ) and is expressed via the following definitions [Chandrasekhar, 1992]

$$\begin{aligned} \alpha &= \frac{\rho}{\Sigma}\sqrt{\Delta} & \omega &= \frac{2GMar}{c^2\Sigma^2} \\ \rho^2 &= r^2 + a^2\cos^2\Theta & \Delta &= r^2 + a^2 - \frac{2GMr}{c^2} \\ \Sigma^2 &= (r^2+a^2)^2 - a^2\Delta\sin^2\Theta & \tilde{\omega} &= \frac{\Sigma}{\rho}\sin\Theta \end{aligned} \tag{3.50}$$

The according metric tensors read

$$g_{\mu\nu} = \begin{pmatrix} \alpha^2 - \tilde{\omega}^2\omega^2 & 0 & 0 & \tilde{\omega}^2\omega \\ 0 & -\frac{\rho^2}{\Delta} & 0 & 0 \\ 0 & 0 & -\rho^2 & 0 \\ \tilde{\omega}^2\omega & 0 & 0 & -\tilde{\omega}^2 \end{pmatrix} \tag{3.51}$$

$$g^{\mu\nu} = \begin{pmatrix} \frac{1}{\alpha^2} & 0 & 0 & \frac{\omega}{\alpha^2} \\ 0 & -\frac{\Delta}{\rho^2} & 0 & 0 \\ 0 & 0 & -\frac{1}{\rho^2} & 0 \\ \frac{\omega}{\alpha^2} & 0 & 0 & -\frac{\alpha^2-\tilde{\omega}^2\omega^2}{\alpha^2\tilde{\omega}^2} \end{pmatrix} \tag{3.52}$$

As stated in [Landau and Lifschitz, 1997] any computation with this metric is quite tedious. However, there is no conceptual difference in the ansatz to formulate the equation of radiative transfer. As the metric is given analytically, the tetrad frames can be determined from it. It is obvious from the off diagonal elements in (3.51) that the tetrad vector fields will be linear combinations of the natural basis vector fields[5].
The tetrad fields can nonetheless be determined by requiring the relations (3.11) to (3.13) to be fulfilled. Using the definitions (3.50) the tetrad fields then read

$$\begin{aligned} e_{(a)}{}^{\alpha} &= \left(\frac{1}{\alpha}\frac{\vec{\partial}}{\partial\tau} + \frac{\omega}{\alpha}\frac{\vec{\partial}}{\partial\Phi}, \sqrt{\frac{\Delta}{\rho^2}}\frac{\vec{\partial}}{\partial r}, \frac{1}{\rho}\frac{\vec{\partial}}{\partial\Theta}, \frac{1}{\tilde{\omega}}\frac{\vec{\partial}}{\partial\Phi} \right) \\ &= \begin{pmatrix} \frac{1}{\alpha} & 0 & 0 & \frac{\omega}{\alpha} \\ 0 & \sqrt{\frac{\Delta}{\rho^2}} & 0 & 0 \\ 0 & 0 & \frac{1}{\rho} & 0 \\ 0 & 0 & 0 & \frac{1}{\tilde{\omega}} \end{pmatrix} \end{aligned} \tag{3.53}$$

$$\begin{aligned} e^{(a)}{}_{\alpha} &= \left(e_{(a)}{}^{\alpha} \right)^{-1} \\ &= \begin{pmatrix} \alpha & 0 & 0 & -\tilde{\omega}\omega \\ 0 & \sqrt{\frac{\rho^2}{\Delta}} & 0 & 0 \\ 0 & 0 & \rho & 0 \\ 0 & 0 & 0 & \tilde{\omega} \end{pmatrix} \end{aligned} \tag{3.54}$$

In order to construct the Ricci-rotation coefficients (see their definition (3.19)), the connection coefficients of the Kerr metric must be known. The number of non-vanishing Christoffel symbols is larger than in the Schwarzschild solution, because all the coefficients in the line element (3.49) depend not only on the radial coordinate but also on the Θ coordinate. The complete list of the Christoffel symbols and the Ricci-rotation coefficients is given in the Appendix B.2.
With the Ricci-rotation coefficients and the tetrad fields known the equation of trans-

[5]The situation is similar to the construction of the comoving tetrad fields in the flow in a spherically symmetric spacetime (see Section 3.4).

fer (3.28) can be calculated. Recalling the relation (3.22) for $p^{(a)}$, the equation of transfer is given as:

$$
\begin{aligned}
& h\lambda^4\eta_\lambda - h\chi_\lambda\lambda^4 I_\lambda \\
= & \left[\frac{h}{\lambda}\frac{\Sigma}{\sqrt{\Delta}\rho}\frac{\partial}{\partial\tau} + \frac{h}{\lambda}\frac{\sqrt{\Delta}\cos\theta}{\rho}\frac{\partial}{\partial r} + \frac{h}{\lambda}\frac{\sin\theta\cos\varphi}{\rho}\frac{\partial}{\partial\Theta} \right. \\
& + \frac{h}{\lambda}\left(\frac{2aMGr}{c^2\sqrt{\Delta}\rho\Sigma} + \frac{\sin\theta\sin\varphi\rho}{\Sigma\sin\Theta}\right)\frac{\partial}{\partial\Phi} \\
& - \frac{\lambda}{h}\left\{ \left(\frac{h^2}{\lambda^2}\,\gamma^{(1)}{}_{(0)(0)} + 2\frac{h^2}{\lambda^2}\sin\theta\sin\varphi\,\gamma^{(1)}{}_{(0)(3)} + \frac{h^2}{\lambda^2}\sin^2\theta\sin\varphi\cos\varphi\,\gamma^{(1)}{}_{(1)(2)}\right.\right. \\
& \quad \left. + \frac{h^2}{\lambda^2}\sin^2\theta\cos^2\varphi\,\gamma^{(1)}{}_{(2)(2)} + \frac{h^2}{\lambda^2}\sin^2\theta\sin^2\varphi\,\gamma^{(1)}{}_{(3)(3)}\right) \times \left(-\lambda\cos\theta\frac{\partial}{\partial\lambda} - \sin\theta\frac{\partial}{\partial\theta}\right) \\
& \quad + \left(\frac{h^2}{\lambda^2}\,\gamma^{(2)}{}_{(0)(0)} + 2\frac{h^2}{\lambda^2}\sin\theta\sin\varphi\,\gamma^{(2)}{}_{(0)(3)} + \frac{h^2}{\lambda^2}\cos^2\theta\,\gamma^{(2)}{}_{(1)(1)}\right. \\
& \quad \left. + \frac{h^2}{\lambda^2}\cos\theta\sin\theta\cos\varphi\,\gamma^{(2)}{}_{(2)(1)} + \frac{h^2}{\lambda^2}\sin^2\theta\sin^2\varphi\,\gamma^{(2)}{}_{(3)(3)}\right) \times \\
& \quad \left(-\lambda\sin\theta\cos\varphi\frac{\partial}{\partial\lambda} + \cos\theta\cos\varphi\frac{\partial}{\partial\theta} - \frac{\sin\varphi}{\sin\theta}\frac{\partial}{\partial\varphi}\right) \\
& \quad + \left(\frac{h^2}{\lambda^2}\cos\theta\sin\theta\sin\varphi\,\gamma^{(3)}{}_{(3)(1)} + \frac{h^2}{\lambda^2}\sin^2\theta\sin\varphi\cos\varphi\,\gamma^{(3)}{}_{(3)(2)}\right) \times \\
& \quad \left.\left.\left(-\lambda\sin\theta\sin\varphi\frac{\partial}{\partial\lambda} + \cos\theta\sin\varphi\frac{\partial}{\partial\theta} + \frac{\cos\varphi}{\sin\theta}\frac{\partial}{\partial\varphi}\right)\right\}\right] [\lambda^5 I_\lambda]
\end{aligned}
\tag{3.55}
$$

In Equation (3.55) the explicit multiplication of the terms has been avoided, because the resulting expressions for the momentum derivatives are lengthy and complicated without offering new physical insight. This is a result of the description of the photon momentum in local tetrads, because these frames change constantly along the null geodesic and the corresponding basis vectors of the momentum are thus complicated functions of the Boyer-Lindquist coordinates. In case of the Kerr metric the coefficients of the momentum derivatives are especially complicated, because there is only axial symmetry. Due to the very tedious and complex computation of the coefficients it is advisable to use a numerical representation of the coefficients that does not rely on the analytical computation. This has not been done in this work as the actual implementation was limited to one-dimensional applications.

3.4 Radiative Transfer in Relativistic Flows

The general relativistic radiative transfer described in Section 3.3 is restricted to a comoving metric. In order to be able to describe the radiative transfer for all possible scenarios, it is desirable to include velocity fields in the treatment. In general relativity the description of flows of matter is included in the comoving metric itself and the framework in Section 3.3 suffices to describe the radiation transport. However, the determination of the comoving metric in the non vacuum case is equivalent to the solution of the field equations of general relativity. In order to avoid this arduous task it is advisable to use an approximation in the description of the radiative transfer. Therefore, the analytic vacuum solutions are retained as static background spacetimes and the relativistic flows must be incorporated into the description of the transport.
The description of the radiative transfer in flows using non-comoving observers has a severe disadvantage for the numerical solution used in this work. The radiation field is beamed towards the direction of the flow and this requires an increase in the angular resolution for the numerical solution of the radiative transfer problem. Furthermore, the Doppler shift of spectral lines requires an increase of the resolution in wavelength to resolve the lines throughout the atmosphere. Consequently, a comoving description of the photon momentum is desirable and the radiative transfer must be described by a comoving observer. In static background spacetimes the flow or equivalently the comoving observers are described by four velocity vectors. These four velocities are defined in the frames of observers that are stationary in the spacetime. If one chooses stationary tetrads as the frames of the stationary observers, the relation to comoving tetrads of the comoving observers is governed by a Lorentz transformation, because the tetrads are locally Lorentzian frames. Therefore, the comoving tetrads can be specified in terms of the natural basis of the background spacetime. The construction of the tetrad fields is then a combination of a Lorentz transformation and the construction of the tetrad fields for stationary observers, that measure the spatial velocity of the flow in their respective tetrad.
The four velocity of the flow must be known at every event in spacetime. It either has to be calculated in relativistic hydrodynamical calculations which explicitly give the four velocity of the flow for a complete set of stationary observers or its value must be somewhat arbitrarily prescribed in the constructed stationary tetrads. For instance one can think of a linear dependence on the radial coordinate as it is customarily assumed for supernova atmospheres. This is justified as the use of an analytic description in this case only attempts to give an estimate of the physical situation. But it should be kept in mind, that the static observer is free in his choice of coordinates and as long as the four velocity and hence the coordinates are not given, these coordinates are not known. Furthermore, the relations between the different coordinate systems cannot be known and an analytic formula for the Lorentz transformation to the comoving observer cannot be given.
The purely analytic case is tractable as long the metric possesses spherical symmetry. In this case all static observers can agree on a method to choose their coordinates as they just use the local natural basis. The functional relation for the Lorentz transformation is then the same for every observer and the transformation itself is free of arbitrary rotations that depend on the observer at hand. This ansatz also works for axially symmetric spacetimes

as long as the velocity field has no component parallel to the axis of symmetry.

When these tetrad fields are known the derivation of the equation of transfer can proceed exactly as in the case of a comoving metric (see Section 3.3.2).
For a spherical symmetric metric of the form (3.37) the tetrad fields can be written as

$$e_{(a)}{}^{\alpha} = \begin{pmatrix} \gamma e^{-\Psi} & \beta_1\gamma e^{-\Lambda} & \beta_2\gamma\frac{1}{R} & \beta_3\gamma\frac{1}{R\sin\Theta} \\ \beta_1\gamma e^{-\Psi} & 1+(\gamma-1)\frac{\beta_1^2}{\beta^2}e^{-\Lambda} & (\gamma-1)\frac{\beta_1\beta_2}{\beta^2}\frac{1}{R} & (\gamma-1)\frac{\beta_1\beta_3}{\beta^2}\frac{1}{R\sin\Theta} \\ \beta_2\gamma e^{-\Psi} & (\gamma-1)\frac{\beta_2\beta_1}{\beta^2}e^{-\Lambda} & 1+(\gamma-1)\frac{\beta_2^2}{\beta^2}\frac{1}{R} & (\gamma-1)\frac{\beta_2\beta_3}{\beta^2}\frac{1}{R\sin\Theta} \\ \beta_3\gamma e^{-\Psi} & (\gamma-1)\frac{\beta_3\beta_1}{\beta^2}e^{-\Lambda} & (\gamma-1)\frac{\beta_3\beta_2}{\beta^2}\frac{1}{R} & 1+(\gamma-1)\frac{\beta_3^2}{\beta^2}\frac{1}{R\sin\Theta} \end{pmatrix} \tag{3.56}$$

$$\begin{aligned} e^{(a)}{}_{\alpha} &= \left(e_{(a)}{}^{\alpha}\right)^{-1} \\ &= \begin{pmatrix} \gamma e^{\Psi} & -\beta_1\gamma e^{\Lambda} & -\beta_2\gamma R & -\beta_3\gamma R\sin\Theta \\ -\beta_1\gamma e^{\Psi} & 1+(\gamma-1)\frac{\beta_1^2}{\beta^2}e^{\Lambda} & (\gamma-1)\frac{\beta_1\beta_2}{\beta^2}R & (\gamma-1)\frac{\beta_1\beta_3}{\beta^2}R\sin\Theta \\ -\beta_2\gamma e^{\Psi} & (\gamma-1)\frac{\beta_2\beta_1}{\beta^2}e^{\Lambda} & 1+(\gamma-1)\frac{\beta_2^2}{\beta^2}R & (\gamma-1)\frac{\beta_2\beta_3}{\beta^2}R\sin\Theta \\ -\beta_3\gamma e^{\Psi} & (\gamma-1)\frac{\beta_3\beta_1}{\beta^2}e^{\Lambda} & (\gamma-1)\frac{\beta_3\beta_2}{\beta^2}R & 1+(\gamma-1)\frac{\beta_3^2}{\beta^2}R\sin\Theta \end{pmatrix} \end{aligned} \tag{3.57}$$

As the tetrad components which are constructed with the aid of the fields (3.56) and (3.57) are linear combinations of all the natural basis vectors, the calculation of the Ricci-rotation coefficients becomes more complicated. This is mostly due to the fact that the components of the tetrad field are functions of the base coordinates. Thus the derivatives in the calculation of the Ricci-rotation coefficients include product- and chain-rules.
For the case of a purely radial velocity field $\beta(\tau, r)$ the calculation is vastly simplified and only this form will be explicitly given here. The tetrad fields for a radial velocity field read

$$\begin{aligned} e_{(a)}{}^{\alpha} &= \left(\gamma e^{(-\Psi)}\frac{\vec{\partial}}{\partial\tau}+\beta\gamma e^{(-\Lambda)}\frac{\vec{\partial}}{\partial r}, \beta\gamma e^{(-\Psi)}\frac{\vec{\partial}}{\partial\tau}+\gamma e^{(-\Lambda)}\frac{\vec{\partial}}{\partial r}, \frac{1}{R}\frac{\vec{\partial}}{\partial\Theta}, \frac{1}{R\sin\Theta}\frac{\vec{\partial}}{\partial\Phi}\right) \\ &= \begin{pmatrix} \gamma\exp(-\Psi) & \beta\gamma\exp(-\Lambda) & 0 & 0 \\ \beta\gamma\exp(-\Psi) & \gamma\exp(-\Lambda) & 0 & 0 \\ 0 & 0 & \frac{1}{R} & 0 \\ 0 & 0 & 0 & \frac{1}{R\sin\Theta} \end{pmatrix} \end{aligned} \tag{3.58}$$

$$\begin{aligned} e^{(a)}{}_{\alpha} &= \left(e_{(a)}{}^{\alpha}\right)^{-1} \\ &= \begin{pmatrix} \gamma\exp(\Psi) & -\beta\gamma\exp(\Lambda) & 0 & 0 \\ -\beta\gamma\exp(\Psi) & \gamma\exp(\Lambda) & 0 & 0 \\ 0 & 0 & R & 0 \\ 0 & 0 & 0 & R\sin\Theta \end{pmatrix} \end{aligned} \tag{3.59}$$

With the connection coefficients (B.2) to (B.17) of the metric (3.37) the Ricci-rotation

coefficients (3.19) for the frames which are comoving with $\beta(\tau, r)$ read

$$
\begin{aligned}
\gamma^{(1)}{}_{(0)(0)} &= \gamma^3 \frac{\partial \beta}{\partial \tau} \exp(-\Psi) + \gamma^3 \beta \frac{\partial \beta}{\partial r} \exp(-\Lambda) + \gamma\beta \frac{\partial \Lambda}{\partial \tau} \exp(-\Psi) + \gamma \frac{\partial \Psi}{\partial r} \exp(-\Lambda) \\
\gamma^{(1)}{}_{(1)(0)} &= \gamma^3 \beta \frac{\partial \beta}{\partial \tau} \exp(-\Psi) + \gamma^3 \frac{\partial \beta}{\partial r} \exp(-\Lambda) + \gamma \frac{\partial \Lambda}{\partial \tau} \exp(-\Psi) + \gamma\beta \frac{\partial \Psi}{\partial r} \exp(-\Lambda) \\
\gamma^{(1)}{}_{(2)(2)} &= -\frac{\gamma}{R} \left\{ \beta \exp(-\Psi) \frac{\partial R}{\partial \tau} + \exp(-\Lambda) \frac{\partial R}{\partial r} \right\} \\
\gamma^{(1)}{}_{(3)(3)} &= \gamma^{(1)}{}_{(2)(2)} \\
\gamma^{(2)}{}_{(2)(0)} &= \frac{\gamma}{R} \left\{ \exp(-\Psi) \frac{\partial R}{\partial \tau} + \beta \exp(-\Lambda) \frac{\partial R}{\partial r} \right\} \\
\gamma^{(2)}{}_{(2)(1)} &= \frac{\gamma}{R} \left\{ \beta \exp(-\Psi) \frac{\partial R}{\partial \tau} + \exp(-\Lambda) \frac{\partial R}{\partial r} \right\} \\
\gamma^{(2)}{}_{(3)(3)} &= -\frac{\cot \Theta}{R} \\
\gamma^{(3)}{}_{(3)(0)} &= \gamma^{(2)}{}_{(2)(0)} \\
\gamma^{(3)}{}_{(3)(1)} &= \gamma^{(2)}{}_{(2)(1)} \\
\gamma^{(3)}{}_{(3)(2)} &= -\gamma^{(2)}{}_{(3)(3)}
\end{aligned}
\tag{3.60}
$$

The resulting equation of transfer reads

$$
\begin{aligned}
&\left[\frac{1}{\lambda} \gamma \exp(-\Psi)(1+\beta\mu) \frac{\partial}{\partial \tau} + \frac{1}{\lambda} \gamma \exp(-\Lambda)(\beta+\mu) \frac{\partial}{\partial r} \right. \\
&+ \left\{ \mu\gamma \left(\gamma^2 \exp(-\Psi)(1+\beta\mu) \frac{\partial \beta}{\partial \tau} + \gamma^2 \exp(-\Lambda)(\beta+\mu) \frac{\partial \beta}{\partial r} \right) \right. \\
&+ \mu\gamma \left(\exp(-\Psi)(\beta+\mu) \frac{\partial \Lambda}{\partial \tau} + \exp(-\Lambda)(1+\beta\mu) \frac{\partial \Psi}{\partial r} \right) \\
&+ \left. \gamma \frac{1-\mu^2}{R} \left(\exp(-\Psi) \frac{\partial R}{\partial \tau} + \exp(-\Lambda)\beta \frac{\partial R}{\partial r} \right) \right\} \frac{\partial}{\partial \lambda} \\
&+ \frac{1}{\lambda} \left\{ \gamma \frac{1-\mu^2}{R} \left(\frac{\partial R}{\partial \tau} \exp(-\Psi)(\beta+\mu) + \frac{\partial R}{\partial r} \exp(-\Lambda)(1+\beta\mu) \right) \right. \\
&- (1-\mu^2) \left(\gamma^3 \exp(-\Psi)(1+\beta\mu) \frac{\partial \beta}{\partial \tau} + \gamma^3 \exp(-\Lambda)(\beta+\mu) \frac{\partial \beta}{\partial r} \right) \\
&\left. \left. - (1-\mu^2)\gamma \left(\exp(-\Psi)(\beta+\mu) \frac{\partial \Lambda}{\partial \tau} + \exp(-\Lambda)(1+\beta\mu) \frac{\partial \Psi}{\partial r} \right) \right\} \frac{\partial}{\partial \mu} \right] \left[\lambda^5 I_\lambda \right] \\
= \quad & \lambda^4 \eta_\lambda - \lambda^4 \chi_\lambda I_\lambda
\end{aligned}
\tag{3.61}
$$

If the specific case of a spherical symmetric solution the Schwarzschild metric (3.42) the equation simplifies further. This is due to the fact that the metric only depends on the radial coordinate. The equation of transfer for a purely radial velocity field in a Schwarzschild

background metric then reads

$$
\begin{aligned}
&\left[\frac{1}{\lambda}\gamma\frac{1+\beta\mu}{\sqrt{1-\frac{2GM}{c^2r}}}\frac{\partial}{\partial\tau}+\frac{1}{\lambda}\gamma\sqrt{1-\frac{2GM}{c^2r}}(\beta+\mu)\frac{\partial}{\partial r}\right.\\
&+\left\{\mu\gamma\left(\gamma^2\frac{1+\beta\mu}{\sqrt{1-\frac{2GM}{c^2r}}}\frac{\partial\beta}{\partial\tau}+\gamma^2\sqrt{1-\frac{2GM}{c^2r}}(\beta+\mu)\frac{\partial\beta}{\partial r}\right)\right.\\
&\qquad\left.+\mu\gamma(1+\beta\mu)\frac{GM}{c^2r^2\sqrt{1-\frac{2GM}{c^2r}}}+\ \gamma\frac{1-\mu^2}{R}\beta\sqrt{1-\frac{2GM}{c^2r}}\right\}\frac{\partial}{\partial\lambda}\\
&+\frac{1}{\lambda}\left\{\gamma\frac{1-\mu^2}{R}(1+\beta\mu)\sqrt{1-\frac{2GM}{c^2r}}\right.\\
&-(1-\mu^2)\left(\gamma^3\frac{1+\beta\mu}{\sqrt{1-\frac{2GM}{c^2r}}}\frac{\partial\beta}{\partial\tau}+\gamma^3(\beta+\mu)\sqrt{1-\frac{2GM}{c^2r}}\frac{\partial\beta}{\partial r}\right)\\
&\left.\left.-(1-\mu^2)\gamma(1+\beta\mu)\frac{GM}{c^2r^2\sqrt{1-\frac{2GM}{c^2r}}}\right\}\frac{\partial}{\partial\mu}\right]\left[\lambda^5 I_\lambda\right]\\
=\quad&\lambda^4\eta_\lambda-\chi_\lambda\lambda^4 I_\lambda
\end{aligned}
\tag{3.62}
$$

The validity of this equation can be tested with the limit for a vanishing velocity field or for a flat spacetime metric. If the velocity field is omitted the static result from Lindquist [Lindquist, 1966] is recovered.

This is not surprising since this result has been the starting point for the construction of the comoving observers in order to formulate the equation. For a vanishing velocity field the comoving observers coincide with the static ones and the two formulations in this limit must be equivalent.

If the spacetime is assumed to be flat and of the form (3.29) the influence of the velocity field remains and we recover the result of Mihalas [Mihalas, 1980]. His work describes special relativistic one-dimensional radiative transfer and this is exactly what Equation (3.62) should describe if the background spacetime is flat.

The recovery of Mihalas' result is a successful test for the concept of describing the radiative transfer in a tetrad frame of a comoving observer. As this is the main idea of the development of Equation (3.62) this suggests the validity of the equation.

This work has been developed independently from the ansatz of [Morita and Kaneko, 1986]. The works share the common idea to use a comoving

observer in the flow to describe the radiative transfer in a background spacetime. Their formulation centers around a fact from special relativity: two sets of orthonormal bases in the inertial and comoving frame follow a Lorentz transformation. In the context of general relativity they refer to the stationary tetrad as the inertial frame. Further they do not give instructions to construct the tetrad fields explicitly from the given metric, but assume them to be given. Besides they assume that the Lorentz transformation between the tetrads is always the same at all events in spacetime. Furthermore, they circumvent the need for a four velocity field describing the flow by prescribing a fluid flow in terms of the base coordinates of the metric. Somewhat arbitrarily they assume that these velocity components of the flow have the same value in their so called inertial frame. Finally they do not construct the equation of transfer by projecting the connection coefficients and momenta into the comoving tetrad but express the Ricci-rotation coefficients and the spatial differential operator in their inertial frame.
However, the ansatz of the work presented here is more clear physically, because the connection with the four velocity of the flow is explicitly constructed. This has the additional advantage that the comoving tetrad is explicitly constructed in terms of the natural basis of the manifold what may prove valuable if nonisotropic opacities must be taken into account.

3.5 Magneto Optical Radiative Transfer in Curved Spacetime

The opacity and emissivity coefficients (see Section 2.3) are macroscopic quantities that describe the interaction of the radiation with matter. Their values depend on the quantum mechanical description of the atoms (and molecules) present in the atmosphere.
In the presence of a magnetic field the Hamilton operator changes and the degeneracy of the according states is removed [Landau and Lifschitz, 1979, Messiah, 1962]. This splitting of the energy levels allows for additional transitions with different energies. Hence the opacity coefficients for a given wavelength or energy will be different. In addition the opacity will depend on the polarization of the photons. Thus it is necessary to include information of the state of polarization into the description of the radiation field.
Chandrasekhar introduced the concept of the Stokes parameters into the context of astrophysics [Chandrasekhar, 1950]. The Stokes parameters are a set of four quantities $\mathbf{I} = (I, Q, U, V)$ that fully describe the properties of a polarized electromagnetic wave [Jackson, 1975]. These parameters cannot be measured for a single electromagnetic wave and hence must be interpreted as average values over time and photons.
The Stokes parameters are often said to form a vector – the Stokes vector. This vector however has no dependencies on the coordinate system used to describe spatial points. The individual components are combinations of intensities of different polarizations. Hence their description is independent from the coordinate system used and is not influenced by the affine connection. In contrast to the wave vector of a photon which is a null vector and its polarization state is directly influenced by the affine connection [Misner *et al.*, 1973]. Thus one must not be confused from the fact that a gravitational field influences the po-

larization of a single photon but does not change the Stokes parameters. The situation is different if there is a source of photons that all are emitted with the same layer of polarization [Connors *et al.*, 1980]. This may occur for instance for photons that are scattered off a accretion disc and obtain the same direction of linear polarization. In this case the wave vector of the photons must be parallel transported along the geodesic in order to obtain the correct emerging polarization. Therefore, in the following it is assumed that there is no preferred direction of polarization.
In this context it should be noted that Stokes parameters for electromagnetic waves in a consistent theory of general relativistic electrodynamics can be formulated [Anile and Breuer, 1974]. However, in this work the electromagnetic wave formulation of classic electrodynamics is used to describe the polarization. This is justified as the influence of the gravitational field on the generation of radiation is negligible.
The independence of the Stokes vector from the affine connection is of importance for the treatment of radiative transfer in curved spacetime. Because this means that the magneto optical radiative transfer equation has the same form as (3.28). However, the specific intensity is replaced by the Stokes vector. Further the source function becomes a vector $\mathbf{S}$ and the absorption becomes a 4×4 matrix $\mathbf{K}$ describing the absorption as well as the change of the Stokes parameter along the affine parameterization.

$$\frac{\mathrm{d}\mathbf{I}}{\mathrm{d}\xi} = -\mathbf{K}\left(\mathbf{I} - \mathbf{S}\right) \tag{3.63}$$

The theory of $\mathbf{K}$ was developed by [Landi Degl'Innocenti, 1983]. The entries of $\mathbf{K}$ are functions of the absorption coefficients and profile functions of the different Zeeman components as well as the geometry of the local magnetic field. Hence the two angles that describe the relative position between the photon momentum and the magnetic field must be known.
As the tetrad fields can be explicitly determined for a given atmosphere, the local coordinate system of the photon momentum is explicitly constructed. Hence the components of the magnetic field can be evaluated in the local coordinate system of the photon and $\mathbf{K}$ can be calculated.
In an exact theory the magnetic field is given as components of the electromagnetic field strength tensor. The tensor must be calculated in a tetrad that must be used to construct the momentum variables for the radiative transfer.
In a first application the field strength tensor will not be self consistently calculated but the magnetic field will be prescribed. Then the magnetic field can be directly given in the natural basis of the metric. Therefore, the magnetic field can be related to the photon momentum in the same way as for instance the affine connection. Consequently, radiative transfer with magnetic fields present in curved spacetimes is possible with the same numerical methods as in classical magneto optical radiative transfer. However, the numerical methods to solve the radiative transfer itself must be adopted to accommodate the coupling of wavelengths due to the gravitational field.

Chapter 4

Photon Paths in Curved Spacetime

It is a well known result that photon paths in a non flat spacetime are curved. This directly influences the radiative transfer as well as the generation of images and spectra. Consequently, this issue is of central importance when modeling general relativistic atmospheres. The solution of the radiative transfer problem used in this work is a characteristic method which solves the transfer along the physical paths of the photons.
Therefore, the photon orbits must be known in order to solve the equation of radiative transfer. In Section 4.1 the different possibilities of describing and calculating the photon paths in curved spacetime are outlined. Furthermore, the method used in this work is compared to the direct integration of the geodesic equation and the results are presented.
The radiative transfer solution only covers the propagation of radiation within the atmosphere and not the generation of the observed spectrum in the curved spacetime. Hence the corrections to the spectrum due to the imaging must be applied after the radiative transfer is done. These corrections are presented in Section 4.2.

4.1 Calculation of the Photon Paths

The solution of the radiative transfer proceeds along the physical paths of the photons (see Chapter 5). For this reason the paths of the photons must be known.
Photon paths are the null geodesics of spacetime. This is a consequence of the wave vector being a null vector [Misner *et al.*, 1973]. The photon orbits are described with the geodesic equation:

$$\frac{\mathrm{d}^2 x^\alpha}{\mathrm{d}\xi^2} + \Gamma^\alpha{}_{\beta\gamma} \frac{\mathrm{d}x^\beta}{\mathrm{d}\xi} \frac{\mathrm{d}x^\gamma}{\mathrm{d}\xi} = 0 \tag{4.1}$$

If the underlying spacetime has symmetries more elegant ways of describing the orbits are possible. In analogy to classical mechanics there are conserved quantities. These quantities are equivalent to constant canonical momenta and can be used to simplify the equations of motion for the system.
This ansatz can either be formulated within the framework of Killing vectors or by the use of the Lagrangian formalism. Here only the latter will be briefly outlined.

For a given metric the Lagrangian is given from the condition $\mathrm{d}s^2 = g_{\mu\nu}\mathrm{d}x^\mu\ \mathrm{d}x^\nu$ and the variational principle

$$\delta \int \mathrm{d}s = 0 \tag{4.2}$$

and can be written as

$$2\mathfrak{L} = g_{\mu\nu}\frac{\mathrm{d}x^\mu}{\mathrm{d}\xi}\frac{\mathrm{d}x^\nu}{\mathrm{d}\xi}\begin{cases} +1 & \text{for particles with mass } m \\ 0 & \text{for massless particles} \end{cases} \tag{4.3}$$

Since the radiative transfer in this work only deals with photons, $\mathfrak{L} = 0$.
For the Schwarzschild metric (3.42) the Lagrangian has two cyclic coordinates t and Φ. The resulting constants of motion can be identified as energy E and angular momentum L [Chandrasekhar, 1992]. In addition, the canonical momentum p_Θ will be constant in the plane with $\Theta = \frac{\pi}{2}$. Due to the rotational symmetry of (3.42) the resulting description with $\Theta = \frac{\pi}{2}$ and $\frac{\partial\Theta}{\partial\xi} = 0$ holds for all orbits.
After the substitution $r = \frac{1}{u}$ [Chandrasekhar, 1992] and a differentiation for u [Misner *et al.*, 1973] the equation of motion reads simply

$$\frac{\mathrm{d}^2u}{\mathrm{d}\Phi^2} = \frac{3}{2}R_s u^2 - u \tag{4.4}$$

with R_s being the Schwarzschild radius.
With Equation (4.4) it is possible to calculate a photon orbit for given initial conditions u and $\frac{\mathrm{d}u}{\mathrm{d}\Phi}$. This description does not need the parameterization via an affine parameter.
However, the radiative transfer equation (3.28) is formulated in terms of the affine parameter ξ. Hence the physical quantities of interest are the path length of ξ and the angle of the direction of propagation seen by the local observer[1] and not the orbits per se.
In this work the ansatz of Mihalas [Mihalas, 1980] was used to obtain the path length and the angles. The photon paths are independent of the energy of the photon and time[2] and hence only the purely spatial part of the differential operator $\frac{\partial}{\partial\xi}$ in equation (3.28) is of interest. This is the full differential operator without the derivative of the time coordinate of the metric and the wavelength derivative

$$\frac{\partial}{\partial\xi}\Big|_{\text{spatial}} = \left\{\sum_{i=1}^{3}\frac{\partial x^i}{\partial\xi}\frac{\partial}{\partial x^i}\right\} + \frac{\partial\mu}{\partial\xi}\frac{\partial}{\partial\mu} + \frac{\partial\varphi}{\partial\xi}\frac{\partial}{\partial\varphi} \tag{4.5}$$

The coefficients $\frac{\partial\cdot}{\partial\xi}$ depend on the spacetime coordinates as well as on μ and φ. For the Schwarzschild metric the system (4.5) reads

$$\frac{\partial}{\partial\xi}\Big|_{\text{spatial}} = \frac{\partial r}{\partial\xi}\frac{\partial}{\partial r} + \frac{\partial\mu}{\partial\xi}\frac{\partial}{\partial\mu} \tag{4.6}$$

[1] Or by any other observer which can relate to the local observer

[2] This is true as long as the structure of the atmosphere does not change on a time scale that is comparable with the time a photon needs to pass the atmosphere in free flight.

with:

$$\begin{aligned}\frac{\partial r}{\partial \xi} &= \sqrt{1-\frac{2MG}{c^2 r}}\mu \\ \frac{\partial \mu}{\partial \xi} &= \frac{1-\mu^2}{r}\left(1-\frac{MG}{c^2 r-2MG}\right)\sqrt{1-\frac{2MG}{c^2 r}}\end{aligned}$$

The spatial operator can be seen as a system of coupled first order ordinary differential equations which can be solved numerically. The integration uses the affine parameterization ξ by design. Hence all needed quantities are available after the integration.
The correctness of this ansatz can be verified by comparing the resulting orbits with those obtained when Equation (4.4) is solved. Several tangent characteristics were calculated with both methods and the resulting orbits were compared. Tangent characteristics were used as the boundary conditions can be easily matched for the different integration variables. For a given radial coordinate r also u is known and the condition of tangency reads either $\frac{\mathrm{d}r}{\mathrm{d}\xi}=0$ or $\frac{\mathrm{d}u}{\mathrm{d}\Phi}=0$.
In Figure 4.1 the results of both methods are compared in polar plots. The mass of the central object is $M=M_{\odot}$ and the radial coordinate of the innermost orbit is $r=4.5\cdot 10^5$ cm. The lower x-axis is given in cm whereas the upper is given in Schwarzschild radii. The same is valid for the left and right y-axis respectively.
The Schwarzschild radius $R_s=\sqrt{1-\frac{2MG}{c^2 r}}$ of the system is plotted as a dashed circle in the plot. The paths are color coded and the propagation is assumed to proceed from the left to the right. The blue color indicates a blue shift whereas red means a redshift of the photon.
The upper plot shows the results of the direct integration of the spatial part of the differential operator (Mihalas ansatz) and the lower plot depicts the solution of Equation (4.4). It is evident that the results from both methods give identical results.
This can even be tested in the regime of unstable orbits. There is an unstable orbit at $r=\frac{3}{2}R_s$ which is a circular orbit. Orbits with a smaller radial coordinate at their tangent point are bound orbits. In Figure 4.2 such an orbit is compared for both methods. The annotation is the same as in Figure 4.1.
The two possible directions of propagation for the photon are shown. The coloring is also retained. However, this time the color is used to distinguish the two parts of the path as the photon would be blueshifted along both parts. The orbit starts at a radial coordinate of $(1-1\cdot 10^{-4})\frac{3}{2}R_s$ and each branch of the ray orbits three times around the center before crossing R_s. From this figure it is also evident that both methods reproduce the same results.
In the case of static atmospheres the affine parameterization can be interpreted as the traveled spatial distance. This is no longer the case for moving atmospheres. Effects like aberration and advection which result from the moving atmosphere increase the effective path length of a photon in a comoving wavelength description. The path length must be interpreted as the integral of the infinitesimal traveled distances measured in the instantaneous local frames.

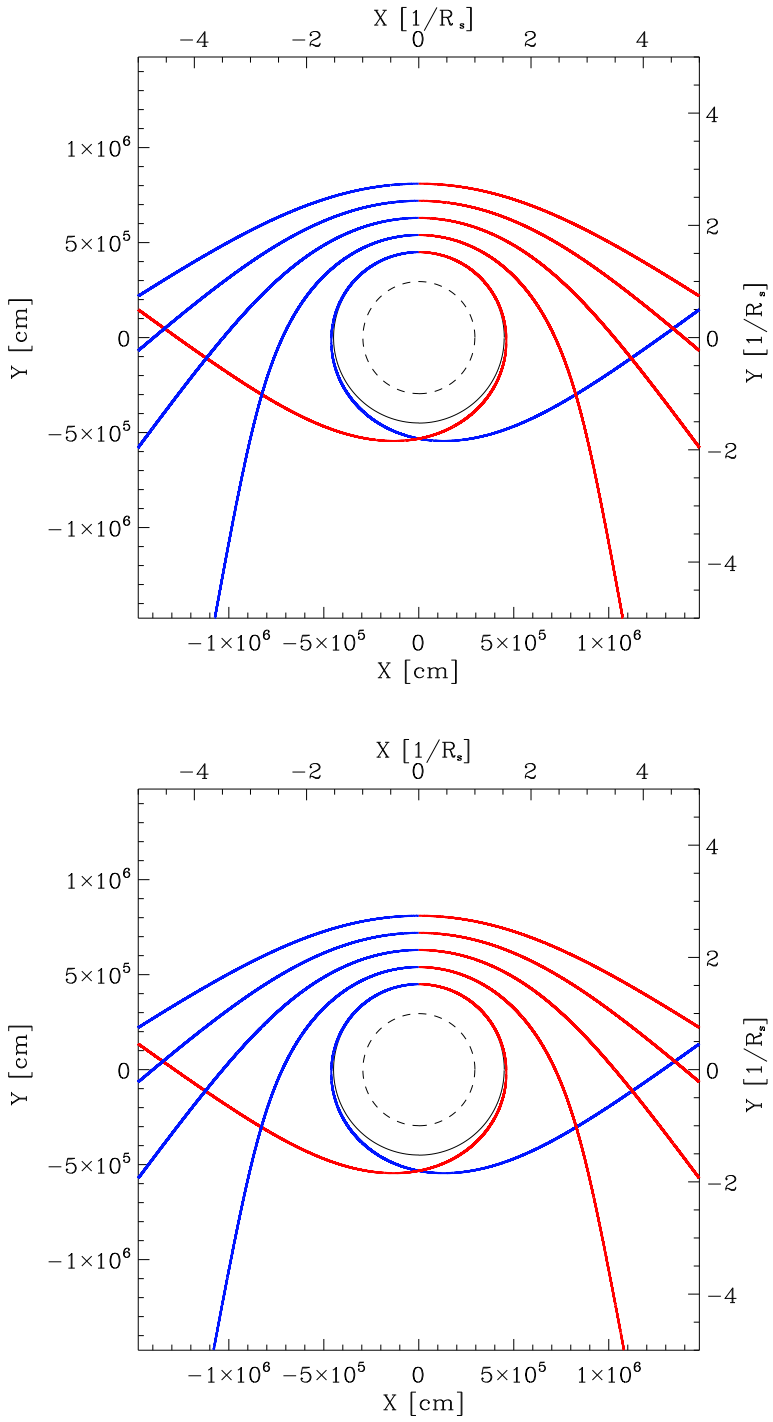

Figure 4.1: Two plots of tangent rays. The upper panel shows rays that were calculated by a direct integration of the spatial part of the differential operator of the equation of transfer.
In the lower panel rays are shown that were directly calculated from Equation (4.4). Both calculations used the same setup of radii. By comparison it is evident that both methods deliver the same results.

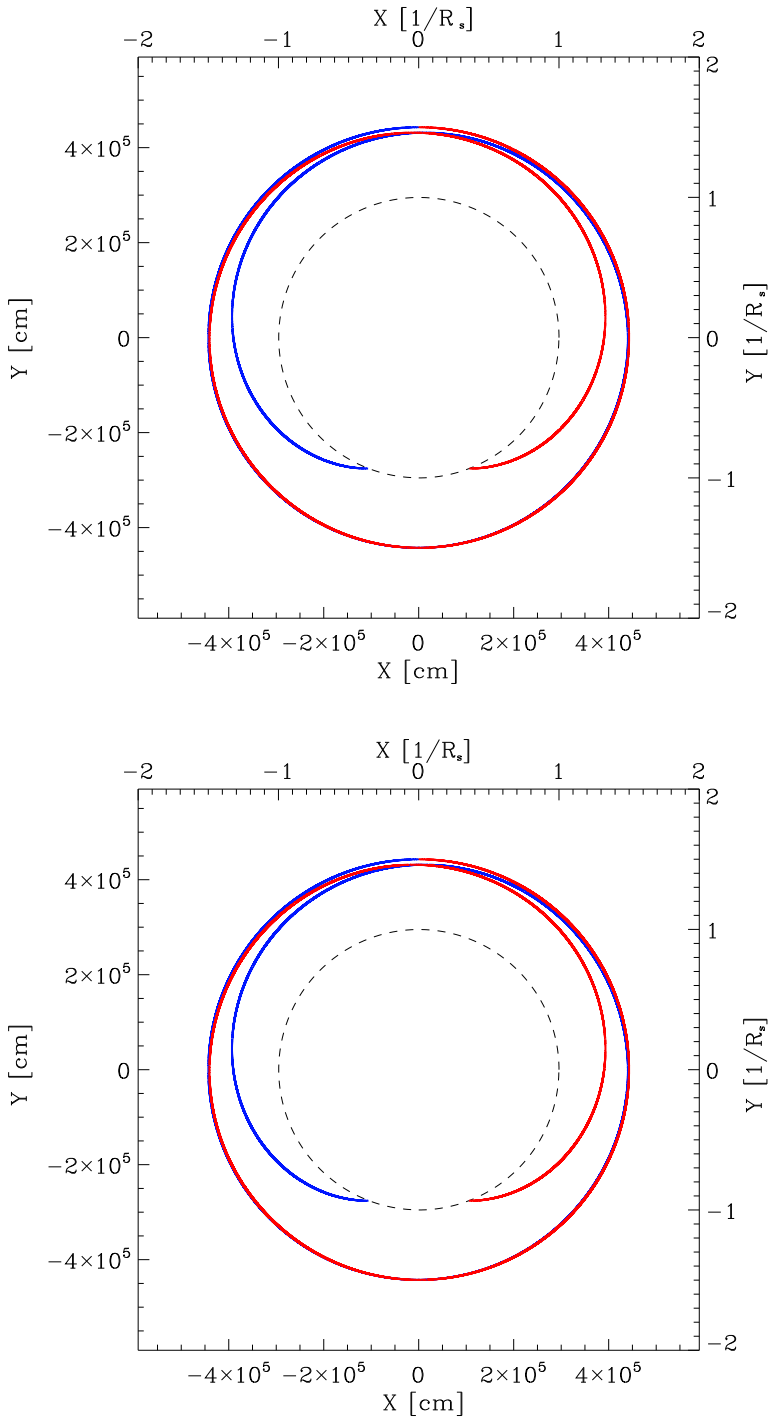

Figure 4.2: Two plots of an unstable orbit around a compact object. The point of tangency has a smaller radial coordinate than the unstable circular orbit at $r = \frac{3}{2}R_s$. As in Figure 4.1 the upper plot shows the result by an integration of the differential operator and the lower plot the result from the solution of Equation (4.4).
Both methods produce the same results.

Since the spatial orbits do not change for a moving atmosphere a relation between the spatial path length and the effective path length of a series of instantaneous rest frames of comoving observers has to be found. This is true for all methods. However, the integration in the case of Mihalas' ansatz [Mihalas, 1980] already uses this effective path length by design and there is no need to find other relations for the geodesic description of the orbits. This fact was the motivation for Mihalas to use this ansatz in the description of flows in flat spacetime.

Another advantage becomes obvious as soon as core intersecting rays are concerned. Because the initial conditions at the starting point of a ray can be chosen freely the method to construct the rays can proceed in the exact same way as for tangential rays. This is not true for the method that relies on the use of constants of motion as it is specialized on tangent rays. Hence this method has to be adapted for the use of core intersecting rays that are important to provide angular resolution in the solution of the radiative transfer problem. It has to be noted that this is only a problem in the case of curved spacetime because in flat spacetime the tangent rays can be constructed with any impact parameter. Therefore truncated tangent rays can represent core intersecting rays. It should be kept in mind that this common point of view cannot be used in curved spacetime as the tangent orbits become instable near the singularity (see Figure 4.2).

In principle the method of solution for the radiative transfer problem used in this work can deal with bound orbits[3]. However, there have to be unbound orbits in order to be able to calculate the observable spectrum. Bound orbits only increase the angular resolution within the atmosphere and otherwise only consume resources during the calculation. Therefore, tangent rays are neglected for very compact atmospheres where the lowest layer is within the unstable circular orbit.

The main advantage of the use of the analytical description of the photon orbits lies in the minimal time that is needed to construct the orbits. In a multidimensional problem, the number of rays that have to be calculated may be enormous. The integration of a large number of differential equations takes a significant amount of time. Hence the analytic method for determining the orbits may be the only feasible one in multidimensional calculations.

As long as the system at hand is one-dimensional the advantages of the direct numerical integration outweigh by far and thus this method is used in this work.

It is useful to visualize the photon paths for a system with reasonable dimensions. A typical neutron star might have a mass of $M = 1.4 M_\odot$ and a maximal radial coordinate of $r = 10^6$ cm. In Figure 4.3 ten tangent and core intersecting rays are shown for this system. The bending of photon paths is only significant near the object. A few Schwarzschild radii away from the center the photon paths are straight. Nonetheless this demonstrates that for a compact atmosphere of the central object the relativistic treatment of the paths cannot be neglected.

The routine that calculates the photon orbits was already tested to reproduce the same results as the integration of the geodesic equations. Another test is the calculation of the orbits in a flat spacetime. The result is known as the orbits are just straight lines. For the test, the same setup as in Figure 4.3 has been chosen, but this time the code used a vanishing mass. The result is shown in Figure 4.4.

[3]The circular orbit must be omitted however, because its optical depth is infinite.

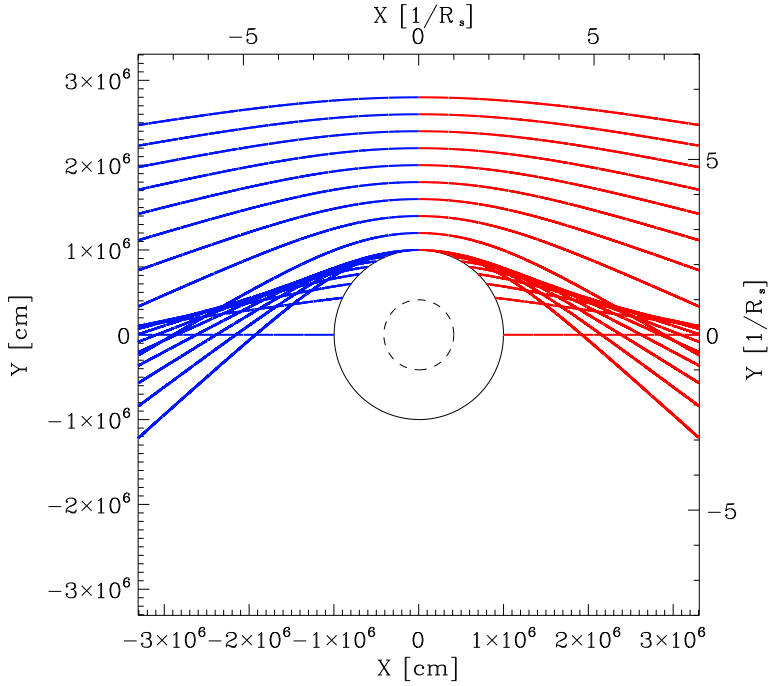

Figure 4.3: Tangent and core intersecting rays for a neutron star like environment. The radial coordinate is $r = 10^6$ cm whereas the mass of the object is $M = 1.4 M_\odot$.

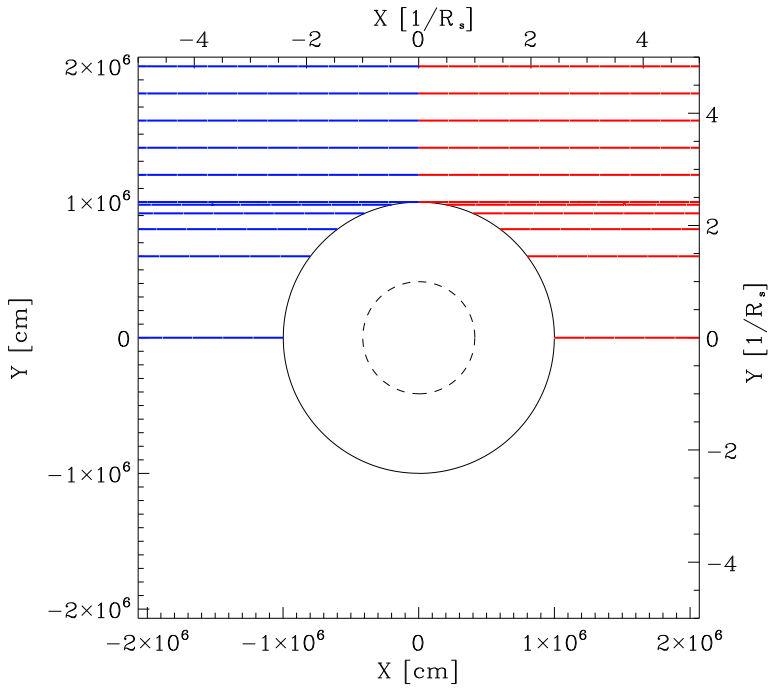

Figure 4.4: The tangent and core intersecting rays for the same spatial dimensions as in Figure 4.3 for are vanishing mass. As expected by theory the paths are straight lines.

In the flat spacetime the path length in a static atmospheres equals spatial distance. Since the length of the characteristics is known analytically in these cases this offers another check of the algorithm. Indeed the path lengths were found to be identical within error margins of the order of 10^{-2} cm.
From the calculations it became clear that a very high accuracy is needed to reproduce the analytical result. A quality controlled ordinary differential equation solver implementation following Burlisch-Stoer [Press *et al.*, 1992] failed to produce photon orbits which had a constant impact parameter. This might not be an intrinsic problem of the method but a lack of exploration of the parameter space of the starting values.
A simple Runge-Kutta implementation [Press *et al.*, 1992] was successful in reproducing the photon orbits. But the step size had to be very small and hence the calculation of all orbits is computationally wise costly. Since the photon orbits have to be calculated only once per radiative transfer calculation that time cost is not critical. Hence further implementations and testing, as well as optimizations were not needed or performed.
It should be noted, however, that the numerical scheme (4.6) has the peculiarity that the integration boundary between two discrete points is not given in terms of the stepping variable ξ. Instead the boundary is given by the radial coordinate itself. Therefore, the standard implementations of the differential equation solvers had to be changed accordingly. The final value for the path length variable at the boundary was determined by linear interpolation.

4.2 Spectra from Compact Objects

The image generation from a compact object for a nearby observer[4] is strongly influenced by the curved spacetime it is embedded in [Viergutz, 1993]. The same is true for the generation of spectra from compact objects. For the calculation of spectra the observer can be assumed to be at infinity just as for spectra in flat spacetime. Therefore, all rays received by the observer can be assumed to be parallel. In the following the atmosphere is described by generalized spherical polar coordinates (τ, r, Θ, Φ).
The observed spectrum is the emitted energy flux measured in a solid angle of the observer. Hence the emitted energy flux $E_{\text{flux}}(\lambda)$ and the spectrum f_λ are related by a factor of the inverse distance squared.

$$f_\lambda = \frac{E_{\text{flux}}(\lambda)}{d^2} \tag{4.7}$$

The emitted energy is the flux integral of the specific intensity in direction of the observer over the surface of the atmosphere.

$$E_{\text{flux}}(\lambda) = \oint_{\partial V^+} I_\lambda(t, \vec{x}, \vec{n}) \vec{n} \cdot \mathrm{d}\vec{A} \tag{4.8}$$

$$= \oint_{\partial V^+} I_\lambda(t, \vec{x}, \vec{n}) \cos\left(\measuredangle(\vec{n}, \mathrm{d}\vec{A})\right) R^2 \sin(\Theta) \mathrm{d}\Phi \, \mathrm{d}\Theta \tag{4.9}$$

[4] Nearby in this context means not at infinity.

$$= \oint_{\partial V^+} I_\lambda(t, \vec{x}, \vec{n}) \mu R^2 \sin(\Theta) \mathrm{d}\Phi \, \mathrm{d}\Theta \tag{4.10}$$

Where ∂V^+ means the surface of the atmosphere which faces the observer and R is the radial coordinate of the outermost layer.
In Figure 4.5 the contribution of a few sample intensities to the total emitted flux in direction of the observer for an arbitrary slice of the atmosphere – that means a fixed Φ coordinate – is shown. The vector $\vec{n}$ which points in the direction of the observer must be determined at all spatial points and the according intensity must be used for the integration.

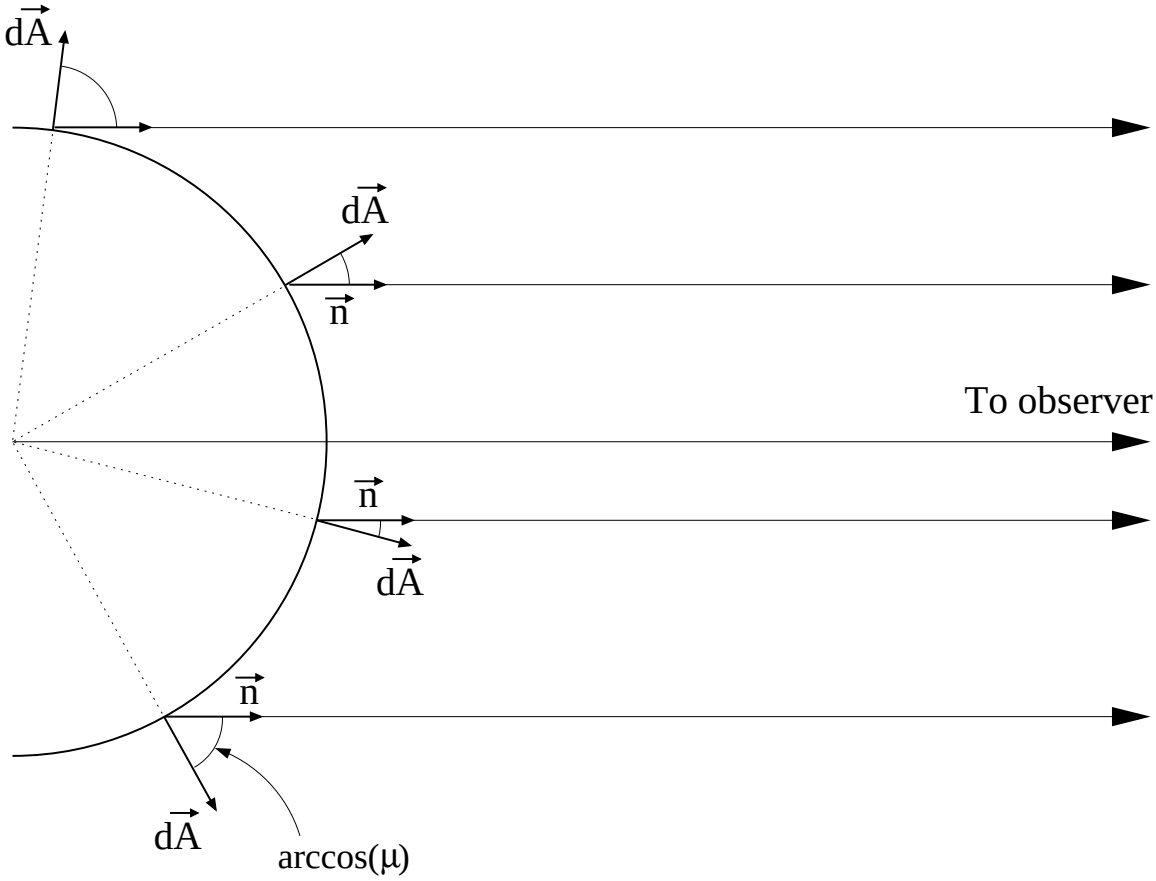

Figure 4.5: The observed spectrum is the sum of the specific intensities in direction of the observer from all surface elements of the atmosphere. Here a slice for a fixed Φ of the atmosphere is shown. The scalar product of $\vec{n}$ and $\mathrm{d}\vec{A}$ determines the visible area of the surface element. It coincides to be the μ component of the photon momentum at the given point.

In spherical symmetry the calculation is much simpler. Because the radiation field is locally the same for each point with identical radial coordinates, the base coordinate system (r, Θ, Φ) can be rotated freely. If the coordinate system is chosen in a way that the axis

which Θ is measured to is aligned with the direction of the observer the coordinates Θ and θ coincide. Further there is no dependence of the specific intensity on the Φ and ϕ coordinates due to the spherical symmetry and Equation (4.10) can be written as

$$E_{\text{flux}}(\lambda) = 2\pi R^2 \int_0^1 I_\lambda(t,\mu)\mu \mathrm{d}\mu \tag{4.11}$$

For no incident radiation the emitted energy is simply related to the Eddington flux H_λ

$$E_{\text{flux}}(\lambda) = 4\pi R^2 H_\lambda \tag{4.12}$$

In curved spacetime the set of angles at the outermost layer of the atmosphere is not suited to calculate the energy flux. This is due to the fact that the photons which are emitted under these angles deviate from straight paths and follow the null geodesics of the spacetime.
Hence we need to find a set of angles at a radial shell of spacetime where the photons do not deviate measurably from straight paths any more. That means that the energy flux integration must be postponed to a point along the null geodesic where the spacetime can be approximated to be flat.
In Figure 4.6 the contribution of a few characteristics to the emitted energy are shown schematically. Neither the photon paths nor the scale of the figure are physically correct, but the principle concept of spectrum generation is depicted correctly.
From Figure 4.6 it is obvious that also the far side of the atmosphere contributes to the spectrum. In the case of nonspherical symmetric atmospheres this may prove to be important. For instance if there is a hot spot of higher local temperature its signature might show up in the spectrum despite being on the far side of the atmosphere. Although the hot spot would have a small effective area due to the almost tangential photon momentum the increase in the specific intensity due to the higher temperature may outweigh this. However, effects like this can only be modeled in a multidimensional simulation and are out of scope for this work (see Section 6.6 for an estimate of the possible influence).
In order to determine if the spacetime at a given event is flat, a method to measure the curvature of spacetime is needed. In the vacuum solutions of Einstein's field equations the Ricci tensor vanishes by definition, $R_{\mu\nu} = 0$, and the most straight forward measure of curvature the Ricci scalar $R = R^{\mu}{}_{\mu}$ vanishes also. But as the Riemann curvature tensor does not vanish, it is possible to construct a scalar via $R_K = R^{\mu\nu\sigma\rho}R_{\mu\nu\sigma\rho}$. For the Schwarzschild metric this can be explicitly given as

$$R_K = 48\frac{G^2M^2}{c^4r^6} \tag{4.13}$$

R_K is called the Kretschmann invariant. It is a measure for the curvature at a given event in spacetime. For the Schwarzschild solution it just depends on the radial coordinate and shows that the origin is a real singularity.
For a given system we can estimate with R_K if the spacetime at the outermost part of the atmosphere is already flat. The spacetime can be somewhat arbitrarily assumed to be flat if R_K is 10^6 times smaller than at the event horizon. This value is reached at a radial coordinate of ten times the Schwarzschild radius $R_{10} = 10R_s$.

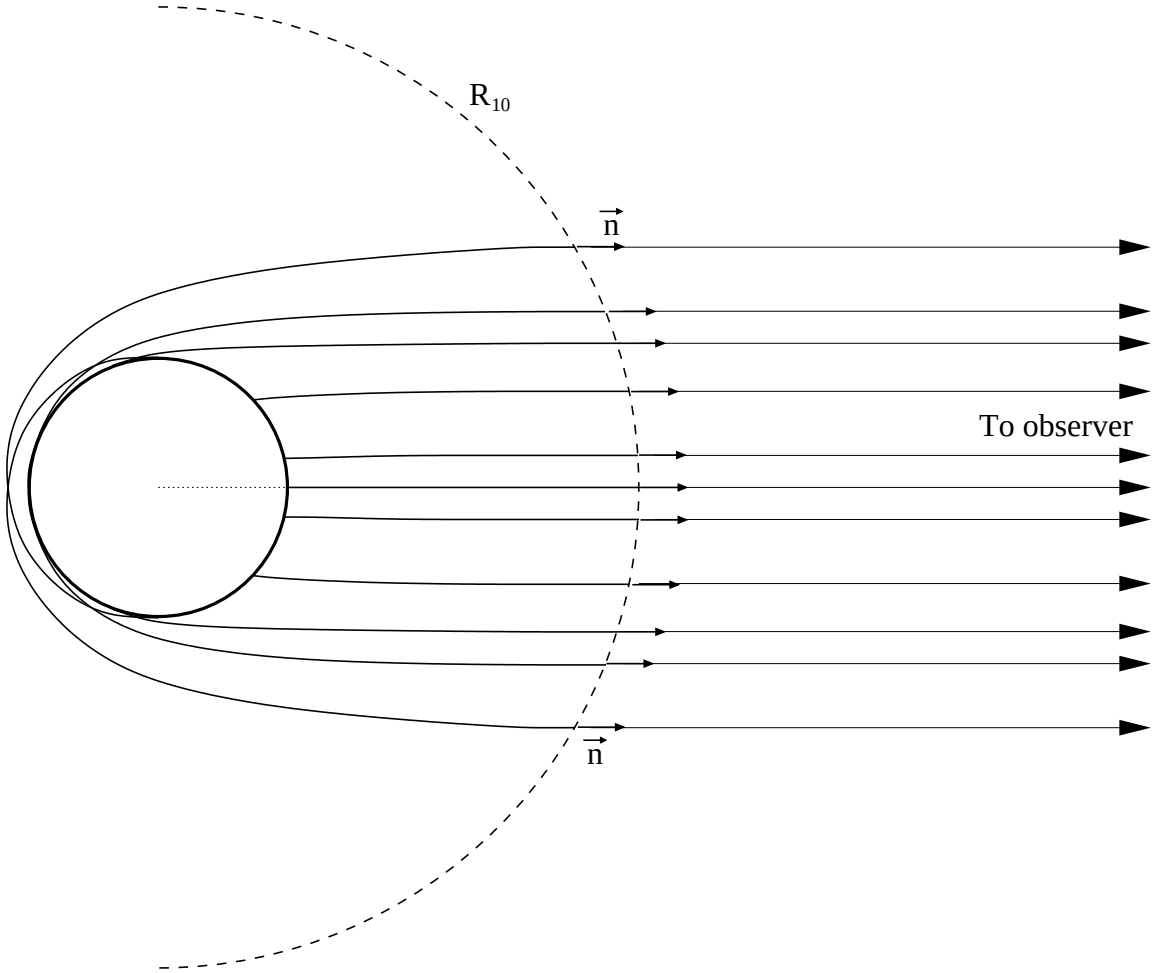

Figure 4.6: A few sample characteristics for the spectrum generation in curved spacetime are shown. At the boundary R_{10} the spacetime is approximately flat and the spectrum can be calculated in the same way as shown in Figure 4.5.

As long as the radial coordinate of the topmost layer of the atmosphere is smaller than R_{10} the spectrum formation is influenced by the curved spacetime. In this case the calculation of the photon paths must be extended up to a radial coordinate of R_{10}. The discrete set of angles obtained at this point is used to calculate the spectrum. It should be noted that the angle between the normal of the surface element and the direction of the observer will be relatively small. Area elements with smaller inclinations do not contribute to the spectrum as no photons in the direction of the observer transverse them.

The specific intensities are only known at the top of the atmosphere after the radiative transfer problem has been solved. If vacuum is assumed outside the atmosphere these intensities can be used to calculate the energy flux at R_{10}. But before the integration over angle can take place the change of the other momentum component of the photon must be taken into account. The energy of the photons changes along their paths. As there is no radiative transfer to be solved anymore the concept of a constant comoving wavelength can be abandoned.

A photon receding from a gravitational source is redshifted. In the Schwarzschild case the redshift does not depend on the taken path, but solely on the change of the radial coordinate. In contrast to the spatial components of the momentum there is no boundary where further tracking of the redshift becomes obsolete. The redshift is trivial to account for as long as the separation of the source and observer is known[5].
The different wavelengths that a photon exhibits between two radial coordinates r_{A} and r_{B} in Schwarzschild geometry are related as follows

$$\lambda\Big|_{r_{\mathrm{A}}} = \lambda\Big|_{r_{\mathrm{B}}} \frac{\sqrt{1-\frac{R_s}{r_{\mathrm{A}}}}}{\sqrt{1-\frac{R_s}{r_{\mathrm{B}}}}} \tag{4.14}$$

If the observer can be assumed to be at infinity the observed redshift just depends on the radial coordinate on top of the atmosphere.

$$\lambda_\infty = \lambda\Big|_{r} \frac{1}{\sqrt{1-\frac{R_s}{r}}} \tag{4.15}$$

In order to accommodate for the redshift of the whole spectrum just the wavelengths that are assigned to the specific intensities must be shifted as the values of the intensities do not change in vacuum. Otherwise the calculation can proceed following relation (4.10).
For a moving atmosphere the calculation of the spectrum is more complicated. This is true for curved as well as flat spacetimes. Since the radiative transfer problem is formulated for a comoving wavelength coordinate, the calculated intensities, angles as well as wavelengths at the top of the atmosphere only hold for the local comoving observer.
In order to resolve this complication the radiative transfer can be smoothly extended to radial coordinates with a vanishing flow. As an alternative the transition to the frame of the observer at infinity can be done via a Lorentz transformation at the top of the atmosphere. The wavelength and the angles are components of the momentum four vector. Hence the Lorentz transformation can directly be used to transform these quantities. However, the intensities are not defined as four vector quantities. Therefore, their relation (2.4) to the Lorentz invariant distribution function must be used.
Since the Lorentz transformation depends on the angle between the velocity field and the propagation vector the resulting wavelength scales are different for all characteristics. Therefore, the transformed intensities must be interpolated on a common wavelength grid. In practice it is not feasible to extend the radiative transfer and the Lorentz transformation is used.
After the transformation the radiation field is given for the top of the atmosphere as seen as a local not comoving observer. The situation is now identical to the spectrum formation in curved spacetime for static atmospheres and the calculation proceeds in the exact same way.

[5]This assumes that the total mass of the compact object was provided in the modeling process.

Chapter 5

Solution of the Equation of Radiative Transfer

The equation of radiative transfer (3.28) has been introduced in Chapter 3. Analytical solutions for physically relevant realistic systems are not known.
However, a lot of work has been done to find approximate solutions as for instance the diffusion approximation for optically thick regions [Rutten, 2003, Mihalas, 1970].
In order to solve the equation without major simplifications besides the assumption of time independence, a numerical approach is used in this work.
In the following the equation of transfer is discretized. This means that all physical quantities are only given at a discrete set of points and the radiation field will be determined for a discrete set of angles and wavelengths.
In its general form (3.28) the equation of transfer is an integro-differential equation. The method employed in this work solves this equation in two steps. In the first part a method is needed to calculate the radiation field for a given source function. This part is called the *formal solution*.
Furthermore a second method is needed to determine the source function self-consistently. As the source function depends on the mean intensity J_λ (see Equation (2.43)) it can be calculated from the radiation field. Hence, with the use of any method for the formal solution, the source function can be determined iteratively. This iterative scheme is called Λ-iteration, as the Λ-operator symbolically represents a formal solution and construction of a new source function.
In practice the Λ-iteration is not usable, because its convergence rate is too small for systems in which scattering is important. Therefore, the ansatz must be modified in order to achieve acceptable convergence rates. The method of choice in this work is an operator splitting technique following [Cannon, 1973, Olson *et al.*, 1986].
All formal considerations are independent from the method of the formal solution used to represent the Λ-operator. Since this work considers the equation of radiative transfer (3.28) in its most general time independent form, the formal solution must be adapted to accommodate this and a generalized formal solution is needed for this work.
In static and special relativistic atmosphere modeling, see [Hauschildt and Baron, 1999] for a summary, the radiative transfer is solved either monochromatic or in a recursive initial

value scheme. This is possible as the coefficient which describes the coupling between the wavelengths (see the coefficient a_λ in Equation (3.44)) in such systems never changes its sign and the direction of the wavelength derivative is always the same.
In case of a general relativistic system this is no longer the case. This can be seen in Equation (3.44) as it is the general form of the equation of radiative transfer with coupling between wavelengths. The wavelength coupling coefficient in this equation is a_λ. Its explicit form for the case of radiative transfer in a Schwarzschild spacetime is given in Equation (3.48). The coefficient a_λ is directly proportional to μ. As the sign of μ is different for in- and outgoing characteristics, the direction of the wavelength derivative is changing in general relativistic systems.
Physically this represents the fact that photons which descend[1] in a gravitational field are blueshifted and ascending photons are redshifted. In Figure 5.1 a sketch of a spherically symmetric scenario is shown.

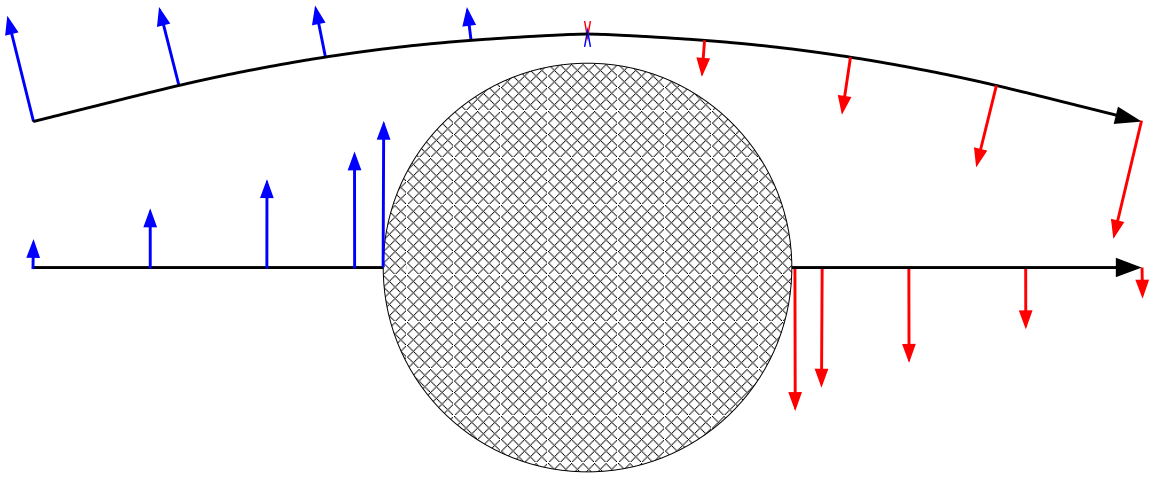

Figure 5.1: Scheme which shows the shift of wavelength along a ray. The shift is represented by arrows that are color coded. Blue means a blueshift and red means a redshift whereas the length of the arrow indicates the magnitude of the shift

The formal solution used in this work is described in Section 5.1. It is a solution along characteristics that is based on the method of Olson and Kunasz [Olson and Kunasz, 1987]. The concept of the Λ-iteration as well as the corresponding operator splitting technique – also called accelerated Λ-iteration (ALI) [Cannon, 1973, Olson *et al.*, 1986] – in the light of the used formal solution are discussed in more detail in Section 5.2. The construction of the approximate operator needed for an ALI step is discussed in Section 5.3.

[1] In spherical symmetric spacetimes this is equivalent to a decrease of the radial coordinate.

5.1 The Formal Solution

The formal solution used in this work solves the equation of radiative transfer along photon paths. Since the photon paths are also referred to as characteristics, the method is called a characteristic method. The solutions on a set of different characteristics give a description of the complete discretized radiation field.

The time independent equation of radiative transfer reads in its characteristic form

$$\frac{\mathrm{d}I_\lambda}{\mathrm{d}s} + a_\lambda \frac{\partial(\lambda I_\lambda)}{\partial\lambda} + 4a_\lambda I_\lambda = \eta_\lambda - \chi_\lambda I_\lambda \tag{5.1}$$

$$\frac{\mathrm{d}I_\lambda}{\mathrm{d}s} + a_\lambda \frac{\partial(\lambda I_\lambda)}{\partial\lambda} = \eta_\lambda - (\chi_\lambda + 4a_\lambda)\, I_\lambda \tag{5.2}$$

whereas the differential $\frac{\mathrm{d}}{\mathrm{d}s}$ and the coefficient a_λ depend on the exact form of the coefficients of the general equation of transfer (3.28).

The following developments assume the general form (5.2) for the equation of transfer and are valid for all a_λ. The description follows closely the work of [Baron and Hauschildt, 2004].

This work is limited to one-dimensional spatial calculations and systems. Hence the discretization needed for the numerical treatment is simplified. The atmosphere is divided into a number of layers and all physical quantities are represented by their values in these layers.

In the following all quantities have an implicit dependence on the spatial position and thus on the layer. Angle dependent quantities – such as the specific intensity – will also depend on the given characteristic. The general dependence on wavelength will always be shown in the equations and an ordered discrete wavelength grid is assumed.

A crucial part of the formal solution is the wavelength derivative in (5.2). Since we describe the transfer on a discrete spatial and wavelength grid the wavelength derivative has to be discretized for the numerical solution. Further, the formal solution must be defined as a mathematical relation which can be solved by a numerical technique.

There are two ways to handle the discretization. If one discretizes before the definition of the formal solution, one part of the derivative is regarded as an additional opacity, whereas the other part is treated as an additional source term. In the second method the discretization is delayed and is implicitly included in the definition of the formal solution.

This second way to discretize the wavelength derivative is used in the following. However, it is possible to mix both discretizations via a Crank-Nicholson scheme to remove possible numerical instabilities of the wavelength discretization scheme [Hauschildt and Baron, 2004].

The discretized equation (5.2) reads:

$$\frac{\mathrm{d}I_\lambda}{\mathrm{d}\tau} = I_\lambda - \hat{S}_\lambda - \tilde{S}_\lambda \tag{5.3}$$

with

$$\begin{aligned} \mathrm{d}\tau &= -\hat{\chi}_\lambda \mathrm{d}s && (5.4)\\ \hat{\chi}_\lambda &= \chi_\lambda + 4a_\lambda && (5.5)\\ \hat{S}_\lambda &= \frac{\eta_\lambda}{\hat{\chi}_\lambda} = \frac{\chi_\lambda}{\hat{\chi}_\lambda} S_\lambda && (5.6)\\ \tilde{S}_\lambda &= -\frac{a_\lambda}{\hat{\chi}_\lambda} \frac{\partial(\lambda I_\lambda)}{\partial \lambda} && (5.7) \end{aligned}$$

In order to ensure numerical stability the discretization has to be a local upwind scheme whose wavelength direction depends on the sign of the coefficient a_λ at any given spatial point. This leads to the definition

$$\begin{aligned} \frac{\partial(\lambda I_\lambda)}{\partial \lambda} &= p_{l-1} I_{l-1} + p_l I_l + p_{l+1} I_{l+1} \\ &= \begin{cases} -\frac{\lambda_{l-1}}{\lambda_l - \lambda_{l-1}} I_{l-1} + \frac{\lambda_l}{\lambda_l - \lambda_{l-1}} I_l + 0 \cdot I_{l+1} & \text{for } a_\lambda \geq 0 \\ 0 \cdot I_{l-1} + \frac{\lambda_l}{\lambda_l - \lambda_{l+1}} I_l - \frac{\lambda_{l+1}}{\lambda_l - \lambda_{l+1}} I_{l+1} & \text{for } a_\lambda < 0 \end{cases} \end{aligned}$$

where the index l is the index of the wavelength λ in the ordered wavelength grid.
Now the transfer problem is solved along a characteristic and the sum of all the solutions of all the different characteristics build up the radiation field. The formal solution along a ray is known when the specific intensity at a point on the characteristic can be expressed through the specific intensities at previous points and can be formally written as

$$I^k_{l,i} = I^k_{l,i-1} \exp\left(-\Delta\tau^k_{l,i-1}\right) + \int_{\tau^k_{l,i-1}}^{\tau^k_{l,i}} \hat{S}_l(\tau) \exp\left(\tau - \tau^k_{l,i}\right) \mathrm{d}\tau + \int_{\tau^k_{l,i-1}}^{\tau^k_{l,i}} \tilde{S}_l(\tau) \exp\left(\tau - \tau^k_{l,i}\right) \mathrm{d}\tau \tag{5.8}$$

where the index k labels the characteristic and the index i labels the point on the given ray. $\tau^k_{l,i}$ is the optical depth along the ray at the given point and $\Delta\tau^k_{l,i-1}$ is the optical depth between the given and the previous point.
Since the source functions (5.6) and (5.7) are only known on the radial grid, the integrands have to be interpolated. The integrals then become analytic and can be expressed for parabolic interpolation between the spatial points i-1, i, and i+1 in the form [Olson and Kunasz, 1987]

$$\begin{aligned} \Delta\hat{I}^k_{l,i} &= \int_{\tau^k_{l,i-1}}^{\tau^k_{l,i}} \hat{S}_l(\tau) \exp\left(\tau - \tau^k_{l,i}\right) \mathrm{d}\tau \\ &= \alpha^k_{l,i} \hat{S}^k_{l,i-1} + \beta^k_{l,i} \hat{S}^k_{l,i} + \gamma^k_{l,i} \hat{S}^k_{l,i+1} && (5.9)\\ &= \frac{\chi^k_{l,i}}{\hat{\chi}^k_{l,i}} \left(\alpha^k_{l,i} S^k_{l,i-1} + \beta^k_{l,i} S^k_{l,i} + \gamma^k_{l,i} S^k_{l,i+1}\right) = \frac{\chi^k_{l,i}}{\hat{\chi}^k_{l,i}} \Delta I^k_{l,i} && (5.10)\\ \Delta\tilde{I}^k_{l,i} &= \int_{\tau^k_{l,i-1}}^{\tau^k_{l,i}} \tilde{S}_l(\tau) \exp\left(\tau - \tau^k_{l,i}\right) \mathrm{d}\tau \end{aligned}$$

$$= \alpha^k_{l,i}\tilde{S}^k_{l,i-1} + \beta^k_{l,i}\tilde{S}^k_{l,i} + \gamma^k_{l,i}\tilde{S}^k_{l,i+1} \tag{5.11}$$

$$\begin{aligned} = \quad & \alpha^k_{l,i}\left\{-\frac{a^k_{l,i-1}}{\hat{\chi}^k_{l,i-1}}\left[p^k_{l-1,i-1}I^k_{l-1,i-1} + p^k_{l,i-1}I^k_{l,i-1} + p^k_{l+1,i-1}I^k_{l+1,i-1}\right]\right\} \\ & + \beta^k_{l,i}\left\{-\frac{a^k_{l,i}}{\hat{\chi}^k_{l,i}}\left[p^k_{l-1,i}I^k_{l-1,i} + p^k_{l,i}I^k_{l,i} + p^k_{l+1,i}I^k_{l+1,i}\right]\right\} \\ & + \gamma^k_{l,i}\left\{-\frac{a^k_{l,i+1}}{\hat{\chi}^k_{l,i+1}}\left[p^k_{l-1,i+1}I^k_{l-1,i+1} + p^k_{l,i+1}I^k_{l,i+1} + p^k_{l+1,i+1}I^k_{l+1,i+1}\right]\right\} \end{aligned} \tag{5.12}$$

The equation (5.8) can be written in matrix notation for a given characteristic

$$\mathbf{I} = \mathbf{A}\cdot\mathbf{I} + \mathbf{\Delta\hat{I}} \tag{5.13}$$

where $\mathbf{I}$ is a vector of specific intensity with $n_\lambda \times n_k$ elements, with n_λ being the number of wavelength points and n_k is the number of points along the given characteristic. $\mathbf{A}$ is a $(n_\lambda \times n_k) \times (n_\lambda \times n_k)$ matrix and contains the information about the wavelength derivative. $\mathbf{\Delta\hat{I}}$ is a vector with $n_\lambda \times n_k$ elements and contains the contribution from the source function.

The elements of $\mathbf{A}$ are the coefficients of the specific intensities in equation (5.12) in combination with the exponential factor from equation (5.8). With the following definitions

$$A^{\mathrm{sub},k}_{l,i} = A^{-}_{l,i} = -\alpha^k_{l,i}\frac{a^k_{l,i-1}}{\hat{\chi}^k_{l,i-1}}p^k_{l-1,i-1} \tag{5.14}$$

$$B^{\mathrm{sub},k}_{l,i} = B^{-}_{l,i} = -\beta^k_{l,i}\frac{a^k_{l,i}}{\hat{\chi}^k_{l,i}}p^k_{l-1,i} \tag{5.15}$$

$$C^{\mathrm{sub},k}_{l,i} = C^{-}_{l,i} = -\gamma^k_{l,i}\frac{a^k_{l,i+1}}{\hat{\chi}^k_{l,i+1}}p^k_{l-1,i+1} \tag{5.16}$$

$$A^{\mathrm{diag},k}_{l,i} = A^{\diagdown}_{l,i} = \exp\left(-\Delta\tau^k_{l,i-1}\right) - \alpha^k_{l,i}\frac{a^k_{l,i-1}}{\hat{\chi}^k_{l,i-1}}p^k_{l,i-1} \tag{5.17}$$

$$B^{\mathrm{diag},k}_{l,i} = B^{\diagdown}_{l,i} = -\beta^k_{l,i}\frac{a^k_{l,i}}{\hat{\chi}^k_{l,i}}p^k_{l,i} \tag{5.18}$$

$$C^{\mathrm{diag},k}_{l,i} = C^{\diagdown}_{l,i} = -\gamma^k_{l,i}\frac{a^k_{l,i+1}}{\hat{\chi}^k_{l,i+1}}p^k_{l,i+1} \tag{5.19}$$

$$A^{\mathrm{super},k}_{l,i} = A^{+}_{l,i} = -\alpha^k_{l,i}\frac{a^k_{l,i-1}}{\hat{\chi}^k_{l,i-1}}p^k_{l+1,i-1} \tag{5.20}$$

$$B^{\mathrm{super},k}_{l,i} = B^{+}_{l,i} = -\beta^k_{l,i}\frac{a^k_{l,i}}{\hat{\chi}^k_{l,i}}p^k_{l+1,i} \tag{5.21}$$

$$C^{\mathrm{super},k}_{l,i} = C^{+}_{l,i} = -\gamma^k_{l,i}\frac{a^k_{l,i+1}}{\hat{\chi}^k_{l,i+1}}p^k_{l+1,i+1} \tag{5.22}$$

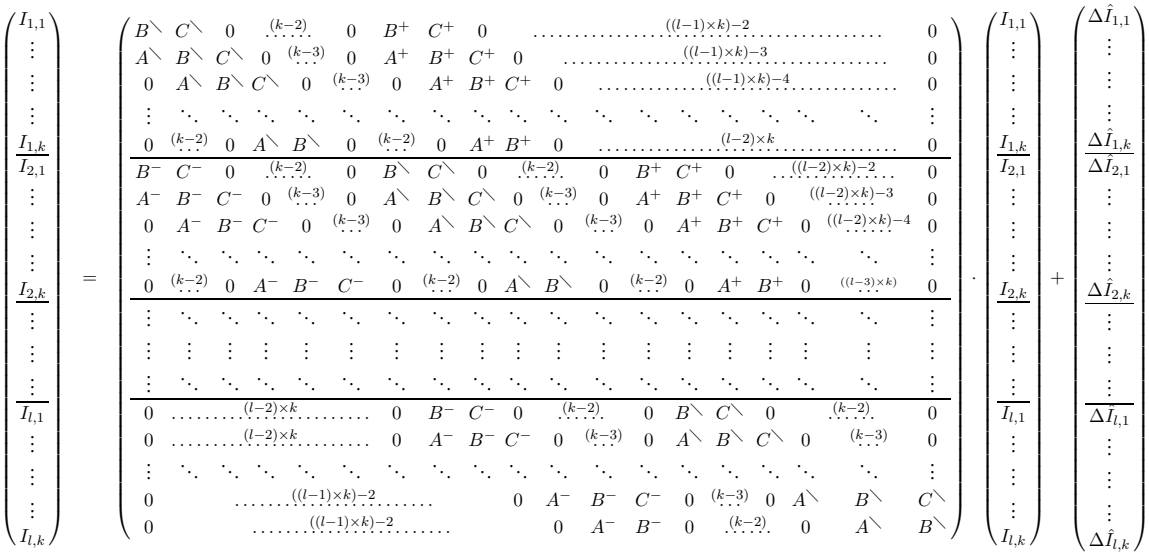

Figure 5.2: The explicit matrix form of the formal solution for a characteristic with length k and l wavelength points. The horizontal lines mark block borders of different wavelengths to clarify the structure.
The matrix has three tridiagonal bands. The one on the main diagonal is called *diag*($= \diagdown$) and the lower and upper accordingly *sub*($= -$) and *super*($= +$). The diagonals of these bands are called *A*, *B*, and *C*.

the formal solution for the specific intensity $I^k_{l,i}$ can be written as

$$\begin{aligned}\left(1 - B^{\mathrm{diag},k}_{l,i}\right) I^k_{i,l} \;=\; & \Delta\hat{I}^k_{l,i} + B^{\mathrm{sub},k}_{l,i} I^k_{i,l-1} + B^{\mathrm{super},k}_{l,i} I^k_{i,l+1} \\ & A^{\mathrm{sub},k}_{l,i} I^k_{i-1,l-1} + A^{\mathrm{diag},k}_{l,i} I^k_{i-1,l} + A^{\mathrm{super},k}_{l,i} I^k_{i-1,l+1} \\ & C^{\mathrm{sub},k}_{l,i} I^k_{i+1,l-1} + C^{\mathrm{diag},k}_{l,i} I^k_{i+1,l} + C^{\mathrm{super},k}_{l,i} I^k_{i+1,l+1} \end{aligned} \tag{5.23}$$

The formal solution along a given ray can be explicitly written in matrix form. For the first wavelength point there are no $\bullet^{\mathrm{sub}}$ matrix elements and there are no $\bullet^{\mathrm{super}}$ elements at the last wavelength point. Besides, there are no $A^{\cdot}_{\cdot,\cdot}$ matrix elements on the first point of a ray and no $C^{\cdot}_{\cdot,\cdot}$ elements on the last point.
This can be seen in the general band structure of the matrix which is shown in Figure 5.2 for a ray with k spatial points and l wavelength points. The complete formal solution is the weighted sum of the contributions of all characteristics.

5.2 The Λ- and the Accelerated Λ-Iteration

The integro-differential equation of radiative transfer can be solved by an iterative scheme called Λ-iteration. The formal solution described in Section 5.1 can be used to construct the Λ-operator needed for this method. For formal completeness the basic concept of the Λ-iteration and its enhancement for convergence improvements – the accelerated Λ iteration – are outlined in the following.

The formal solution is the calculation of the mean intensity for a given source function[2]. This can be symbolically written as

$$J_\lambda = \Lambda_\lambda \left[S_\lambda\right] = J_\lambda^{\mathrm{FS}} \tag{5.24}$$

Here Λ is an operator and has the form of a matrix[3] which acts on the source function vector to produce a mean intensity vector. The general form of S_λ reads

$$S_\lambda = (1-\epsilon)J_\lambda + \epsilon B_\lambda \tag{5.25}$$

with ϵ being the thermal coupling parameter and B_λ being Planck's function at the given wavelength.
The combination of Equation (5.24) and (5.25) gives

$$J_\lambda^{\mathrm{new}} = \Lambda_\lambda \left[S_\lambda^{\mathrm{old}}\right] \quad \text{and} \qquad S_\lambda^{\mathrm{new}} = (1-\epsilon)J_\lambda^{\mathrm{new}} + \epsilon B_\lambda \tag{5.26}$$

and as a simple iterative scheme for S_λ

$$S_\lambda^{\mathrm{new}} = (1-\epsilon)\Lambda_\lambda \left[S_\lambda^{\mathrm{old}}\right] + \epsilon B_\lambda \tag{5.27}$$

Unfortunately, this method does not converge quickly enough although it is contracting [Olson *et al.*, 1986] and cannot be used in situations in which scattering is important. The method of operator splitting [Cannon, 1973] speeds up the convergence rate dramatically, however. This method involves an approximate operator Λ^* and the Λ-operator is split in the following way

$$\Lambda_\lambda = \Lambda_\lambda^* - (\Lambda_\lambda^* - \Lambda_\lambda) \tag{5.28}$$

This splitting does not change the formal step (5.24) yet. But at this point an inaccuracy is introduced. The argument of the first Λ_λ^* is replaced by the – at this point unknown – new source function, and

$$J_\lambda^{\mathrm{new}} = \Lambda_\lambda \left[S_\lambda^{\mathrm{old}}\right] \tag{5.29}$$

$$J_\lambda^{\mathrm{new}} = \Lambda_\lambda^* \left[S_\lambda^{\mathrm{old}}\right] - (\Lambda_\lambda^* - \Lambda_\lambda) \left[S_\lambda^{\mathrm{old}}\right] \tag{5.30}$$

[2] In this context the main property of the formal solution is the connection of the mean intensity and the source function. The formal solution from (5.23) sufficiently provides the mean intensity for a given source function as it gives the complete radiation field.

[3] For a discretization in wavelength and a radial grid.

becomes

$$J_\lambda^{\mathrm{new}} = \Lambda_\lambda^* \left[S_\lambda^{\mathrm{new}}\right] - \left(\Lambda_\lambda^* - \Lambda_\lambda\right) \left[S_\lambda^{\mathrm{old}}\right] \tag{5.31}$$

If the iteration has converged then $S_\lambda^{\mathrm{new}} = S_\lambda^{\mathrm{old}}$ holds and the inaccuracy is removed. The improved convergence rate of the operator splitting method becomes obvious when the change of the mean intensity during one iteration step is considered. Using the linearity of the operators and relation (5.25) it follows

$$\begin{aligned} J_\lambda^{\mathrm{new}} &= \left[1-(1-\epsilon)\Lambda_\lambda^*\right]^{-1} \left\{J_\lambda^{\mathrm{FS}} - (1-\epsilon)\Lambda_\lambda^* \left[J_\lambda^{\mathrm{old}}\right]\right\} && (5.32)\\ J_\lambda^{\mathrm{new}} &= \left[1-(1-\epsilon)\Lambda_\lambda^*\right]^{-1} \left\{J_\lambda^{\mathrm{FS}} - J_\lambda^{\mathrm{old}} + \left[1-(1-\epsilon)\Lambda_\lambda^*\right] J_\lambda^{\mathrm{old}}\right\} && (5.33)\\ \rightarrow \quad J_\lambda^{\mathrm{new}} - J_\lambda^{\mathrm{old}} &= \left[1-(1-\epsilon)\Lambda_\lambda^*\right]^{-1} \left\{J_\lambda^{\mathrm{FS}} - J_\lambda^{\mathrm{old}}\right\} && (5.34) \end{aligned}$$

The matrix $\left[1-(1-\epsilon)\Lambda_\lambda^*\right]^{-1}$ amplifies the convergence of the normal Λ-iteration step $J_\lambda^{\mathrm{FS}} - J_\lambda^{\mathrm{old}}$. The iteration (5.32) is called accelerated Λ-iteration (ALI).

5.3 The Construction of the Λ^*-Operator

In the split of the Λ-operator (5.28) no constraints to the choice of the Λ^*-operator were specified. It was shown in the case of ALI [Olson *et al.*, 1986] that an approximate operator constructed from original entries of the Λ-operator results in superior convergence rates and guarantees convergence for the adoption of just the diagonal of the original Λ-matrix. The convergence rate is optimal if $\Lambda^* = \Lambda$ is used. However, the construction of the approximate operator and the inversion of the matrix $\left[1-(1-\epsilon)\Lambda_\lambda^*\right]$ in the ALI (5.32) are more costly in time the more elements of the original Λ-operator are used in Λ^*. The optimal configuration is different for different problems and computer architectures [Hauschildt *et al.*, 1994].

The Λ-operator can be explicitly constructed with the help of a formal solution. The jth column of the Λ-operator equals the formal solution (5.24) for a test source function that is zero everywhere but for the jth entry. This entry equals one and is called a pulse. If the full operator is not desired or needed, as in the case of the Λ^*-operator, the formal solution can be halted appropriately.

$$\begin{pmatrix} \Lambda_{1j} \\ \Lambda_{2j} \\ \vdots \\ \Lambda_{jj} \\ \vdots \\ \vdots \\ \Lambda_{lj} \end{pmatrix} = \mathbf{\Lambda} \cdot \begin{pmatrix} 0 \\ \vdots \\ 0 \\ 1 \\ 0 \\ \vdots \\ 0 \end{pmatrix} \leftarrow j \tag{5.35}$$

In the case of the formal solution from Section 5.1, the situation is more complex. A

pulse inserted at a point on a characteristic for a given wavelength will propagate to longer and/or shorter wavelengths and in both directions along the ray. This is due to the fact that within the formal solution the specific intensity at a given wavelength and point on a ray is influenced by the intensities from previous and later points both spatially and in wavelength.

Since it would require a computational wise costly formal solution for every layer in the atmosphere to construct the complete operator according to relation (5.35), it is desirable to provide explicit formulae for the construction of the operator. Then only the required elements of the operator can be calculated.

Because the wavelength direction of the coupling can change from a spatial point to the next, all wavelengths are coupled. In case of parabolic interpolation of the wavelength derivative (5.7) the specific intensity I_λ at a spatial point can not be determined independently from the specific intensities at spatial points further along the ray. Since these intensities are also dependent on the intensities at earlier points, an explicit formula for a specific intensity is equivalent to the solution of the Equation (5.23). In order to keep the construction procedure tractable the explicit construction of the operator is simplified. Only the two neighboring wavelengths are considered for a given wavelength and the dependence on later spatial points is ignored.

This effectively limits the construction of the Λ^*-operator to linear interpolation in the wavelength derivative. The operator is only tridiagonal in wavelength but still can have the full bandwidth in the spatial part. If there is the need for a parabolically wavelength interpolated Λ^*-operator, it can be calculated with the help of the formal solution. It should be noted that the α, β-interpolation coefficients for the linear interpolation of the wavelength derivative are different from those of the α, β, γ coefficients from the parabolic interpolation of the source function. In case of linear interpolation of the source function the interpolation coefficients coincide again.

The construction of the Λ^*-operator proceeds similar to the construction described in [Hauschildt and Baron, 1999] with the use of tangent and core intersecting characteristics. In Figure 5.1 a tangent characteristic is shown as the upper ray, whereas two core intersecting rays, which are distinguished between ingoing and outgoing characteristics, are shown as the lower rays.

A given tangential characteristic k has $2k+1$ intersection points with the layers $1 \ldots k+1$. For every point i on the ray there is a mirror point $i_{\mathrm{mirror}} = 2k+1-i$ for which the physical conditions are identical. A given core characteristic k has as many intersection points as there are layers.

As in Equation (5.35), a source function pulse is injected into the formal solution. Due to the interpolation of the source function (5.9), the propagation of the pulse starts one spatial point "before" the actual pulse. In case of the topmost layer there is no interpolation and the propagation starts at the pulse.

If the pulse is at layer j and wavelength l then the element of the Λ-operator can be ex-

pressed as

$$\begin{aligned}\Lambda_{mj,l} &= \delta_m{}^i\Big\{\sum_{\substack{\{k\in k_{\rm tang}\}\\ \{i:i\le k+1\}}} w^k_{i,j}\lambda^k_{i,j,l} + \sum_{\{k\in k_{\rm core}\}} w^k_{i,j}\lambda^k_{i,j,l}\Big\} \\ &\quad + \delta_m{}^{(2k+1)-i+1}\sum_{\substack{\{k\in k_{\rm tang}\}\\ \{i:i>k+1\}}} w^k_{(2k+1)-i+1,j}\lambda^k_{(2k+1)-i+1,j,l} \qquad (5.36)\end{aligned}$$

where $w^k_{i,j}$ are angular quadrature weights, $k_{\rm tang}$ is the locus of the tangent, and $k_{\rm core}$ of the core intersecting rays. The $\lambda^k_{i,j}$ are auxiliary quantities which are calculated in the following. We start at the first point of the propagation $i_{\rm start}$ and define

$$X_{\rm start} = \begin{cases} \frac{\chi^k_{l,1}}{\hat\chi^k_{l,1}}\beta^k_{l,1} & \text{if } i_{\rm start}=1\wedge j=1 \\ \frac{\chi^k_{l,i_{\rm start}}}{\hat\chi^k_{l,i_{\rm start}}}\gamma^k_{l,i_{\rm start}} & \text{if } i_{\rm start}>1 \end{cases}$$

$X_{\rm start}$ replaces the contribution of the thermal source function $\Delta\hat I^k_{l,i}$ in the explicit formal solution (5.23). With the other intensities being zero at the first point we have

$$\lambda^k_{i_{\rm start},j,l} = \frac{X_{\rm start}}{1+\beta^k_{l,i_{\rm start}}\frac{a^k_{l,i_{\rm start}}}{\hat\chi^k_{l,i_{\rm start}}}p^k_{l,i_{\rm start}}} = \frac{X_{\rm start}}{1-B^{{\rm diag},k}_{l,i_{\rm start}}} \qquad (5.37)$$

$$\lambda^k_{i_{\rm start},j,l-1} = \frac{B^{{\rm super},k}_{l-1,i_{\rm start}}}{1-B^{{\rm diag},k}_{l-1,i_{\rm start}}}\lambda^k_{i_{\rm start},j,l} \qquad (5.38)$$

$$\lambda^k_{i_{\rm start},j,l} = \frac{B^{{\rm sub},k}_{l+1,i_{\rm start}}}{1-B^{{\rm diag},k}_{l+1,i_{\rm start}}}\lambda^k_{i_{\rm start},j,l} \qquad (5.39)$$

Note that depending on a_λ only $\lambda^k_{i_{\rm start},j,l-1}$ or $\lambda^k_{i_{\rm start},j,l}$ can be different from zero but not both. The next $\lambda^k_{i,j,l}$ can be defined recursively. However, the auxiliary expression X has to be redefined at every point of the propagation.

$$X_i = \begin{cases} \frac{\chi^k_{l,i}}{\hat\chi^k_{l,i}}\beta^k_{l,i} & \text{if } i=j \\ \frac{\chi^k_{l,i}}{\hat\chi^k_{l,i}}\alpha^k_{l,i} & \text{if } i=j+1 \\ \frac{\chi^k_{l,i}}{\hat\chi^k_{l,i}}\gamma^k_{l,i} & \text{if } i=i_{\rm mirror}-1 \\ \frac{\chi^k_{l,i}}{\hat\chi^k_{l,i}}\alpha^k_{l,i}+\frac{\chi^k_{l,i}}{\hat\chi^k_{l,i}}\gamma^k_{l,i} & \text{if } i=j+1\wedge i=i_{\rm mirror}-1 \\ \frac{\chi^k_{l,i}}{\hat\chi^k_{l,i}}\beta^k_{l,i} & \text{if } i=i_{\rm mirror} \\ \frac{\chi^k_{l,i}}{\hat\chi^k_{l,i}}\alpha^k_{l,i} & \text{if } i=i_{\rm mirror}+1 \\ 0 & \text{else} \end{cases}$$

Since the $\lambda^k_{i,j,l}$ depend on $\lambda^k_{i,j,l-1}$ or $\lambda^k_{i,j,l+1}$ the correct coefficient has to be calculated before the $\lambda^k_{i,j,l}$. The sign of $a^k_{l,i}$ decides whether the propagation of the wavelength information proceeds from red to blue or vice versa.

Instead of using the general form (5.12) of the wavelength dependent pulse propagation, a simplified version is used (see above).

For linear interpolation all terms with γ coefficients vanish and any dependence on $\lambda^k_{i,j,l-2}$ or $\lambda^k_{i,j,l+2}$ is ignored.

This results in a simple construction for the $\lambda^k_{i,j,l}$. Just remove all $C^{\cdot,\cdot}_{\cdot,\cdot}$ terms from Equation (5.23) and omit all coefficients which use a $l+2$ or $l-2$ subscript. Replace the contribution $\Delta\hat{I}^k_{l,i}$ with the X_i factor. Finally, remove either all $\cdot^{\mathrm{sub}}$ terms for $a_\lambda < 0$ or all $\cdot^{\mathrm{super}}$ terms for $a_\lambda \geq 0$.

It follows for $a_\lambda < 0$ (from red to blue)

$$\lambda^k_{i,j,l+1} = \left[1 - B^{\mathrm{diag},k}_{l+1,i}\right]^{-1} \left\{ A^{\mathrm{diag},k}_{l+1,i-1} \lambda^k_{i-1,j,l+1} \right\} \tag{5.40}$$

$$\lambda^k_{i,j,l} = \left[1 - B^{\mathrm{diag},k}_{l,i}\right]^{-1} \left\{ X_i + A^{\mathrm{diag},k}_{l,i} \lambda^k_{i-1,j,l} + A^{\mathrm{super},k}_{l,i} \lambda^k_{i-1,j,l+1} + B^{\mathrm{super},k}_{l,i} \lambda^k_{i,j,l+1} \right\} \tag{5.41}$$

$$\lambda^k_{i,j,l-1} = \left[1 - B^{\mathrm{diag},k}_{l-1,i}\right]^{-1} \left\{ A^{\mathrm{super},k}_{l-1,i} \lambda^k_{i-1,j,l} + A^{\mathrm{diag},k}_{l-1,i} \lambda^k_{i-1,j,l-1} + B^{\mathrm{super},k}_{l-1,i} \lambda^k_{i,j,l} \right\} \tag{5.42}$$

and for $a_\lambda \geq 0$ (from blue to red)

$$\lambda^k_{i,j,l-1} = \left[1 - B^{\mathrm{diag},k}_{l-1,i}\right]^{-1} \left\{ A^{\mathrm{diag},k}_{l-1,i} \lambda^k_{i-1,j,l-1} \right\} \tag{5.43}$$

$$\lambda^k_{i,j,l} = \left[1 - B^{\mathrm{diag},k}_{l,i}\right]^{-1} \left\{ X_i + A^{\mathrm{sub},k}_{l,i} \lambda^k_{i-1,j,l-1} + A^{\mathrm{diag},k}_{l,i} \lambda^k_{i-1,j,l} + B^{\mathrm{sub},k}_{l,i} \lambda^k_{i,j,l-1} \right\} \tag{5.44}$$

$$\lambda^k_{i,j,l+1} = \left[1 - B^{\mathrm{diag},k}_{l+1,i}\right]^{-1} \left\{ A^{\mathrm{sub},k}_{l+1,i} \lambda^k_{i-1,j,l} + A^{\mathrm{diag},k}_{l+1,i} \lambda^k_{i-1,j,l+1} + B^{\mathrm{sub},k}_{l+1,i} \lambda^k_{i,j,l} \right\} \tag{5.45}$$

In Figure 5.3 a scheme for the relations in (5.40) to (5.42) and (5.43) to (5.45) is shown for an example. In the scheme the A^{diag} terms are represented by green arrows, blue arrows represent the A^{super} and B^{super} terms, and the red arrows are the A^{sub} and B^{sub} terms.

The point of the pulse is marked by a cross. Due to the interpolation of the source function this results in a contribution at the spatial point prior to the location of the pulse. Since the coupling term a_λ is assumed to be negative in the example the same spatial point at the shorter wavelength is also influenced. At the next spatial point the sign of a_λ is reversed and now the contributions influence longer wavelengths. Since there is also an influence of later spatial points of the same wavelength, the point of insertion can already be influenced by up to three other points both spatial and in wavelength. For the following points the pulse propagates in exactly the same way and the approximate operator can be constructed.

The scheme outlined is valid for a given ray at a given wavelength. The construction of the complete Λ^*-operator is outlined in Figure 5.4 as a flowchart. The construction is repeated over all characteristics. Then for every wavelength, a pulse is inserted once

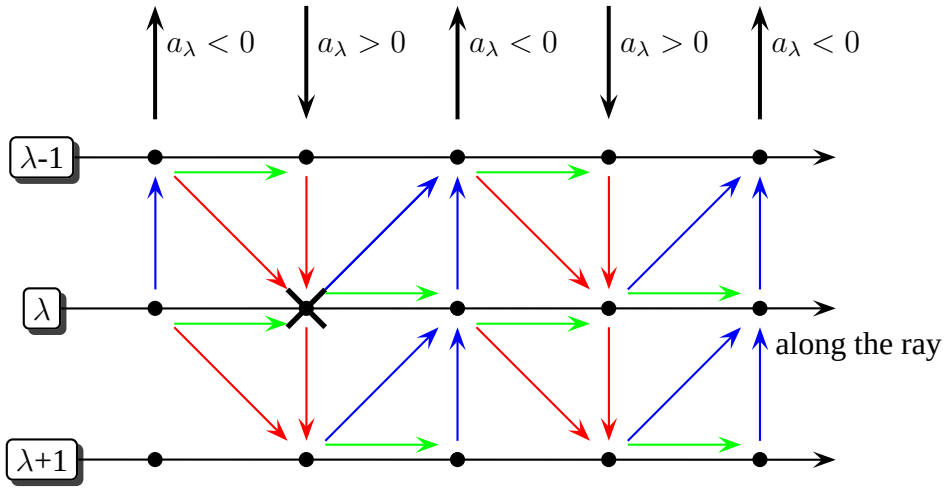

Figure 5.3: Scheme of the pulse propagation for the construction of the Λ^*-operator. The cross marks the position of the pulse. The influence of the different points on each other is color coded. Red arrows indicate an influence on longer and blue on shorter wavelengths. Green represents an influence without a change of wavelength.
In this case the wavelength derivative direction changes from point to point. Hence a point may influence the next spatial point at the same wavelength in several ways. Both directly without a change of wavelength and indirectly due to the wavelength shift.

per layer and propagated along the ray. During the propagation the $\lambda^k_{i,j,l}$ coefficients are computed, weighted, and summed up according to relation (5.36) at the end of the ray. It is noteworthy that there are differences between the tangent and core intersecting rays. The core intersecting rays pass all layers only once and the tangent rays pass all layers above the layer of tangency twice. Therefore, the pulse must only be inserted up to the layer of tangency, because the deeper layers have no means to contribute to the given ray.
The form of equation 5.36 is not yet fully correct. It indicates that it holds for a given wavelength and hence the Λ-operator Λ_l would just have S_λ as an argument. However, the two neighboring wavelengths have also to be taken into account. Hence the Λ-operator is split into three parts

$$\Lambda^*_l\left[S_l\right] = \Lambda^*_{l,l-1}\left[S_{l-1}\right] + \Lambda^*_{l,l}\left[S_l\right] + \Lambda^*_{l,l+1}\left[S_{l+1}\right] \tag{5.46}$$

where $\Lambda^*_{l,l(l-1,l+1)}$ is just the weighted sum of the $\lambda^k_{i,j,l(l-1,l+1)}$. The system (5.32) can be solved by the same means as for a standard ALI step.

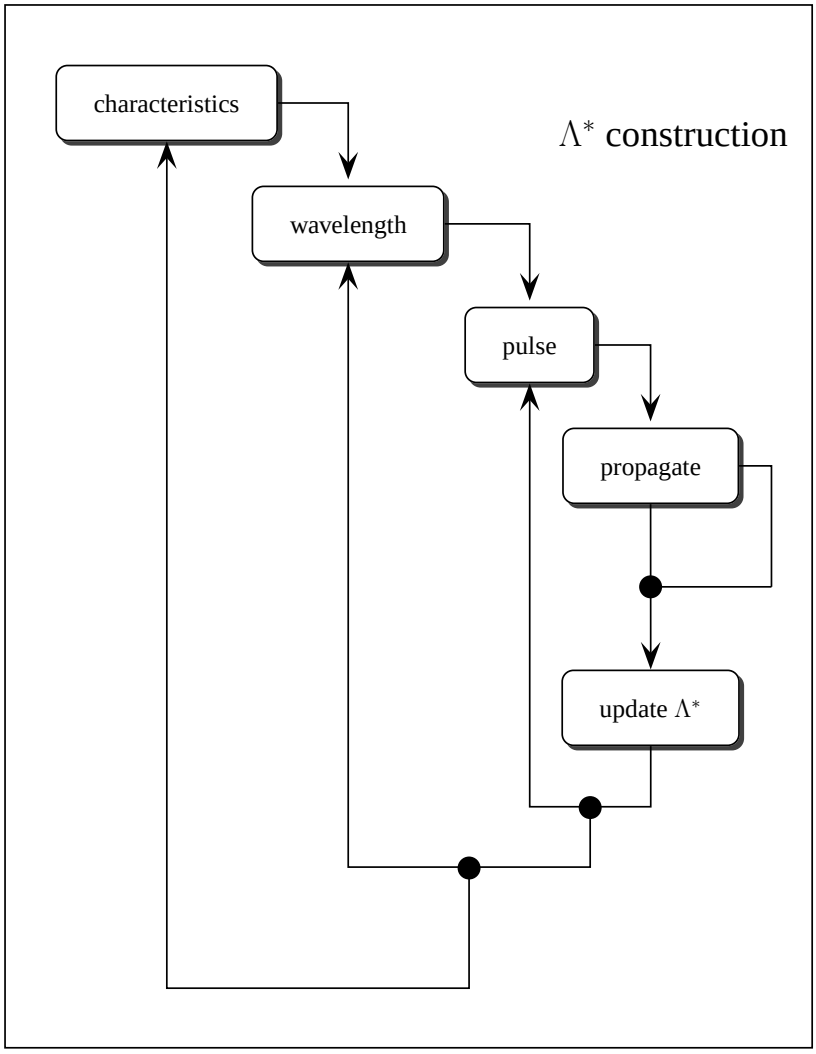

Figure 5.4: A flowchart of the Λ^* construction. The arrows indicate a loop and the dots are the continuation points after the loop has finished.
The construction proceeds through several loops. The contributions to the Λ^*-operator are calculated ray by ray for every wavelength. At every layer passed by the ray a pulse is inserted and propagated along the remaining ray. At the end of the ray the contribution at the layer of the pulse for the given wavelength is added to the operator.

Chapter 6

A Testing Environment

A new implementation of a radiative transfer solver is tested best in a well controlled testing environment. In order to do so the solution of the general relativistic radiative transfer problem has been tested in a very simple atmosphere model which has been derived from the model employed in [Baron and Hauschildt, 2004].
The atmosphere consists of a gas of two-level atoms. In addition, an over wavelength constant background opacity and Planckian are assumed. Due to this setup there is only one spectral line in an otherwise flat continuum. Hence the influence of general relativity on the radiative line transfer on one transition can be investigated without the superposition of other effects.
It cannot be claimed that this atmosphere has any physical significance and it is not intended to model a real physical system. However, the general relativistic effects on the radiative transfer found in this environment will also apply in a more sophisticated physical model. The unphysical oversimplifications in the following must be seen in this light.
Section 6.1 gives a short overview of the implementation of the new radiation transport solver and summarizes its initial tests. The details of the construction of the model atmosphere are given in Section 6.2. As a first application the general relativistic transfer in a compact atmosphere is introduced in Section 6.3 whereas Section 6.4 deals with the results of more extended atmospheres and the addition of relativistic flows.
In Section 6.5 gray continuum transfer for compact atmospheres is described as a further test of the numerical framework. The influence and the expected effects of multi-dimensional modeling in the context of imaging in curved spacetimes are discussed in Section 6.6.

6.1 The Testing Code

The general form of the characteristic equation of radiative transfer (5.2) requires the use of the formal solution introduced in Chapter 5 in the solution of the radiative transfer.
The radiative transfer code is based on the code described in [Baron and Hauschildt, 2004]. It provides a framework for the formal solution and the accelerated Λ-iteration.
In order to be usable for general relativistic radiative transfer several additions to the code

have been made. At first, code has been added which calculates the photon orbits for a given atmosphere structure and images the spectrum in curved spacetime as described in Chapter 4. It has been ensured that the added routines provide the correct interface for the radiative transfer solver.

Furthermore, code has been added which allows for the integration of the atmosphere structure. The physical assumptions made in regard of the atmosphere are described in Section 6.2. Besides, several improvements to the code base have been made and additional options for the setup and an improved radial optical depth grid generation have been included.

Independent checks are crucial to the testing of the new implementation. However, the inclusion of general relativity means that new physics are included in the calculations. This new physics cannot be described by other radiative transfer implementations available and no fully independent check of the new implementation is possible. The perspective can be reversed, however, and the general relativistic framework can be used as an independent check for the standard radiative transfer solver.

For a system with a vanishing mass, the a_λ term as defined in Equation (3.48) for the Schwarzschild spacetime vanishes. Thus the coupling of the different wavelengths is removed. Then the radiative transfer can be calculated for every single wavelength independently. A solution to the uncoupled (or monotonically coupled) radiative transfer problem is well known with the ALI method as described for instance in [Hauschildt, 1992, Hauschildt and Baron, 1999]. The new general relativistic solver still solves the matrix equation (5.13) in order to test the framework.

Since both methods are physically equivalent, they must produce identical results. In Figure 6.1a the relative flux for a line calculated with both methods for a vanishing mass is plotted. The results have a relative error of about 10^{-4}. The main contribution to this error comes from the differences in the path length. The old method uses the analytical result while the general solver integrates the numerical system (4.6) for a vanishing mass M. Although the path lengths were accurate to at least 10^{-2} cm, the differences were large enough to produce the error. The different path lengths are effectively equivalent to different opacities. From the constancy of the relative error it can be learned that the calculation of the radiative transfer is otherwise perfectly identical. This can also be seen from additional data points which are marked by crosses in Figure 6.1a. These mark the relative error of the fluxes when the analytical result for the path length is used in the general framework instead of integrating the orbits. Only a few points are shown, because for most points the match is perfect and the corresponding errors are zero.

From this test it can be learned that the new framework produces the same results as a well tested and well trusted method if the same atmospheric structure is used. Conversely, this is a strong indication that the solution of the general relativistic transfer is reliable. The inaccuracy of the order of 10^{-4} due to the numerical calculation of the orbits must be kept in mind and the need for improving the accuracy must be reevaluated for every model atmosphere.

Another less rigorous test is the calculation of a spectrum from an atmosphere which has a non vanishing mass but the line opacity is omitted. Since the remaining continuous opacity

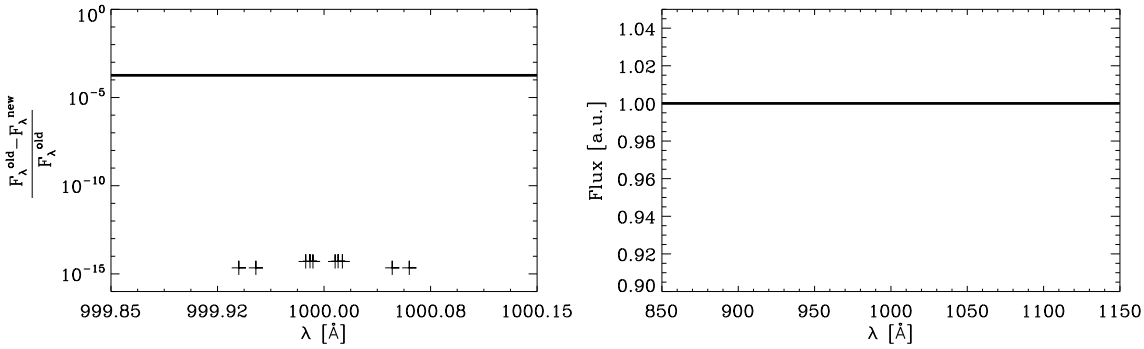

(a) **(b)**

Figure 6.1: In Figure 6.1a the relative error of the fluxes calculated with the new and the old radiative transfer solvers is shown. The crosses mark the nonzero data points if both methods use identical path lengths.
In Figure 6.1b the flat continuum for a general relativistic calculation with an omitted spectral line is shown.

is constant over wavelength the gravitationally induced shift cannot produce deviations from a flat continuum. This expected result is indeed found and shown in Figure 6.1b. Therefore, the implementation of the general relativistic radiative transfer test solver and seems to be working correctly. Thus the results of further calculations with the general relativistic code can be trusted as it passed the available tests. However, one has to question the results as long as alternative solutions become available for confirmation.

6.2 The Physical Parameters of the Atmosphere

The structure of a model atmosphere is normally determined from the solution of appropriate physical equations such as the hydrostatical equation.
Since for the construction of a testing environment the physical relevance is not of primary interest, the description of the model structure can be simplified. In order to keep the treatment as simple as possible in the following an analytic relation for the density in terms of the radial coordinate of the given background spacetime is assumed.
As general relativity is only important in compact objects an exponential density law with an appropriate scale height is assumed

$$\varrho(r) = \varrho_0 \exp\left(\frac{r - r_{\mathrm{out}}}{r_{\mathrm{scale}}}\right) \tag{6.1}$$

The parameters ϱ_0, r_{out}, and r_{scale} must be chosen in such a way that the calculation results an atmosphere of the desired extent. For simplicity the scale height r_{scale} is chosen to be constant throughout the atmosphere. It should be noted that in Equation (6.1) the variable r is the radial spacetime coordinate as the relation which is motivated by Newtonian physics is adopted for curved spacetime.

The radiation transport is solved along characteristics with optical depths that cover the atmosphere from optically thick regions to the outermost layers. In order to resolve the physical radial structure given by (6.1) in terms of optical depth an expression is needed which relates the opacity to the radial coordinate.
For the testing atmosphere model it suffices to assume that the opacity is linearly proportional to the density.

$$\chi(r) = \chi_0 \varrho(r) \tag{6.2}$$

A prescribed optical depth grid with the desired resolution can be related to the radial structure. This is done via the relation of the differentials of the radial coordinate and of the radial optical depth (see Equation (2.35))

$$\frac{\mathrm{d}r}{\mathrm{d}\tau} = -\frac{1}{\chi(r)} \tag{6.3}$$

where $\chi(r)$ is given by (6.2).
The sign of (6.3) is negative as the optical depth is measured from the outside of the atmosphere. It should be noted that $\chi(r)$ represents only the continuum extinction. Within the spectral line of the two level atom the optical depth scale will be different.
To describe the single spectral line of the two-level-atom, we define a wavelength λ_{line} as the center of the line and construct the line profile with a Gaussian profile centered on this wavelength. The redistribution function (see Section 2.3.2) is assumed to be isotropic and completely redistributed. The emission and absorption profiles are then equal and the profile function for the transition can be written as

$$\int R(\lambda, \lambda')\mathrm{d}\lambda' = \Phi(\lambda) = \frac{\omega_{\mathrm{line}}}{\sqrt{\pi}} \exp\left(-\frac{\lambda - \lambda_{\mathrm{line}}}{\omega_{\mathrm{line}}}\right)^2 \tag{6.4}$$

with ω_{line} being the width of the Gaussian. The opacity associated with the line $\chi_{\mathrm{line}}(\tau, \lambda)$ is linearly related to the opacity of the continuum $\chi_\kappa(\tau)$

$$\chi_{\mathrm{line}}(\tau, \lambda) = \chi_\kappa(\tau) R_{\mathrm{line}} \frac{\Phi(\lambda)}{\int \Phi(\lambda')\mathrm{d}\lambda'} \tag{6.5}$$

whereby the factor R_{line} determines the strength of the line relative to the continuum.
Since the opacities of the continuum and the line generally consist of a true absorption and a scattering part, the parameters ϵ_κ and ϵ_{line} must be specified in order to define the scattering albedo. The true absorption and scattering part for the continuum is then described by

$$\kappa(\tau) = \epsilon_\kappa \chi(\tau) \tag{6.6}$$
$$\sigma(\tau) = (1 - \epsilon_\kappa)\chi(\tau) \tag{6.7}$$

whereas for the line opacity we have

$$\kappa_{\mathrm{line}}(\tau, \lambda) = \epsilon_{\mathrm{line}} \chi_{\mathrm{line}}(\tau, \lambda) \tag{6.8}$$

$$\sigma_{\text{line}}(\tau,\lambda) \;=\; (1-\epsilon_{\text{line}})\chi_{\text{line}}(\tau,\lambda) \tag{6.9}$$

Now the total opacity with contributions from both the continuum and the line can be written as

$$\begin{aligned}\chi_{\text{total}}(\tau,\lambda) \;=\;& \kappa(\tau)+\sigma(\tau)\\ &+\kappa_{\text{line}}(\tau,\lambda)+\sigma_{\text{line}}(\tau,\lambda)\end{aligned} \tag{6.10}$$

while the emissivity reads:

$$\begin{aligned}\eta_{\text{total}}(\tau,\lambda) \;=\;& \big(\kappa(\tau)+\kappa_{\text{line}}(\tau,\lambda)\big)\; B(T(\tau))\\ &+\sigma(\tau)\; J(\tau,\lambda)+\sigma_{\text{line}}(\tau,\lambda)\; \bar{J}(\tau)\end{aligned}$$

with $\bar{J}$ being the mean intensity averaged over the line profile.
With the source function prescribed at every point of the atmosphere there is no need to introduce further physical quantities on the radial optical depth grid. In an application to a physical system these physical quantities would have been needed to calculate the opacity and emissivity which are already given here.
This is true for all quantities but the temperature, because it is needed to describe the thermal non-scattering emission of the atmosphere. Further the temperature is needed to provide boundary conditions for the radiation field at the bottom of the atmosphere. Hence we need to provide a temperature structure in the radial optical depth scale. We use the formalism of the Hopf function $q(\tau)$ [Chandrasekhar, 1950] to describe the gray atmosphere. Thus we can relate a temperature to an optical depth depending on an effective temperature which describes the total energy output of the atmosphere.

$$T^4(\tau) = \frac{3}{4}T_{\text{eff}}^4(\tau+q(\tau)) \tag{6.11}$$

The physical description of the testing environment is complete, but is still very flexible due to the strong dependence on parameters, as the scale height, outer radius, scattering albedos, effective temperature, or the opacity.

6.3 A Compact Atmosphere

The most compact object without an event horizon is a neutron star. Its is large enough that a general relativistic treatment is crucial. Therefore, a neutron star like environment is a good starting point for the testing of the general relativistic radiative transfer. The atmospheres of these compact objects are also very compact and have a scale height of only a few centimeters.
In order to simulate a neutron star like atmosphere with the testing environment from Section 6.2 the parameters outer radius, scale height, and the density at the outer radius must be chosen appropriately.
A possible configuration is shown in Figure 6.2. The atmosphere covers optical depths in

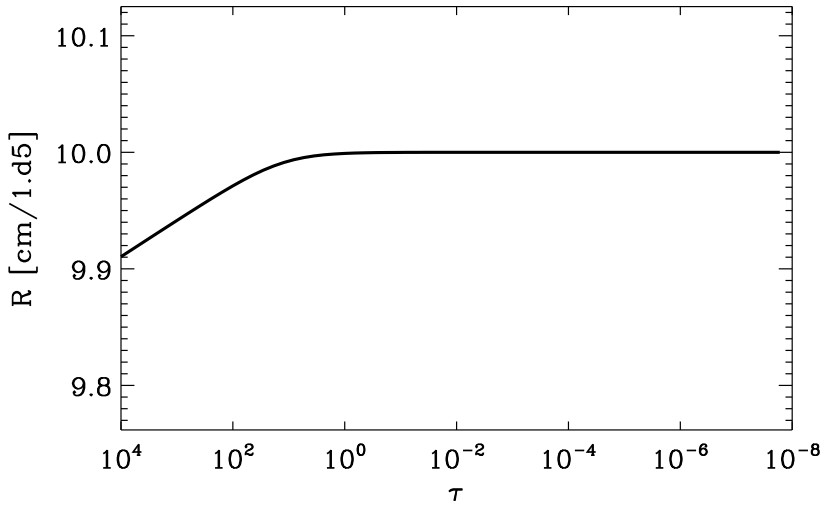

Figure 6.2: Radius is plotted over optical depth. The optical depth was calculated from the wavelength independent continuous opacity. The atmosphere is about 90 meters thick, but the layers with an optical depth around one lie just centimeters below the outermost layer.

the range from $\tau = 10^{-8}$ up to $\tau = 10^{4}$. The total extent of the atmosphere in this range is circa 90 meters.

The atmosphere can be truncated at the maximal optical depth as the solution of the radiative transfer in these deep layers is described by the diffusion approximation [Mihalas, 1970] and must not be solved for.

In situations with strong scattering albedos and Gaussian line profiles, the maximal optical depth must be chosen to be larger than the inverse of the destruction probability ϵ [Avrett, 1965, Mihalas, 1978].

The radiative transfer is solved only over a small wavelength range. Therefore, the Planckian can be assumed to be constant over wavelength. This simplifies the spatial boundary conditions as well as the emissivity of the spectral line.

The resulting atmosphere model is not intended as a realistic scientific model and is not suited to investigate the physics of a neutron star. However, the effects of the general relativistic theory on the radiative transfer in atmospheres of similar scale as well as their extent are reproduced correctly. Hence conclusions drawn from these calculations can be directly applied to the expected observations of real objects.

Since the atmospheres are very compact and the range of the radial coordinate covered in the models is small, the intra atmospheric wavelength shift due to general relativity is small. Hence the width of the Gaussian line ω_{line} is taken as a small enough value $\omega_{\mathrm{line}} = 10^{-2}$. In such a line the extent of the relativistic effects on the radiative transfer is expected to be clearly visible.

In practice this means that general relativistic transfer in compact atmospheres will be most

important for rapidly changing opacities. Such a situation may also occur in a blend of several spectral lines which results in spikes in the run of the opacity [Hauschildt *et al.*, 1995]. In the following the spectra of compact atmospheres are presented for different combinations of the scattering albedos. In order to allow for identifications of general relativistic effects the spectra for the massless cases were also calculated. These non relativistic cases have the same physical structure and use the same code to calculate the radiative transfer.

If one compares relativistic and non relativistic spectra from the same structure it becomes apparent that the flux in the continuum is different. This may be surprising at first as the physical structure and the continuous opacity and thus the radial optical depth grid are the same. However, the coupling term a_λ acts like an additional "opacity source" in the radiative transfer (see Equation 5.5). Although this additional opacity has no physical interpretation in terms of atomic transitions as it is just a consequence of the comoving wavelength description, it still influences the radiative transfer since the optical depth along a given characteristic is different from the massless case. There is no contradiction as the radial optical depth grid is solely used to describe the sampling of the physical structure in terms of optical depth and the radiative transfer uses its own optical depth scale for every ray and wavelength.
From this it follows, that fits to observations obtained with classical radiation transport codes would determine a wrong temperature in order to match the flux in the continuum. Hence the structures derived from non general relativistic radiative transfer modeling of compact atmospheres will contain a systematic temperature error.
The main interest in the comparison of the classical and general relativistic line transfer lies in the observable changes of the emerging line profile. The spectra for the massless and the general relativistic case are thus best compared if the continuum is normalized. Hence in the following the flux is given in normalized arbitrary units.
In Figures 6.3 and 6.4 the results of a non-scattering atmosphere, $\epsilon_{\rm line} = \epsilon_\kappa = 0$, are shown. The radial optical depth grid in these calculations covers a range from $\tau = 10^{-8}$ up to $\tau = 10^4$ and the outer radial coordinate of the atmosphere is $r = 10^6$ cm.
The emerging line profiles are contained in one plot in order to be easily compared. Due to the gravitational redshift the center of the line is shifted in case of the imaged spectra and two different wavelength scales are used to align the central wavelengths. The wavelength scale at the bottom corresponds to the massless case and the upper to the $M = M_\odot$ case. Both scales cover the same absolute range in wavelength. This is noteworthy as the wavelength bins are scaled up by the gravitational redshift.
In Figure 6.3 the relativistic spectrum, shown in red, was not imaged but was taken directly from the top of the atmosphere. Hence the two wavelength scales are identical. The emerging line profiles are very different, however.
The line profile in the massless case, shown in black, is symmetric around the line center as one would expect because the profile function of the transition is symmetric. Further the line is saturated in the core.
The general relativistic line is also saturated but is asymmetric with an extended red wing and a slightly less extended blue wing than the classical result.
As the atmosphere is completely non-scattering, this is a basic result of the general rela-

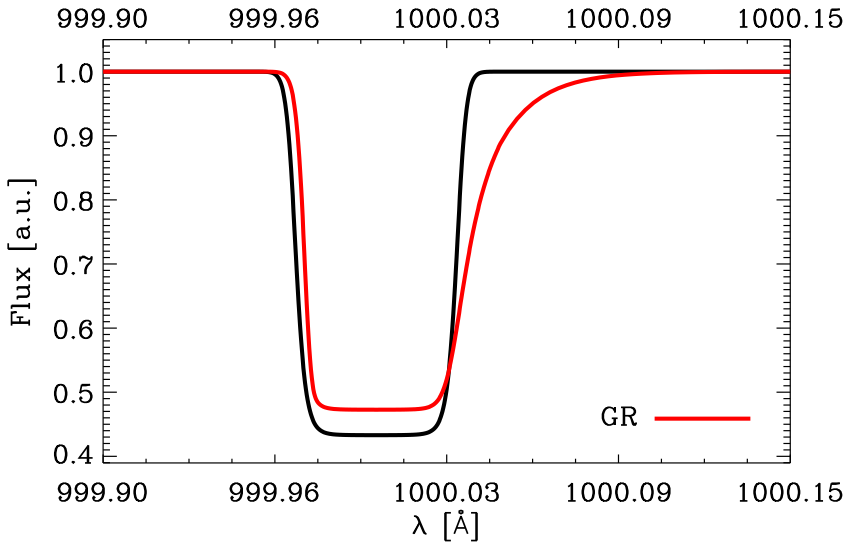

Figure 6.3: The spectra of a massless and a relativistic compact non scattering atmosphere are compared. The outer radius of the atmosphere is 10^6 cm. The relativistic spectrum is not imaged in curved spacetime but taken from the top of the atmosphere.

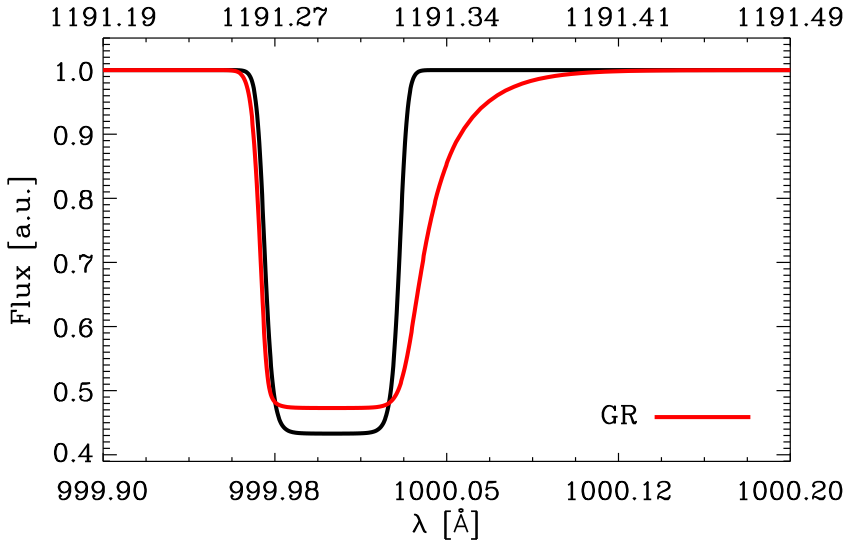

Figure 6.4: The spectra of a massless and a relativistic compact non scattering atmosphere are compared. The outer radius of the atmosphere is 10^6 cm. The spectrum of the relativistic atmosphere was imaged in curved spacetime and thus exhibits a strong redshift of wavelength.

tivistic radiative transfer. Due to the coupling of the wavelengths the influence of the line is shifted to longer wavelengths. For the blue side of the line this results in a reduced extension of the wing as the stronger intensities of the continuum get shifted into the line profile. In the red part of the line the lower intensities of the line get shifted outside the line profile and cause the extended red wing.
In Figure 6.4 the same emerging line profile as in Figure 6.3, shown in red, is compared to the classical result, shown in black. However, this time the spectrum has been imaged in curved spacetime. According to the procedure described in Section 4.2, a proper set of angles was used for the integration and the redshift of the wavelength was applied to the intensities.
Now the wavelength scales are very different as one expects from the gravitational redshift. The principal shape of the line profile did not change significantly however. This can be attributed to the fact that the change of angles is most important for those characteristics which have a small μ at the outermost layer of the atmosphere. These characteristics contribute very little to the angular integration of the flux and have in relation to the core intersecting rays lower values for the specific intensities. Therefore, the imaging in curved spacetime for compact atmospheres has no large effect on the spectrum. The situation is different if multidimensional calculations with a varying structure are taken into account. See Section 6.6 for an estimate of the possible effects.
Although the shape of the line profile is nearly unchanged there is an obvious change in the observed spectrum which must be attributed to the imaging in curved spacetime. The redshift causes the width of the line to become larger according to relation (4.15). Consequently, the observed line in numbers of absolute wavelength is broader than the unshifted line. This phenomenon is especially visible in the blue wing of the line profile. In Figure 6.3 the blue part of the line was less extended in comparison to the classical case and in Figure 6.4, the relativistically imaged spectrum, it extends even more into the blue part of the spectrum.

Up to now scattering has been neglected. The inclusion of scattering is crucial to the modeling of astrophysical atmospheres. The concept of an ALI was included in the radiative transfer solution in order to solve the scattering problem. Consequently, in the following the scattering albedos will no longer vanish, but instead the results of calculations with different combinations of line and continuum scattering will be presented. In Figures 6.5 and 6.6 spectra from atmospheres with $M = M_{\odot}$ are compared. Therefore, the lower and upper wavelength scales are identical.
In Figure 6.5 a scattering line, $\epsilon_{\mathrm{line}} = 10^{-2}$, is compared to the non scattering case from Figure 6.3. The scattering case is plotted in red whereas the non scattering is shown in black. Both spectra are directly taken from the top of the atmosphere and use the same atmosphere structure and mass as before.
With scattering present in the line, the photons can escape from deeper layers. Hence the saturation of the core of the line is removed. Otherwise the spectra are very similar. This is due to the fact that in wavelength regions outside the profile the physical situation is the same. The continuum is not scattering and the radiative transfer proceeds the same way as in the non scattering atmosphere.

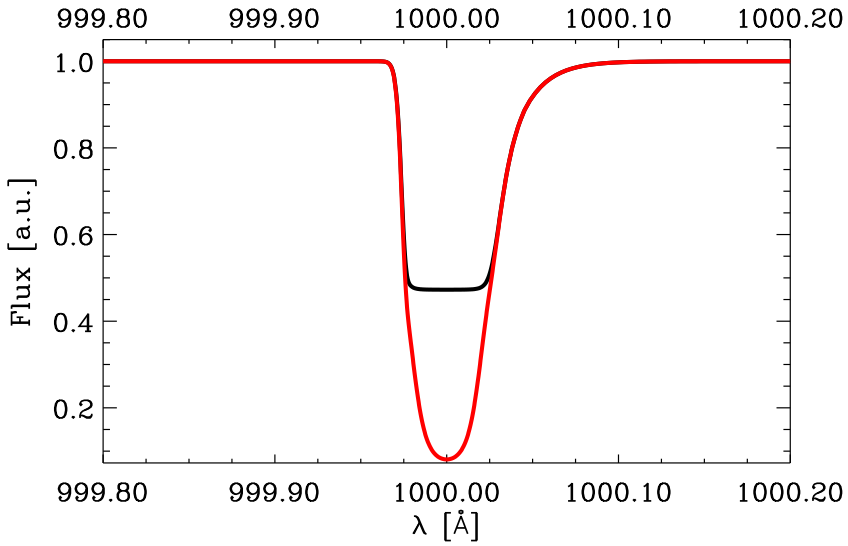

Figure 6.5: The spectra of two compact atmospheres are shown which were directly taken at the atmosphere. The black spectrum is from a completely non scattering atmosphere whereas the red spectrum was taken from an atmosphere with a scattering line, $\epsilon_{\rm line} = 10^{-2}$.

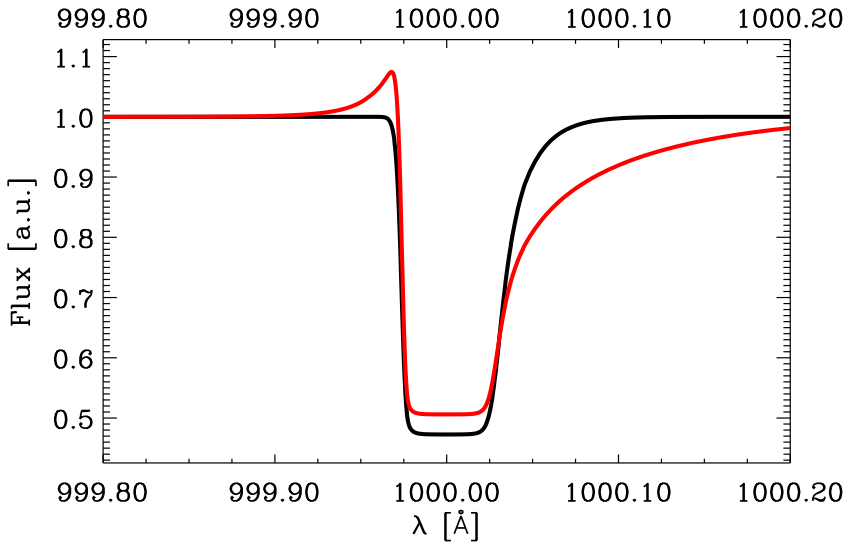

Figure 6.6: The spectra of two compact atmospheres are shown which were directly taken at the atmosphere. The black spectrum is from a completely non scattering atmosphere whereas the red spectrum was taken from an atmosphere with a continuous scattering albedo of $\epsilon_\kappa = 10^{-2}$.

In Figure 6.6 a non scattering line with a coherent scattering continuum, $\epsilon_\kappa = 10^{-2}$, is compared to the non scattering atmosphere. The scattering case is plotted in red.

The most notable difference is the emission feature on the blue side of the line. It can be attributed to the Schuster mechanism [Mihalas, 1970, Gebbie and Thomas, 1968].

Normally the Schuster mechanism is symmetric if symmetric line profiles are assumed. However, the whole spectrum formation process in the given atmosphere is subject to a wavelength shift. As seen in Figure 6.3 this leads already to an asymmetric emergent line profile. In this case the blue emission feature can be seen as a sum of contributions from a Schuster mechanisms that were merged through the shift of wavelength and cut off due to the strong opacity of the line. There is no emission feature on the red side of the line as it got smeared out and suppressed by the lower intensities shifted out of the line profile.

Since due to the scattering the photons in the continuum originate from deeper and hotter layers, the atmosphere has a larger apparent continuum flux. Further the radiative transfer is influenced by the change of the source function which explains the changed depth of the line.

The extended red wing in Figure 6.6 can also be attributed to the continuum scattering. Since the photons are scattered they can cover greater distances without getting absorbed. Hence they are redshifted further and transport the information about the line opacity to longer wavelengths and thereby cause the extended red wing.

In Figures 6.7 and 6.8 the emerging spectra for a scattering compact atmosphere are shown. The scattering takes now place in the continuum as well as in the line, $\epsilon_{\rm line} = \epsilon_\kappa = 10^{-2}$. The general relativistic cases are shown in red and correspond to the upper wavelength scale.

In Figure 6.7 the relativistic spectrum was taken from the top of the atmosphere without being imaged in curved spacetime.

The emerging line profile is a combination of the results from Figures 6.5 and 6.6. The saturation in the core is removed due to the scattering in the line. Furthermore, the blue emission feature and the extended red wing of the line due to the continuous scattering are present.

For comparison, the same but imaged spectrum is shown in Figure 6.8. The basic shape of the line stays the same. But besides the shift of wavelength the apparent broadening of the profile is again clearly visible.

For cases with even stronger scattering in the continuum, the effects of the Schuster mechanism become more visible. In Figure 6.9 the imaged spectrum of a strongly scattering, $\epsilon_{\rm line} = \epsilon_\kappa = 10^{-4}$, compact atmosphere is shown in red. The massless case is shown in black. The scattering is now so strong that even the non relativistic atmosphere shows emission in the wings of the line by the Schuster mechanism.

In order to avoid introducing errors in the boundary conditions the radial optical depth grid was extended to $\tau = 10^5$ in these calculations.

The emerging line profile in the relativistic case resembles the profile from Figure 6.8, however, the blue wing emission feature is stronger and the line is deeper as in the weaker scattering case. The stronger Schuster mechanism is a direct result of the stronger continuous scattering whereas the stronger line scattering causes the absorption line to deepen.

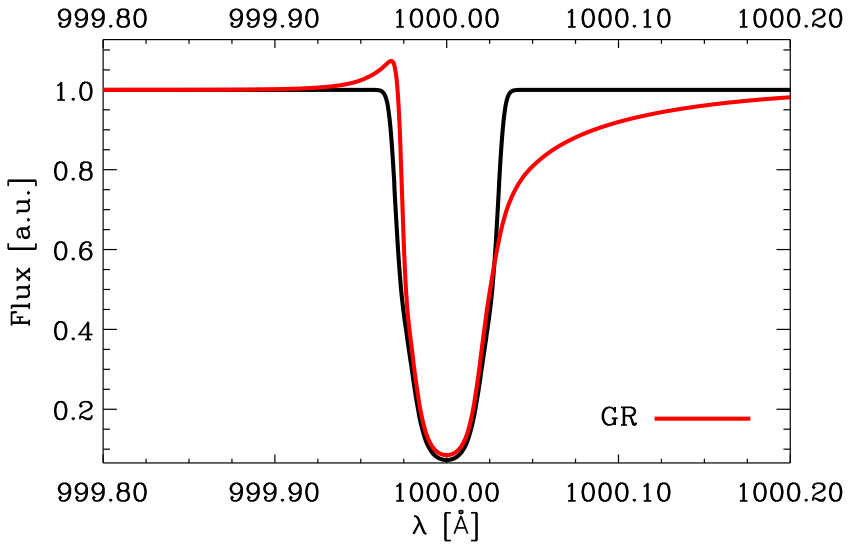

Figure 6.7: The spectra of a massless and a relativistic compact atmosphere are compared. The scattering albedos are $\epsilon_{\rm line} = \epsilon_\kappa = 10^{-2}$. The outer radius of the atmosphere is 10^6 cm. The relativistic spectrum is not imaged in curved spacetime but taken from the top of the atmosphere.

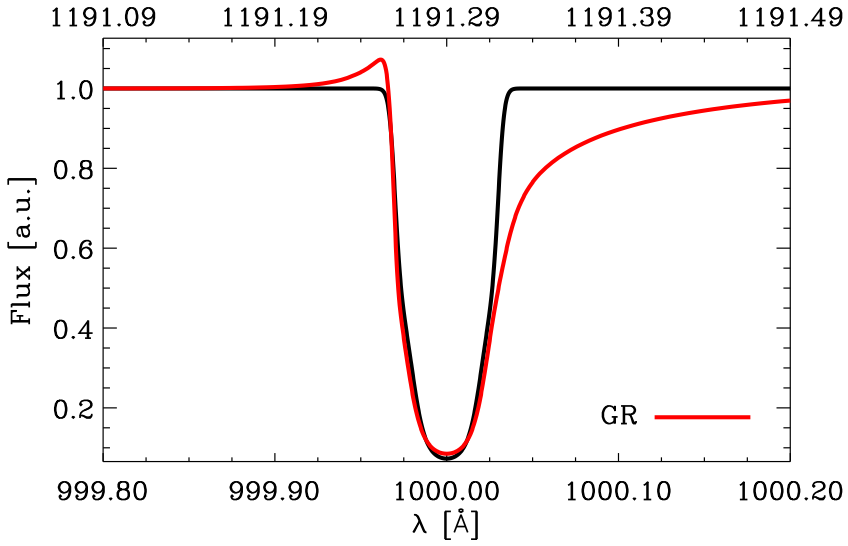

Figure 6.8: The spectra of a massless and a relativistic compact atmosphere are compared. The scattering albedos are $\epsilon_{\rm line} = \epsilon_\kappa = 10^{-2}$. The outer radius of the atmosphere is 10^6 cm.

In Figure 6.10 the spectrum for a compact atmosphere with pure scattering, $\epsilon_\kappa = 0$, in the continuum and no line scattering is shown. Physically this means that the two kinds of scattering are no longer coupled via the thermal pool because the photons in the continuum are always scattered.
The pure scattering in this context is realized by a scattering albedo of $\epsilon_\kappa = 10^{-20}$. The strong emission feature on the blue side of the line has a visible counterpart on the red side. In the over relativistic line profiles the red counterpart was never visible as it was smeared out over wavelength. In this case the Schuster mechanism is strong enough so that the emission peak is still visible over the continuum. However, the peak is small in height and very spread out. The large wavelength range is a result of the very strong scattering albedo in the continuum. The photons travel very long distances without being destroyed and are subject to the full wavelength shift along the characteristic. In the other cases the photons lost the information about the wavelength shift in an absorption process.

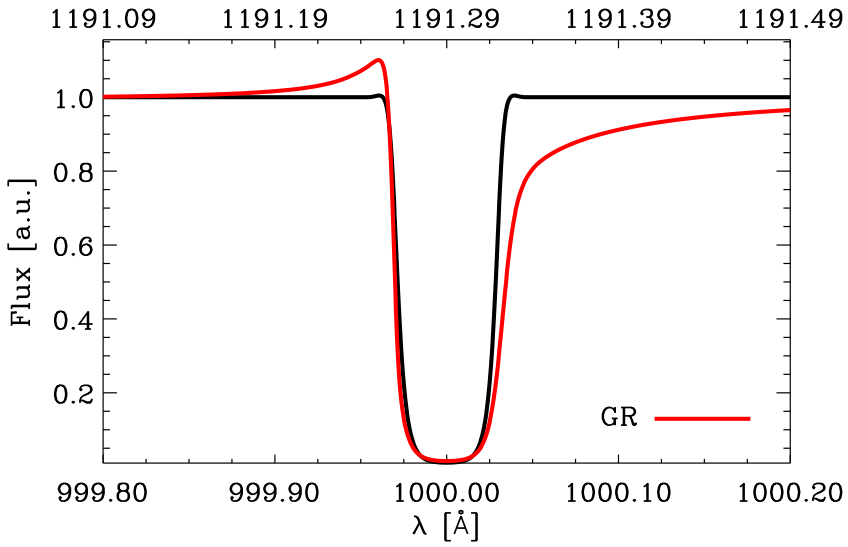

Figure 6.9: The spectra of a massless and a relativistic compact atmosphere are compared. The scattering albedos are $\epsilon_{\rm line} = \epsilon_\kappa = 10^{-4}$. The outer radius of the atmosphere is 10^6 cm.

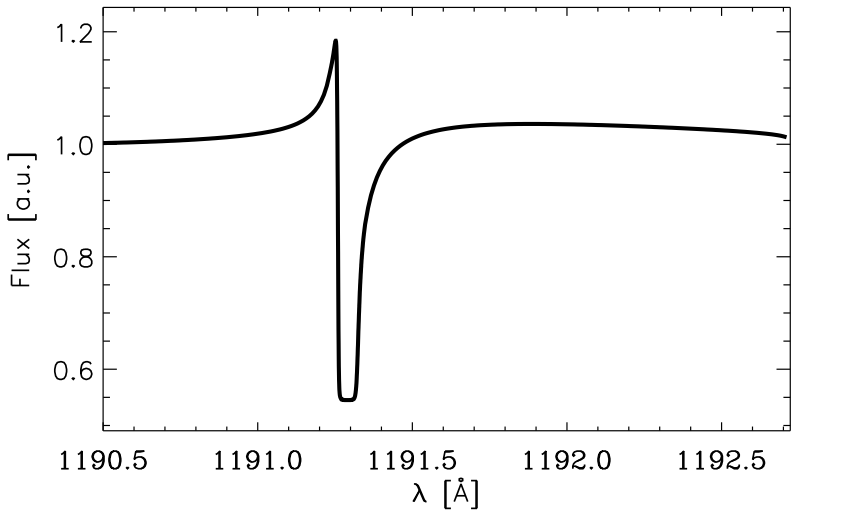

Figure 6.10: The imaged emerging line profile for a very strong continuous scattering albedo $\epsilon_\kappa = 10^{-20}$ for a general relativistic compact atmosphere is shown. The spectral line is not scattering.

6.4 An Extended Atmosphere

The range of the radial coordinate covered in the calculations of the compact atmospheres in Section 6.3 is only about 100 meter. Therefore, the intra atmospheric wavelength shift was accordingly small. In order to increase the spatial extent the description of the atmosphere structure must be changed.
Instead of assuming an exponential run of the density as in Section 6.2 the density can also be described by a power law

$$\varrho(r) = \varrho_0 \left(\frac{r_{\max}}{r}\right)^n \tag{6.12}$$

Otherwise the construction of the atmospheric structure proceeds exactly as in Section 6.3. This setup allows for a gentler change of the opacity with the radial coordinate.
At first an atmosphere of similar spatial dimensions like a compact atmosphere is calculated. Its radial structure for a linear run of the density, $n = 1$, is plotted over the radial optical depth in Figure 6.11. The according emergent line profile for the scattering albedos $\epsilon_{\text{line}} = \epsilon_\kappa = 10^{-2}$ is shown in Figure 6.12. The relativistic case is plotted in red whereas the classical spectrum is depicted in black. The upper wavelength scale corresponds to the imaged spectrum.

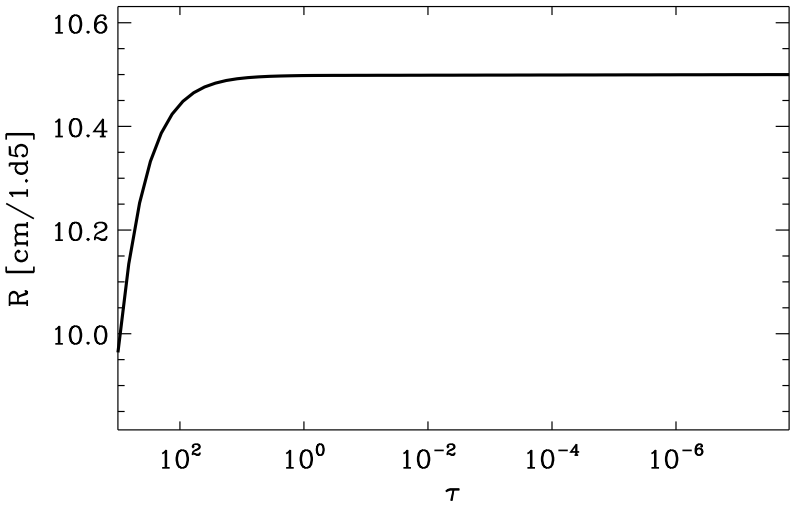

Figure 6.11: The radial coordinate is plotted over optical depth. The structure is slightly more extended than the one from Figure 6.2. However, the relation (6.12) instead of an exponential ansatz was used in the construction of the atmosphere. This results in a less steep gradient especially in the optical thick layers.

The relativistic line shape is vastly different compared to the results of the exponential atmospheres in Section 6.3. A second line profile is visible which is shifted to longer wavelengths than the original line. This satellite line is present in all angles which con-

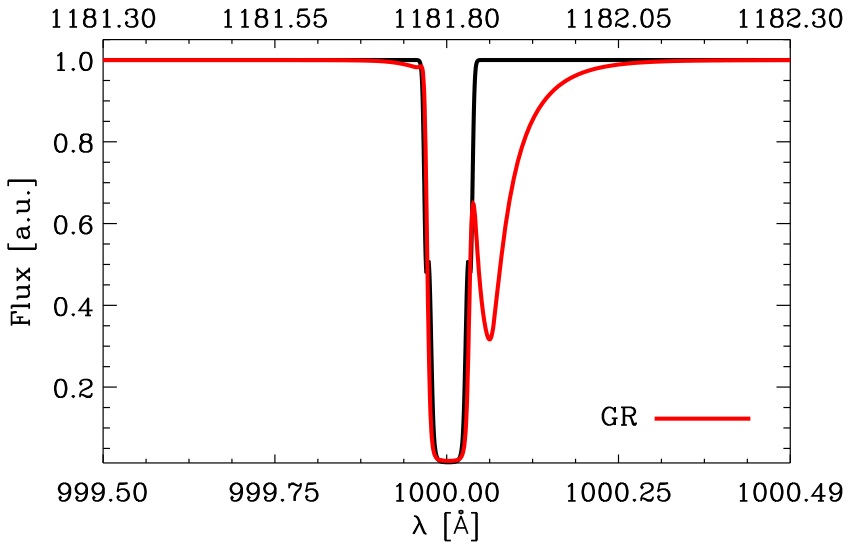

Figure 6.12: The spectra of a massless and a relativistic compact atmosphere are compared. The scattering albedos are $\epsilon_{\mathrm{line}} = \epsilon_{\kappa} = 10^{-2}$. The atmosphere is constructed with relation (6.12) and $n = 1$. The according radial structure is shown in Figure 6.11.

tribute to the integrated spectrum. Hence an artifact from a failed integration can be ruled out.

If one takes a closer look at the classical spectrum it becomes evident that there are small spectral features present in the line wings. These features can again be attributed to the Schuster mechanism. In the general relativistic case the Schuster mechanism also applies. This can be seen at the transition of the line into the blue continuum. The emission peak is subject to the wavelength shift and remains visible only as an perturbation in the line. The Schuster feature in the red line wing is influenced by the gravitational shift of wavelength. Since it lies in the wing it is not swept into the continuum but remains visible. The intensities from within the line profile get redshifted and produce the peak within the line. Without the spectral feature of the Schuster mechanism, these intensities would be shifted into the continuum and would have produced similar line shapes to those in Section 6.3.

In addition the gradient $\frac{\mathrm{d}\tau}{\mathrm{d}r}$ is smaller for the extended atmosphere than for the exponential atmosphere and hence the region of line formation has a larger radial extent which translates into a larger wavelength shift. Thus the spectrum formation is stronger influenced by the internal wavelength shift. From this can be learned that the emerging line profiles for physically different structures are very different. Hence the general radiative transfer seems to be suited to produce constraints for the atmosphere model structure.

The structure in Figure 6.11 is more spatially extended than the structure in Figure 6.2. However, the range of the radial coordinate covered is still only a few hundred meters. Therefore, a more extended atmosphere is presented in the following.

Compact objects are often subject to accretion. The resulting atmospheres include velocity

fields. With the results of the equation of radiative transfer in the presence of velocity fields from Section 3.4 models for such atmospheres can be calculated.

Normally the description of accretion is a multidimensional problem. But this work is restricted to one-dimensional solutions of the radiative transfer and the main interest lies in the effects of general relativity on the radiative transfer in a given system and not proper modeling of realistic physics. Therefore, instead of using physical solutions as standard disk [Shakura and Sunyaev, 1973, Novikov and Thorne, 1973] or advection dominated accretion flows [Narayan and Yi, 1994], we assume a variation of the density according to Equation (6.12).

The velocity field is purely radial due to the restriction to one dimension and is described by the following relation

$$v(r) = -v_{\max}\left(\frac{r - r_{\max}}{r_{\min} - r_{\max}}\right) \tag{6.13}$$

where $v_{\max}$ means the maximal velocity at the minimal radius $r_{\min}$ of the atmosphere. The velocity is directed inward, hence the negative sign and is zero at the outer radius $r_{\max}$ of the atmosphere.

The velocity field causes a Doppler shift and thus adds to the coupling of the wavelengths (see Equation (3.62)) as the coupling term a_λ reads

$$\begin{aligned} a_\lambda &= \mu\gamma\left(\gamma^2\frac{1+\beta\mu}{\sqrt{1-\frac{2GM}{c^2r}}}\frac{\partial\beta}{\partial\tau} + \gamma^2\sqrt{1-\frac{2GM}{c^2r}}(\beta+\mu)\frac{\partial\beta}{\partial r}\right) \\ &\quad + \mu\gamma(1+\beta\mu)\frac{GM}{c^2r^2\sqrt{1-\frac{2GM}{c^2r}}} + \gamma\frac{1-\mu^2}{R}\beta\sqrt{1-\frac{2GM}{c^2r}} \end{aligned} \tag{6.14}$$

For time independent velocity fields the derivative over proper time can be dropped, but relation (6.14) remains a function of the velocity field $\beta(r)$.

Hence the velocity field directly contributes to the generalized absorption along the characteristics. If the derivative of the velocity over the radial coordinate is too steep the opacity along a ray changes too quickly and numerical instabilities occur. These instabilities can be removed via an increase of the resolution of the optical depth grid. But this strategy is not favorable as it is too demanding in terms of computing resources.

In order to avoid the numerical instabilities altogether the extent of the atmosphere is increased as this reduces the steepness of the derivative of the velocity. The larger radial coordinates demand a higher central mass of the atmosphere, because otherwise the general relativistic effects would be negligible.

One disadvantage of this more extended setup is the lack of exploration of strong tidal effects as those are expected to be largest near the central mass. However, the resulting model still suffices in analyzing the basic properties of general relativistic radiative transfer in the presence of velocity fields.

In Figure 6.13, the resulting line profiles for a massless atmosphere, in black, and for the general relativistic case, in red, are plotted. The relativistic case has a central mass of

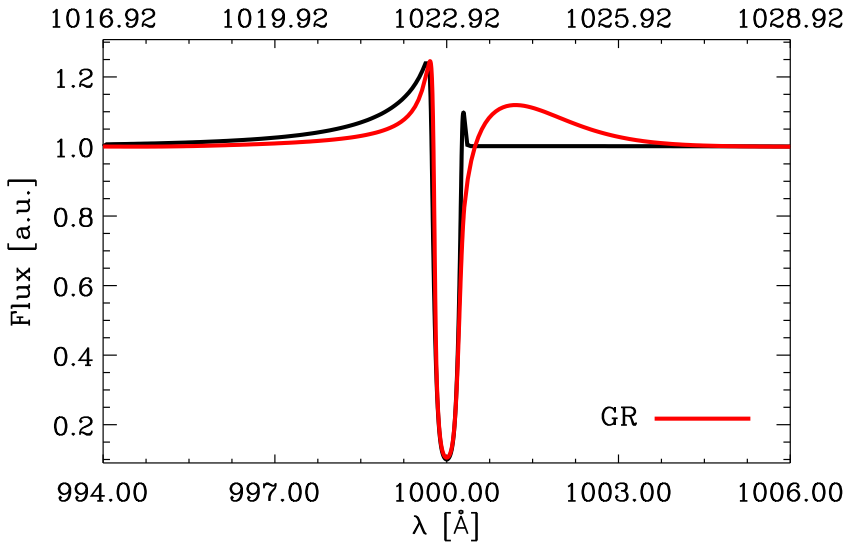

Figure 6.13: Comparison of emerging line profiles of a massless and a $M = 15M_{\odot}$, shown in red, atmosphere. The maximal velocity at the innermost layer of the atmosphere is $10^4\,\mathrm{km/s}$.

$M = 15M_{\odot}$. Both models have an outer radius of $r = 10^8\,\mathrm{cm}$ and a density exponent of $n = 3$ (See Equation (6.12)). The scattering parameters are $\epsilon_{\mathrm{line}} = \epsilon_{\kappa} = 10^{-2}$.

For the massless atmosphere the line profile resembles an inverse P-Cygni profile [Mihalas, 1978]. This is an expected behavior as the velocity field is pointing inwards opposed to for instance stellar winds where P-Cygni profiles can be observed.

Due to the relation (6.13) the velocity field vanishes at the outermost layer and no Lorentz boost due to a velocity field is necessary. The general relativistic line is however still redshifted due to the gravitational field. The redshift is smaller than in the previous Sections because the radial coordinate of the top layer is much larger than before and dominates over the Schwarzschild radius in the relation (4.15) that determines the redshift.

The influence of general relativity reduces the extent of the blue emission feature and a very spread out emission feature on the red side is visible. In order to emphasize the effect of the radiation field on the emerging spectrum the line profiles for three different velocities are shown in Figure 6.14. The structure is the same as in Figure 6.13. The velocity field influences the extent of the blue emission feature. A larger velocity partly compensates the redshifting effect of the gravitational field. This can also be seen at the red emission feature as it is confined to smaller wavelengths for larger velocities.

The strong effect of general relativity is expected and was the main motivation for the calculation of the line profiles in a spatially extended atmosphere. Therefore, the general relativistic treatment of relativistic flows may be very important for the modeling in such environments. However, this holds only under the premise that the underlying structure in a realistic model is not very different.

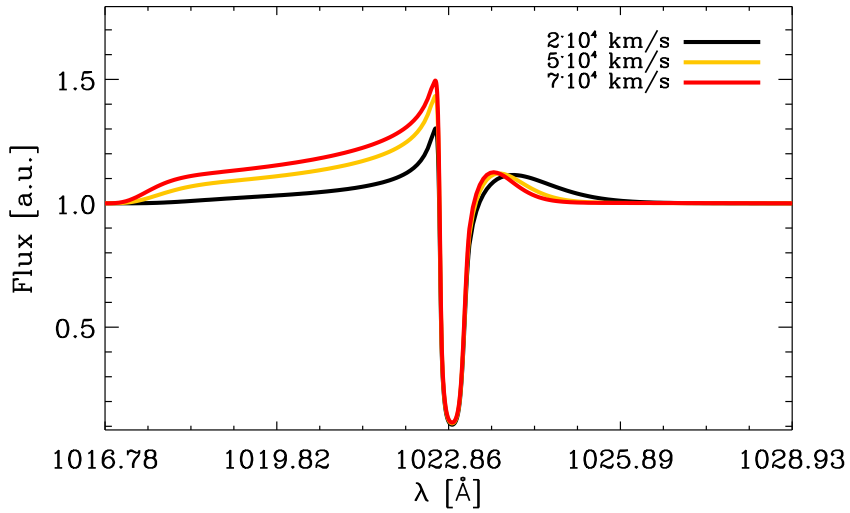

Figure 6.14: The general relativistic line profiles for different maximal velocities, $2 \cdot 10^4\,\mathrm{km/s}$, $5 \cdot 10^4\,\mathrm{km/s}$, and $7 \cdot 10^4\,\mathrm{km/s}$, are shown.

6.5 Continuous Spectra from a Gray Atmosphere

In the preceding Sections 6.3 and 6.4 the radiative line transfer has been calculated. If the spectral line is omitted the testing environment from Section 6.2 can also be used to calculate purely continuum radiative transfer [Knop *et al.*, 2007].
In order to do so one has to omit the opacity of line. Furthermore, the approximation of a wavelength independent Planckian is no longer valid, because now the interest lies in the radiative transfer in a broader wavelength region. This influences directly the thermal part of the source function and the spatial boundary conditions which are implemented by the wavelength dependent diffusion approximation [Mihalas, 1970].
As there are still no physical data used in the construction of the model the opacity is best treated as gray.
In the following, the effective temperature of the atmosphere has been arbitrarily chosen as $T_{\mathrm{eff}} = 10^4\ \mathrm{K}$. The structure of the atmosphere has been constructed as described in Sections 6.2 and 6.3. In the construction of the compact atmosphere a mass of $M = M_\odot$ and an outer radius of $r = 10^6\ \mathrm{cm}$ have been used.
In the following Figures 6.15a to 6.15e the gravitational redshift is assumed to be known and is corrected for in the plot. Black body spectra are overplotted. In order to match the spectra the blackbody and the continuous spectra were normalized on the maximum in arbitrary units.
In Figure 6.15a the emerging spectrum for a vanishing scattering albedo ϵ_κ is shown. The according black body spectrum with the T_{eff} of the model atmosphere is overplotted with dashes in red. The spectra match very well and in case of a non-scattering atmosphere the temperature determination via a black body fit would have been successful.

The situation is however different if scattering is taken into account. In Figure 6.15b the spectrum for a modestly scattering, $\epsilon_\kappa = 10^{-1}$, atmosphere is shown. The black body spectrum for the effective temperature $T_{\rm eff} = 10^4$ K of the atmosphere model is overplotted. It is obvious that the black body does not fit the observation as it appears to be too cold.
In Figure 6.15c the same spectrum is shown with a black body fit. The temperature of the fit is $T = 12400$ K. Hence the apparent temperature of the continuous spectrum is significantly higher than the model temperature would have suggested.
For a stronger scattering albedo the effect is even more significant. In Figures 6.15d and 6.15e a strongly scattering, $\epsilon_\kappa = 10^{-3}$, atmosphere is shown. The black body spectrum has the temperature $T = 10^4$ K in Figure 6.15d and the temperature $T = 2.14/, \cdot 10^4$ K in the fit shown in Figure 6.15e. The apparent temperature is more than two times higher than the effective temperature of the model structure. In this case even the redshifted continuous spectrum peaks at shorter wavelengths than the black body spectrum of the model temperature.
In order to check the validity of the calculations the thermalization depth for the different scattering albedos is determined. The thermalization depth $\tau_{\rm th}$ is the optical depth where $J_\lambda = B_\lambda$ [Mihalas, 1970].
For coherent scattering the thermalization depth is related to the thermalization parameter as follows

$$\tau_{\rm th} = \frac{1}{\sqrt{\epsilon_\kappa}} \tag{6.15}$$

Since the emergent spectra are Planckian, $\tau_{\rm th}$ is the optical depth where the temperature of the atmosphere equals the temperature of the blackbody fit.
The resulting optical depth $\tau_{\rm th}$ is plotted over the scattering albedo in Figure 6.15f. The results match the prediction from the theory sufficiently well.
These results are valid for all temperature regimes. From this follows, that in order to model the temperature structure of compact astrophysical atmospheres, e.g. neutron stars, it is necessary to fully include the effects of scattering in the modeling process as scattering determines the fit. Besides the problem of scattering is fully entangled in the general relativistic radiative transfer theory. Thus for realistic neutron star models the radiative transfer including the treatment of general relativity and scattering must be self consistently solved. Otherwise systematic errors would be introduced into the calculations.

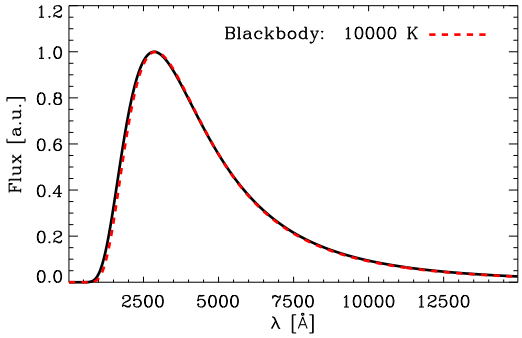

(a) $\epsilon_\kappa = 1$

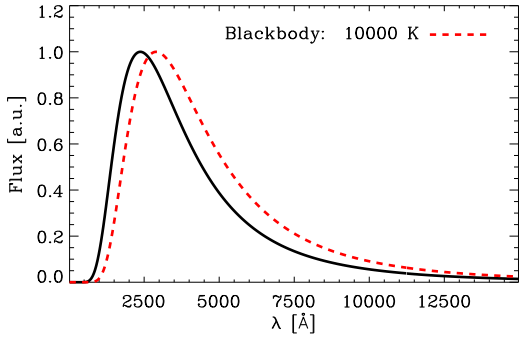

(b) $\epsilon_\kappa = 10^{-1}$

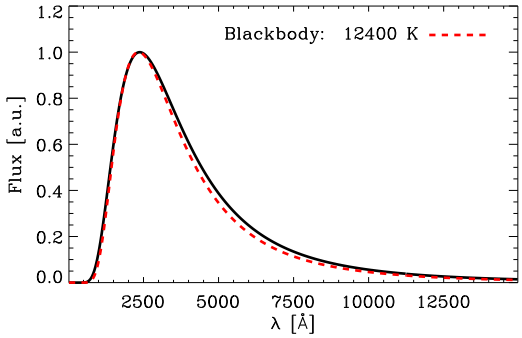

(c) $\epsilon_\kappa = 10^{-1}$

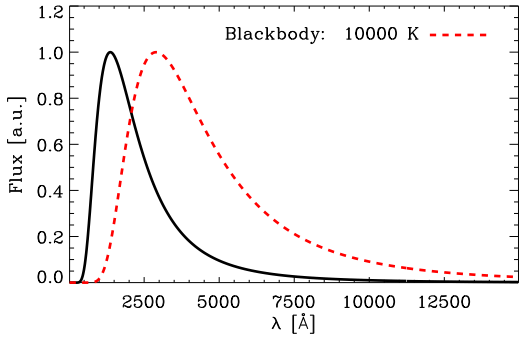

(d) $\epsilon_\kappa = 10^{-3}$

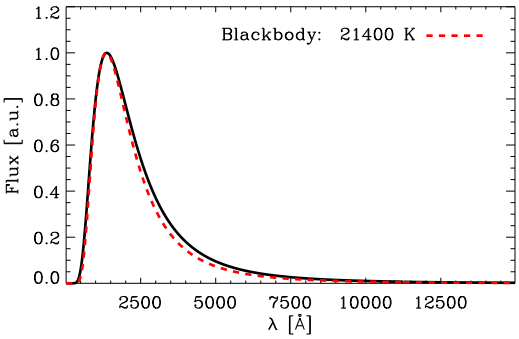

(e) $\epsilon_\kappa = 10^{-3}$

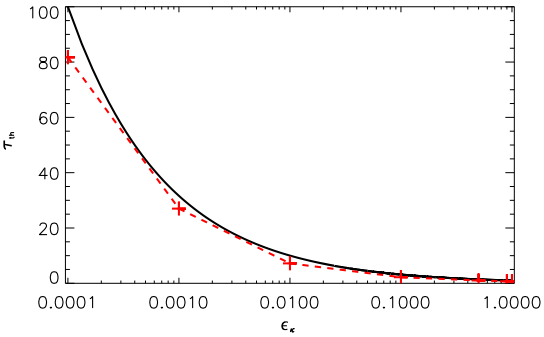

(f)

Figure 6.15: In Figures 6.15a to 6.15e continuous spectra from compact, gray atmospheres with varying scattering albedos with overplotted black body fits are shown. The continuous spectra are imaged in curved spacetime but are corrected for the gravitational redshift.
In Figure 6.15f the thermalization depth is plotted for various values for the coherent scattering albedo as small red crosses. The run of the thermalization depth according to the theory is plotted as a solid black line. The calculations match the theory reasonably well.

6.6 The Influence of Imaging on Emerging Line Profiles

The influence of curved spacetime and the according transformation for synthetic spectra have been introduced in Chapter 4. In Section 6.3 it has been shown that the gravitational redshift of the spectrum has a discernible effect on the width of images spectral lines. But the basic shape of the line seems to be uneffected by the imaging.
This result is reasonable because the characteristics which are most effected by the imaging are the topmost tangent rays with small values for μ which do not contribute much to the overall spectrum due to the small effective area of the according surface element.
The situation would be different in multidimensional models. In such models varying surface temperatures and for instance hot spots from accretion flows can be included. The emission of such a hot spot can contribute to the spectrum even if it is on the back side of the atmosphere due to the imaging in curved spacetime.
As noted before this work is limited to one-dimensional calculations and thus consistent multidimensional models are not possible. Hence the model is an approximation that still allows to estimate the extent of the effects on the spectrum.
In order to do so two calculations of different temperatures are combined. Since the spectrum calculation cannot be performed internally the complete radiation fields for two different temperatures are used.
A number of tangent rays in the calculation get replaced by the corresponding rays of a model with a higher effective temperature. The new combined radiation field does not represent exactly a hot spot but a hot annulus on the far side of the atmosphere. However, this still represents the effects of an inhomogeneous surface temperature sufficiently well and in the following the term hot spot refers to this annulus.
Two quantities in this combination affect the observable spectrum directly. First there is the number of angles of the radiation field that are exchanged. It determines the surface of the spot or annulus and therefore directly affects the spectrum. Secondly there is the effective temperature of the hotter model atmosphere itself. The total radiated flux of an atmosphere is proportional to the temperature to the fourth power and thus the spectrum strongly depends on the combination of the effective temperatures.
In Figure 6.16a, two spectra of a compact atmosphere from Section 6.3 are compared. The dashed red line represents the combination of the two temperature models and the black one is the normal spectrum for the cooler temperature. The cooler model atmosphere has a temperature of $T_{\text{eff}} = 10^4$ K whereas the hotter atmosphere has a 50 times higher temperature, $T_{\text{eff}} = 5 \times 10^5$ K. The spectra were normed on the continuum of the unchanged model to be easily compared.
The first 20 angles of the hot model were used in the calculation of the combined spectrum. In terms of the direction cosine μ these rays cover the range $0 < \mu < 10^{-4}$. This rather small range is a result of the compactness of the atmosphere as in the outer part the radial coordinate is not changing much from layer to layer and hence the outer tangent characteristics are very similar.
The shape of the line is not strongly affected by the hot spot as only the depth relative to the continuum is slightly increased and the main observable difference is caused by the increased flux in the continuum. In a real application the influence of spectral lines formed

in hot spots could be significantly larger. This is due to the possible dependence of the profile function on the temperature and more importantly due to the change of the chemical composition. For instance transitions of highly ionized atoms may only be present in the hot spot and these signature wavelengths could be detectable in the emerging spectrum.
In the model at hand the effect on the continuum was the dominant one. The description of the continuum is simplified, however, as a non varying continuum for the radiative line transfer was assumed.
The gray atmosphere models from Section 6.5 treat the continuum physically more correct. Hence effects due to the imaging on the continuum are investigated best with these models. Analogue hot spot calculations for the gray atmosphere models from Section 6.5 were performed. The result for a $T_{\rm eff} = 10^4\,{\rm K}$ atmosphere and a 20 angle annulus of $T_{\rm eff} = 1 \times 10^5\,{\rm K}$ is shown in Figure 6.16b.
A second peak at shorter wavelengths is visible. Due to the different effective temperatures the maximal emission occurs at different wavelengths respectively. As the short wavelength slope of the blackbody like spectrum is very steep the emission of the hotter part of the atmosphere takes place at wavelengths where the flux of the cold model essentially vanishes. Hence the signature of the hot spot is clearly visible.
The signatures in the spectrum due to the modeling of hot spots are primarily a consequence of multidimensional modeling. Therefore, the contributions would not be limited to the outermost tangent rays that originate from the far side of the atmosphere. In this general case the effects can be expected to be much larger, because the contribution to the flux integral for, say, core characteristics would be significantly larger.
Nevertheless, the result shows that imaging must be used in multidimensional calculations and especially in configurations where the topology of the system relative to the observer is known, e.g. an accretion funnel on the far side of the object.

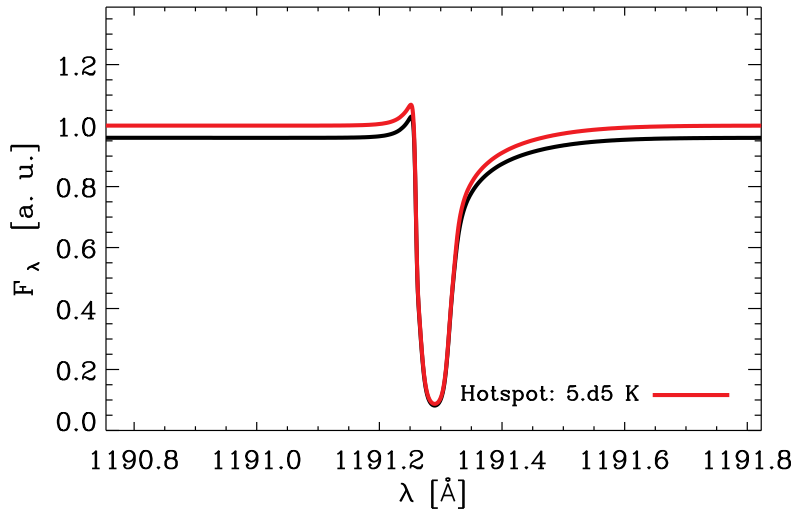

(a)

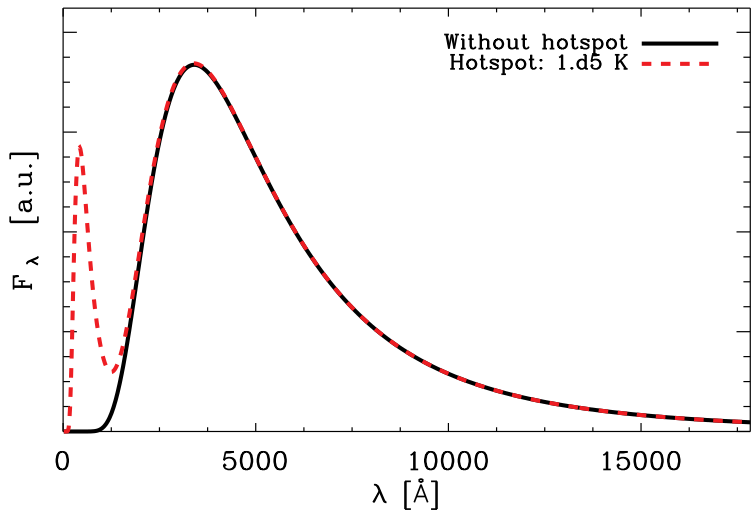

(b)

Figure 6.16: The effects of a hot spot on the emerging spectrum are shown. In (a) the influence on a line profile is shown whereas in (b) the continuous spectra of a gray atmosphere are compared.

Chapter 7

Numerical Implementation

The calculations from Chapter 6 are based on a numerical implementation of the technique described in Chapter 5. This implementation is a test driver of the radiative transfer routines as there is no input of physical quantities as for instance abundances and opacities of species. Instead the atmosphere is crudely described by a few parameters.
A physical description of model atmospheres is used in sophisticated atmosphere codes. In order to utilize the framework provided by such a code the numerical solution of the radiative transfer must be inserted into the atmosphere code.
The general stellar atmosphere code package `PHOENIX` is used for the implementation in this work. The existing framework of `PHOENIX` and its previously implemented radiative transfer solution allow for convenient testing of the new implementation. In the following the `PHOENIX` solution will be referred to as the default or old method of solution while the technique from Chapter 5 will be referred to as new or general radiative transfer solution.

The memory resources needed by the new radiative transfer solver are discussed in Section 7.1.
The inclusion of the general radiative transfer into the code package `PHOENIX` is described in Section 7.2.
Section 7.3 describes the testing of the implementation and discusses the results whereas the numerical performance and possible improvements are discussed in Section 7.4.

7.1 Memory Demands of the General Relativistic Radiative Transfer

The formal solution and the ALI scheme which have been introduced in Sections 5.1 and 5.2 have a numerical disadvantage. They are formulated in matrix notation with the number of wavelength points being one of the factors which determine the size of the matrix. Since the different wavelengths used in the calculation of a typical spectrum is usually quite large the matrices involved in the solution will be also large.
In order to perform a formal solution along a given ray, all matrix elements as well as all interpolation coefficients for all wavelengths and all spatial points must be known. In the

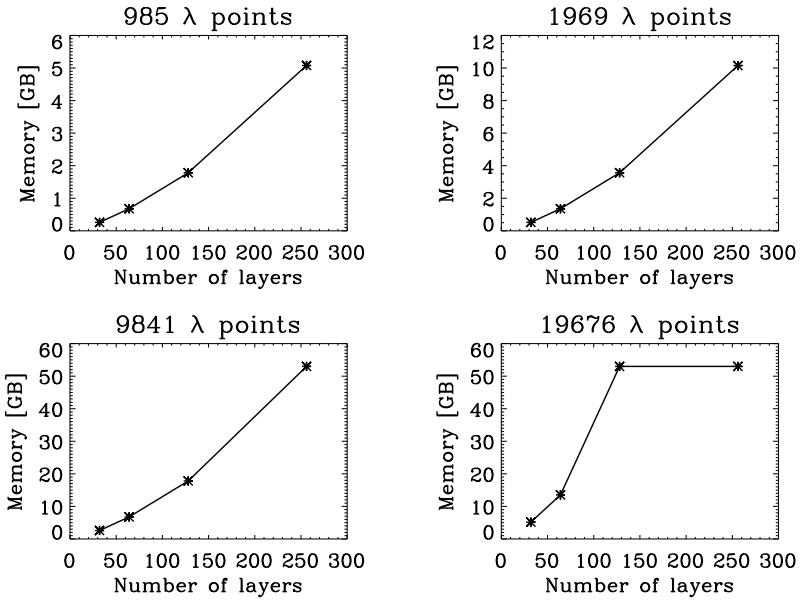

Figure 7.1: The used memory is plotted over number of layers of the model atmosphere for four different number of wavelength points.

work of [Baron and Hauschildt, 2004] this data was saved on disk for every characteristic. The memory demand is even increased as there is the approximate Λ-operator structure which is needed for the ALI step and must also be allocated during the radiative transfer. This structure has a number of $\approx 3 \times n_\lambda \times n_{\mathrm{layer}}^2$ entries that hold an 8 byte long variable, where n_λ means the number of wavelength points and n_{layer} the number of radial layers in the model atmosphere.

Test calculations have been performed with the serial version of the test driver of the radiative transfer which has also been used to calculate the radiative transfer in Chapter 6 to determine the memory demand. The values for the maximal allocated memory are not exact, because not every memory allocation is tracked. The dominant contributions however are tracked and indicate the approximate consumed resources.

In Figure 7.1 the maximal allocated memory during a ALI step is shown for four different sets of wavelength points: 985, 1968, 9841, and 19676 points.

The allocated memory shows an approximate quadratic dependence on the number of layers. However, the calculations were performed only for a small set of different n_{layer}: 32, 64, 128, and 256.

For 19676 wavelength points the memory is capped at 53 GB as the calculations failed for these configurations as the available memory was exhausted. The calculations were performed on a node of the HLRN[1] with 53 GB available memory. Hence the 53 GB in the plots must be seen as a minimum of the real demand for that calculation.

In Figure 7.2 the variation of the allocated memory over the number of wavelength points

[1] Norddeutscher Verbund für Hoch-und Höchstleistungsrechnen (HLRN). `http://www.hlrn.de`

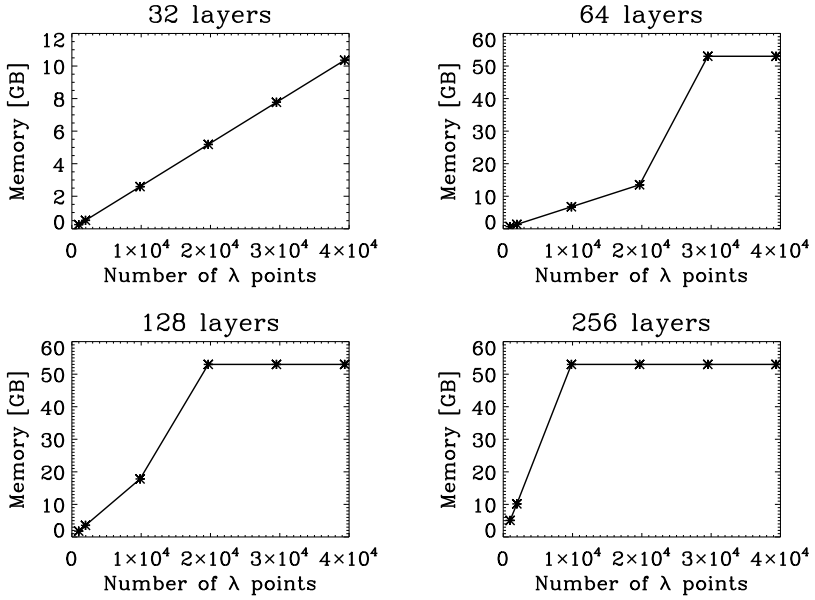

Figure 7.2: The used memory is plotted over number of wavelength points for different numbers of layers of the model atmosphere.

is shown for four different numbers of layers – 32, 64, 128, and 256. In addition to the numbers of wavelength points used in Figure 7.1, 29519 and 39357 wavelength points were used to create the data points.

The more layers are used in the model the stronger the allocated memory depends on the number of used wavelength points. For models with a larger number of layers the available memory is quickly exhausted.

The information from the Figures 7.1 and 7.2 can be combined into a surface plot of the maximal allocated memory which is shown in Figure 7.3. The maximal available memory of 53 GB is reached for several combinations of parameters.

At first glance these tests indicate that the new general numerical method is not feasible for use on the available hardware because of the high memory demand. However, using domain decomposition in the parallelized version of the code the memory demand per processor can be decreased. With a processor working only on a few characteristics in the formal solution, the storage requirements for the characteristics data is decreased accordingly. In an optimal situation there is the same number of processes as there are characteristics and every process just has to keep the data for one characteristic in memory. Hence an increase in the number of processes will minimize the memory requirements for every single process and the memory allocation is dominated by the data structure for the approximate Λ-operator alone.

For instance in the calculations shown in Figures 7.1 to 7.3 the maximal allocated memory for 64 layers and 9841 wavelength points is ≈ 6.8 GB for a serial run. A parallelized version of the code with 12 tasks used for similar parameters, 64 layers and 10389 wavelength points, only ≈ 2.5 GB of memory per processor. As the size of the approximate Λ-operator

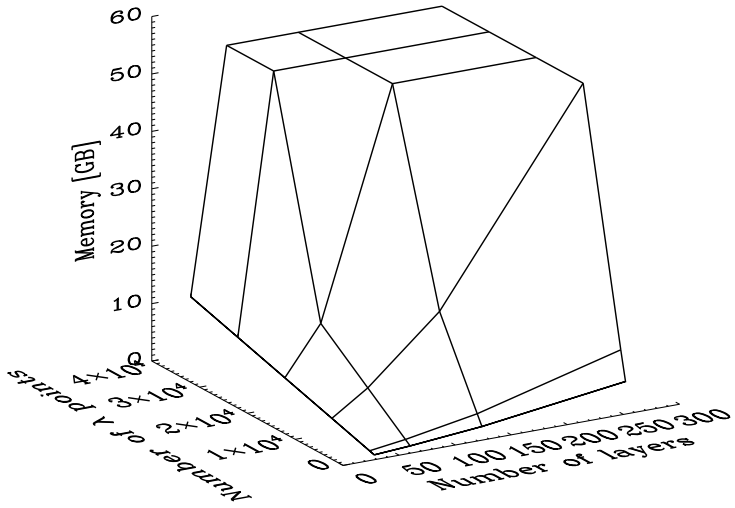

Figure 7.3: Two-dimensional plot of the used memory over the number of layers and wavelength points. The plot is capped at 53 GB since this was the maximal available memory. It is obvious that large a number of either layers or wavelength points can exhaust the available memory very quickly.

depends linearly on the number of wavelength points detailed models with $\approx 10^5$ different wavelengths would need $\approx$ 25 GB of memory. Such calculations can already be performed with state of the art shared memory supercomputers. However, in order to realize this, most of the processors on a shared memory node must remain unused to increase the effective memory per processor while computing.

7.2 Implementation in PHOENIX

In the following the integration of the general radiative transfer implementation into an existing code package is outlined. The code package of choice is the PHOENIX code. It is a general stellar atmosphere code which is capable of the calculation of atmospheres and spectra for a wide range of objects.
All features of PHOENIX as for instance multi level NLTE calculations and dynamic opacity sampling are not subject to change[2] in general relativistic atmosphere modeling and are not influenced by the method used to obtain the radiation field.
That means that in order to model general relativistic objects with PHOENIX only routines for the calculation of an appropriate structure and the general solution of the radiative transfer must be added.

[2]The need to adopt the model description to the extreme environments of compact objects not withstanding.

This work focused on the inclusion of the radiative transfer, because its implementation is the same for all possible model structures – from neutron star atmospheres to accretion flows.

A general PHOENIX radiative transfer iteration is schematically shown in the left part of Figure 7.4 and can be summarized as follows. At first the structure of the atmosphere is calculated. The details of the calculation are different for different model types, but have in common that from the structure information – temperature T and occupation numbers $[n]$ – the opacities can be calculated. Then for every wavelength present in the model the opacities, the Λ^*-operator and the radiative transfer are calculated in a wavelength loop. Depending on the model type of the atmosphere the radiative transfer at a given wavelength is either independent from other wavelengths or depends on the prior wavelength point. This dependence is resolved by a recursive upwind scheme in a sorted wavelength grid. Hence the radiative transfer can be calculated wavelength by wavelength. With the radiation field known the contribution to a radiative rate of a transition for each wavelength can be calculated. The complete rate is the sum of all contributions whose wavelength fall within the line profile of the transition. In order to solve the statistical equations the rates are stored in another approximate operator R^* can be used [Hauschildt, 1993, Hauschildt and Baron, 1999] which is constructed from the diagonal components of the Λ^*-operator at the given wavelength.
After the wavelength loop the radiation field and the rates are known, the rate equations are solved, and the new occupation numbers $[n]$ are calculated.

The current scheme must be modified, because the general relativistic radiative transfer must be solved for all wavelengths simultaneously. The equivalent radiative transfer scheme is shown on the right of Figure 7.4.
The main difference to the default PHOENIX scheme is that all opacities for all wavelengths must be known before the solution of the radiation transport can proceed. Hence instead of solving the radiative transfer in the loop over wavelength the opacities are saved for every wavelength. Then the radiative transfer can be calculated after the wavelength loop.
After the radiative transfer calculation the radiation field and the Λ^*-operators for all wavelengths are known. Therefore, the same framework used in the default PHOENIX scheme can be used for the general radiative transfer solver. In order to do so, a second wavelength loop is required which calculates the rate operators in the same way as before with the radiation field being provided for each wavelength and all calls which are purely related to the radiative transfer were omitted. After the rates are complete the iteration step proceeds exactly the same way as for the standard radiative transfer.

In order to make the computation of detailed atmosphere models feasible, the PHOENIX code is parallelized in several ways [Hauschildt *et al.*, 1997, Baron and Hauschildt, 1998, Hauschildt *et al.*, 2001]. Hence the implementation and the setup of the general radiative transfer solver must also be parallelized accordingly.
Most of the parallelization present in PHOENIX does not affect the radiative transfer. Only the wavelength parallelization is of interest, because the opacity data is exclusively known

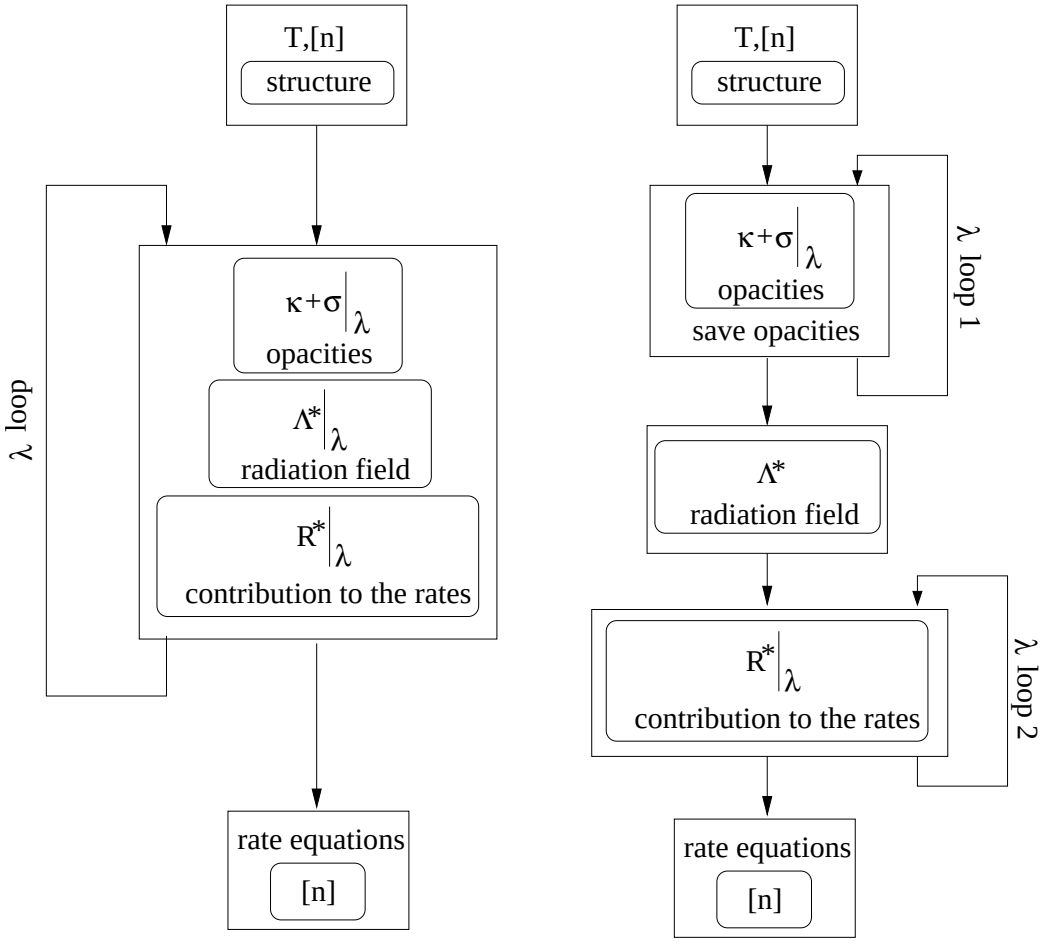

Figure 7.4: Flowcharts of the principle solution to the radiative transfer in PHOENIX. Rounded boxes indicate that the contained quantities are calculated at that step.
Left: The default PHOENIX scheme for a radiative transfer iteration is shown. All wavelength dependent quantities are calculated in one wavelength loop.
Right: The general radiative transfer iteration is shown. Since the radiative transfer cannot be solved for a given wavelength alone, the scheme needs two wavelength loops to calculate the same data as a default PHOENIX iteration.

on a wavelength cluster and must be broadcasted to all other processes in order to perform a radiative transfer step within the new general framework. The broadcast of the opacity data takes place after the wavelength loop is completed. This minimizes the communication overhead between the processes during the wavelength loop.
With all the data in place after the first wavelength loop, every process can then perform a general radiative transfer iteration. This iteration itself is also parallelized but is independent from other parallelizations in PHOENIX.
The calculation of the matrices for the formal solution is parallelized over wavelength whereas the formal solution itself is parallelized over the characteristics. The actual ALI step however is performed on every process.
From this follows that in contrast to the default PHOENIX framework there is no need to send wavelength dependent quantities between the wavelength clusters, because every process computes these itself.

7.3 Test of the Implementation

It is essential to have a reliable test for the results from a new code (see Section 6.1). In case of the implementation of the general radiative transfer in PHOENIX the well tested default radiative transfer solver offers such a reliable test. Besides the solution of the radiative transfer nothing has changed in the setup of PHOENIX and the results must be identical up to the prescribed accuracy of the radiative transfer solvers.
In order for the test results to be comparable the radiative transfer must be solvable by either method. Hence the gravitational mass was set to zero and a monotonic velocity field was used.
In a monotonically expanding atmosphere the coupling term a_λ is always positive. The intensities at a given wavelength only depend on the shorter wavelengths. This is shown in Figure 7.5 in which the dependence of the specific intensity at a point is indicated by arrows.
This system can be solved recursively or with the use of the matrix equation. However all $\bullet^{\mathrm{super}}$-terms of the matrix (see relations (5.20) to (5.22)) will be consequently zero. Nonetheless the full method and framework of the general solution is used.
At first the two different implementations have been tested as serial versions. This has allowed for quick testing and debugging on a standard desktop computer. However, this has limited the possible number of wavelength points, because the memory demand per CPU for serial calculations is significantly higher (see Figure 7.3). Hence approximately 1000 wavelength points have been used in the calculations. This small size of the numerical system proved to be valuable in the debugging process, since the detection of boundary effects was not suppressed by the sheer number of wavelength points. Hence inconsistencies in the construction of the approximate operator, the spatial boundary conditions and the wavelength boundary conditions could be removed.
Further the states of allocated arrays and pointers were adjusted to allow for multiple successive iterations without memory leaks.

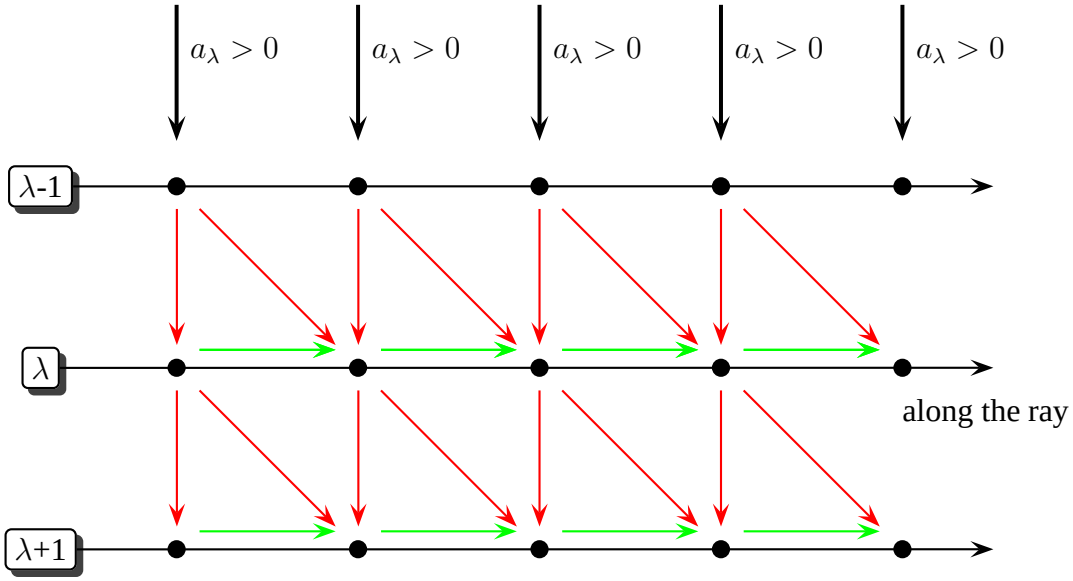

Figure 7.5: The influence of the different points on each other is color coded – red arrows indicate an influence on longer wavelengths while green represents an influence without a change of wavelength.
With the sign of a_λ being always positive the wavelength derivative sense does not change from point to point and the radiative transfer can be solved recursively.

An parallelized version has been first tested against the results from the serial runs with a small number of wavelength points. With the results being perfectly identical for all versions the implementation has been tested in a more realistic model iteration.

PHOENIX has been used in the supernova mode, with $\approx 10^4$ wavelength points and neutral hydrogen treated in NLTE. In order to investigate the differences due to the different radiative transfer solver the structure has been held constant from iteration to iteration. This assured that any occurring differences were purely related to the radiative transfer.

A good indicator for the agreement of the results from both methods besides the radiation field itself are the departure coefficients b_i (see Section 2.4). The b_i depend directly on the radiative rates which directly depend on the radiation field and are very sensitive to variations of the mean intensity.

In the following b_i^{old} means the departure coefficients resulting from the default PHOENIX framework, and b_i^{new} the departure coefficients for the new general framework.

The results for the converged departure coefficients of neutral hydrogen are shown in Figure 7.6. The upper panel shows the default values whereas the lower shows the new coefficients. All calculated levels of the hydrogen atom are shown and there is no obvious deviation visible.

However, the detailed values of the departure coefficients for half of the levels are different in one or more layers of the atmosphere. These differences are best visible in a relative plot.

In Figure 7.7 the ratio $\frac{b_i^{\mathrm{old}} - b_i^{\mathrm{new}}}{b_i^{\mathrm{old}}}$ is plotted over the radial optical depth grid τ. The y-axis is scaled with the factor 10^{-5} and hence larger amplitudes around zero mean larger deviations. The points which belong to one level of hydrogen are connected by a line. The jagged appearance of the line shows that in no consecutive layers in the atmosphere the coefficients were different, although multiple deviations for a single level also occurred.

The maximal deviation from zero is of the order of 10^{-4}. For all practical purposes the NLTE calculations driven by the two radiative transfer method can be assumed to deliver equal results.

It should be noted that the lack of deviation for most of the levels is not due to the exactness of radiative rates calculated by the radiative transfer, but is a consequence of the five leading digits of the departure coefficients saved. Hence all b_i are different internally, but only in a few cases the differences add up to fall short of the desired accuracy.

The other obvious test for the quality of the agreement of the radiative transfer calculations are the spectra themselves. In Figure 7.8 the comoving spectra of the same supernova models which were used in the departure coefficient comparison are shown. The top panel shows the spectrum from the old default radiative transfer, whereas the lower panel shows the result for the new general method.

From a check by eye the spectra seem perfectly identical. In order to allow for a direct comparison the spectra are shown in one plot in Figure 7.9. The old spectrum is plotted in a thick black line and the new one is overplotted in red. For a clearer comparison of the spectral details the plot range was reduced to only 250 Å.

The agreement appears to be flawless in a mere inspection by eye. In order to quantify the

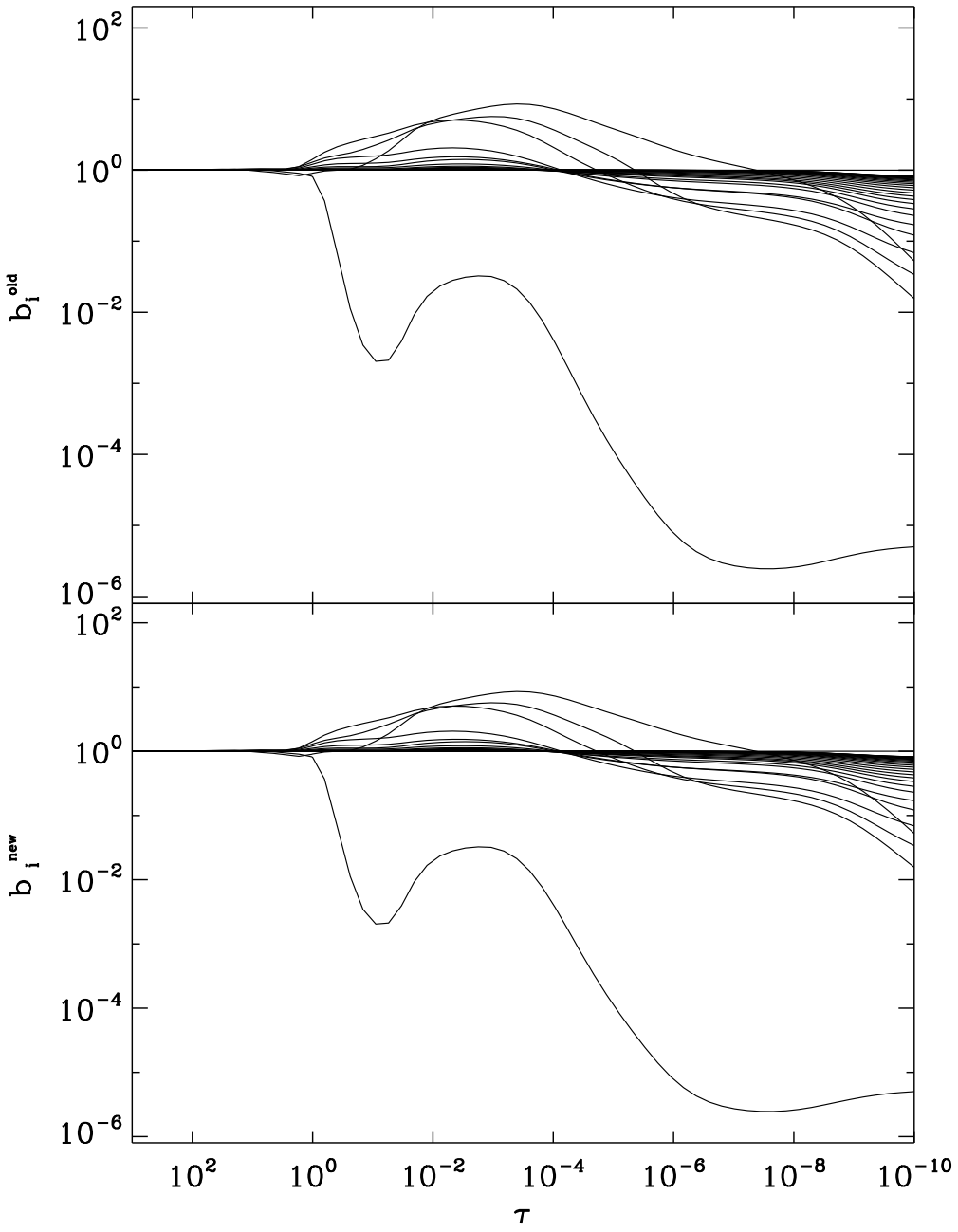

Figure 7.6: The departure coefficients for the first 30 level of neutral hydrogen are shown for two cases. The upper panel shows the results for the old default implementation in PHOENIX, whereas the results for the new general method are shown in the lower panel.

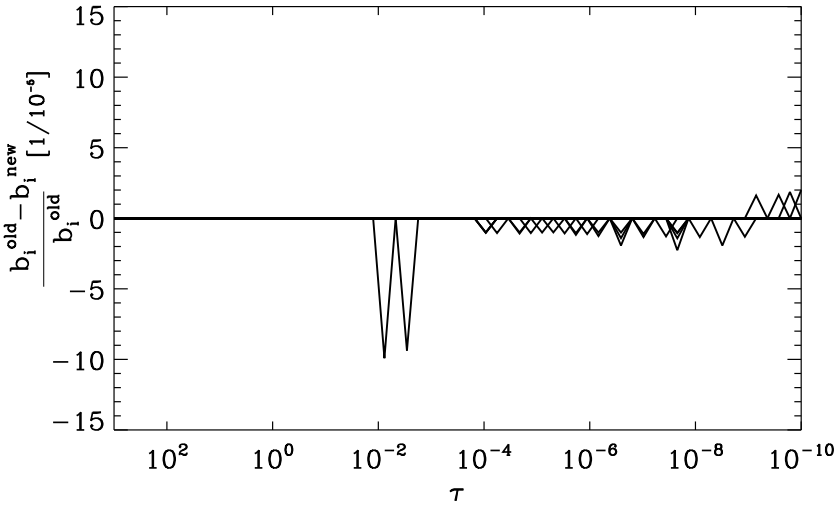

Figure 7.7: The relative differences of the departure coefficients derived from calculations with the old as well as the new general radiative transfer solver for the first 30 levels of neutral hydrogen are shown.

similarity the ratio

$$\left| \frac{F_\lambda^{\mathrm{old}} - F_\lambda^{\mathrm{new}}}{F_\lambda^{\mathrm{old}}} \right| \tag{7.1}$$

is plotted in Figure 7.10. The absolute value of the ratio is plotted, because a logarithmic scaling is used as a large range of values is covered in the plot.
Every point represents the ratio at the according wavelength point. For most points the match is indeed very good as the bulk of the ratios have value of the order of 10^{-5}.
Some data points even show smaller errors down to the order of 10^{-10}. However, there are a couple of data points at around 950 Å which show a difference in the spectra of up to a few percent.
The according part of the spectrum of the spectra is shown in detail in Figure 7.11. There is no evidence that there is a problem regarding the radiative transfer.

In all preceding tests of the implementation the structure has been held constant and just the occupation numbers and the radiation field have been iterated. Since the new radiative transfer can be considered as consistent after the testing its effect on the temperature correction must be investigated.
Within the limits of the model assumptions made in regard to the structure of the model atmosphere, the physical accuracy of the calculated structure depends on the consistency between the radiation field and the given structure. This consistency is checked via the energy conservation in the comoving frame of the local observer. This check is valid as long as there is no time independence in the calculation allowed for and the model atmosphere is assumed to be stationary.

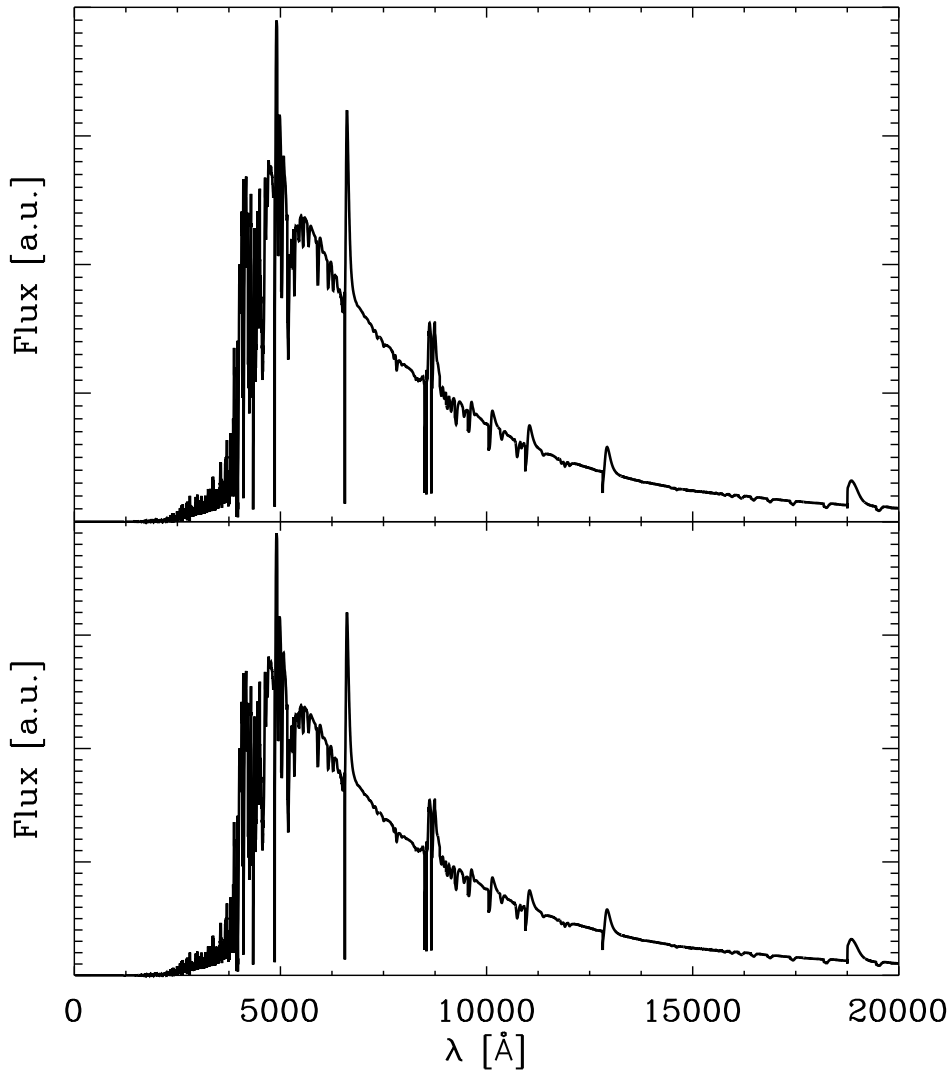

Figure 7.8: The upper panel shows the comoving spectrum of a default radiative calculation with PHOENIX. The comoving spectrum from the according calculation with the new general radiative transfer solver is shown in the lower panel.

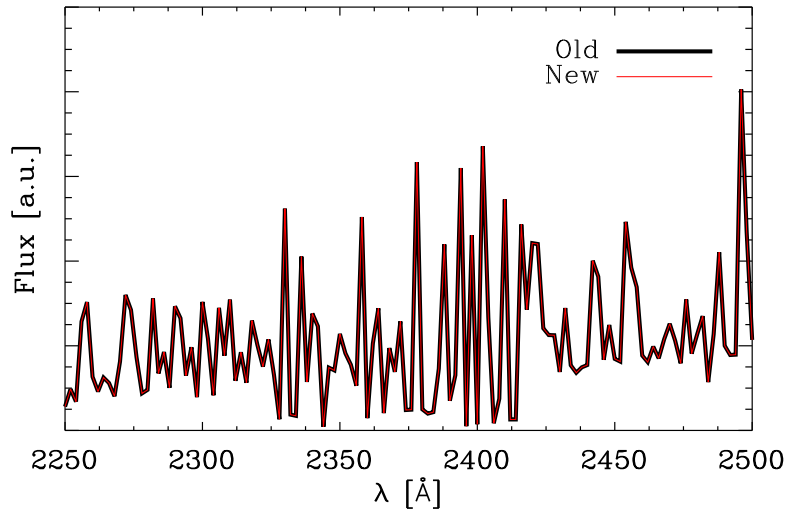

Figure 7.9: A 250 Å broad section from Figure 7.8 is shown. The spectra from the two different methods for the solution of the radiative transfer are plotted over each over.

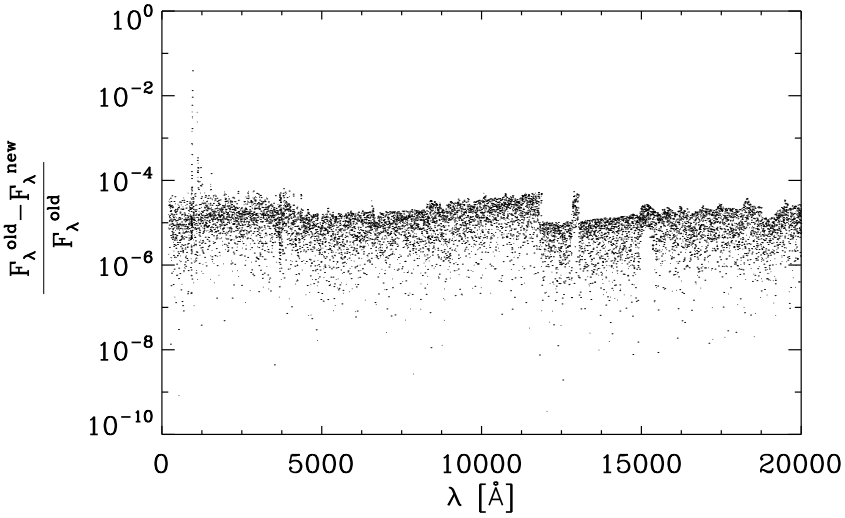

Figure 7.10: The relative ratio of the comoving spectra that were calculated with the old and the new radiative transfer solution is shown. The absolute value of the ratio is plotted in order to use a logarithmic scale.

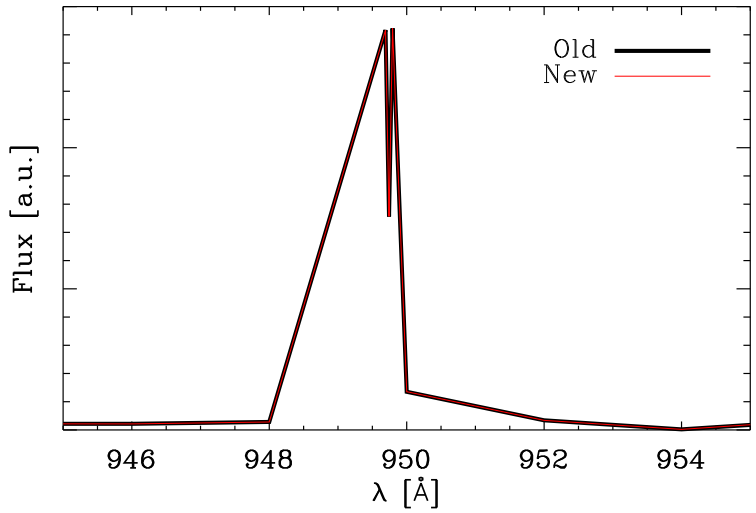

Figure 7.11: A detailed part from both spectra in Figure 7.8 is shown in one plot. It covers the wavelength range where the deviation of the two different spectra is of the order of a few percent (see Figure 7.10). The original spectrum is plotted as a thick black line and the new one is overplotted in red.

The energy conservation is determined by the condition that the absorbed energy in a volume element balances the emitted energy. When energy transport via material flows, for instance by convection, is absent this energy balance is fully determined by the radiation field [Hauschildt *et al.*, 2003]. In order to balance the energy conservation the local temperature of the gas is corrected. This change of the model structure means that a new radiation field must be calculated. This changes the energy balance and a new temperature structure can be calculated.
In the case of a sufficiently small temperature correction and errors the model atmosphere can be regarded as physically consistent.

The accuracy of the radiation field itself is determined by the prescribed accuracy in the ALI step (See Equation (7.2)). The accuracy of the convergence is a quantity which is averaged over all layers in the model. From this follows that although globally converged the radiation field in some layers might not already be converged up to the prescribed accuracy. Hence it must be expected that the energy balance in these layers can be different for two different solutions of the radiative transfer.
Indeed this is found in a comparison of two calculations – one with the new the other with the old method of solution – of the same atmosphere model. The differences in the radiation field added up in the flux integral over wavelength. This was especially true for the deepest layers where the differences were as large as one tenth of a percent.
The temperature correction procedure produced a slightly different temperature structure. This results in a change of the occupation numbers and the opacity. Further the departure

coefficients start to be different, because they are very sensitive to changes in the temperature.
After convergence according to the energy conservation in both models the structures are different. However, the structures did not diverge and are physically still similar. This can also be seen in the spectra as they are still very alike.
Both model atmospheres are consistent within the accuracy of their according radiative transfer solution. None of the radiative transfer solvers assures the prescribed accuracy for the radiation field in all layers. Hence there is no way to favor the results from one method over those from the other. As both methods produce physically similar consistent atmospheres there is no obvious reason for tightening the accuracy checks in order to improve the energy balance. The increase in the computational cost is not justified by the small improvement of the physics. This is especially true for the general radiative transfer method because its computational cost is already very high.

7.4 Numerical Performance

The time needed for a general radiative transfer iteration directly depends on the time needed for a formal solution.
This dependence is crucial for the overall numerical performance, because the formal solution is used very often during an iteration. In numbers the formal solution gets called $n_{\mathrm{ray}} \times n_{\mathrm{ALI}}$ times, with n_{ray} being the number of characteristics and n_{ALI} the number of ALI steps.
The formal solution is of the form

$$\begin{aligned} x &= \mathbf{A} \cdot x + b \\ (\mathbf{1} - \mathbf{A})\, x &= b \\ \mathbf{M} x &= b \end{aligned}$$

The explicit form is given in Figure 5.2.
In [Baron and Hauschildt, 2004] several different solvers have been tested. The overall best solver has been the SuperLU package [Demmel *et al.*, 1999]. It has also offered very good performance in the testing of the implementation in `PHOENIX`. However, the large size of the numerical system to be solved is well suited for iterative solvers. Hence the feasibility of iterative methods for the formal solution has been investigated.
At first a Jacobi type solver [Golub and Van Loan, 1989, Zurmühl and Falk, 1986] has been implemented. The right hand side of the linear system has been used as starting values and the system was iterated to a relative accuracy of 10^{-10}. The method works reasonably well as it reproduces the results of SuperLU. The performance has been very bad, however. In case of the longest tangent characteristics the solver would use up to 1000 iterative steps.
In order to speed up the convergence rate a Ng type acceleration [Ng, 1974] has been implemented. In principle it saves the result from previous – in this case three – iterations

and extrapolates the expected result. The acceleration was successful as the solver indeed needed approximately half as much iterations.

It should be noted that the starting point of the Ng acceleration can affect the overall performance. In some cases a start of the Ng method before the 20th iteration could in fact slow down the whole iteration process.

The performance of the Jacobi type solver nonetheless could not match the performance of the SuperLU package as it has been up to ten times slower. Hence an other iterative solver – a Gauss-Seidel type solver [Golub and Van Loan, 1989, Zurmühl and Falk, 1986] – has been implemented. The Gauss-Seidel method not only iteratively updates the variables locally, but uses these new calculated values in the calculation of the following entries of the solution. This potentially speeds up the convergence of the solution.

In the case of the formal solution this is indeed the case. The Gauss-Seidel method is very quickly reaching convergence in a few steps. Depending on the size of the matrix usually two up to 15 iterations suffice for convergence. The resulting computational times are comparable to those of the SuperLU package. Further there was no evidence found that the size of the matrix system would pose a problem to the method of solution.

However, the numerical performance should still be improved when possible. An iterative solution converges faster the better the initial guess of the variables is. This fact leaves room for improvement. The formal solution is performed between two ALI steps in order to update the source function for the following ALI step. Thereby the matrix itself remains unchanged and only the right hand side – essentially the source function – was changed by the last ALI step.

In the first implementation the solver would use this right hand side as a starting condition, because of the lack of a more sophisticated guess. For two successive formal solutions however there is such a guess, since the last solution of the radiation field along the characteristic can be used. This starting condition is much better suited than the right hand side especially if the source function did not change significantly in the last ALI step.

In order to use the last result as a starting condition it must be saved on the process which worked on it. The memory demand is minimized as the distribution of the formal solutions to different process is a round robin scheme. Hence every process can determine in advance which characteristics it will work on and allocate the appropriate arrays.

The impact on the total allocated memory will be minimized if enough processes are used since then only one solution must be saved additionally in memory.

The improvement of the initial guess indeed reduces the time for a Gauss-Seidel step by a factor of five. The final performance of the different solvers for a test model with 64 layers and 6432 wavelength points is compared in Figure 7.12. The logarithmic time in seconds is plotted over the number of formal solutions performed. The results for the standard SuperLU package and for the two iterative solvers of Jacobi and Gauss-Seidel type with the improved initial guesses are shown. The time for the first formal solution is significantly higher than the following for all solvers. This is due to the construction of the Λ^*-operator which is recognized by the timing procedure as a part of the formal solution.

The Jacobi solver profits from the improved starting conditions, however its performance is too bad in order to be a viable replacement for the SuperLU package. The contrary is

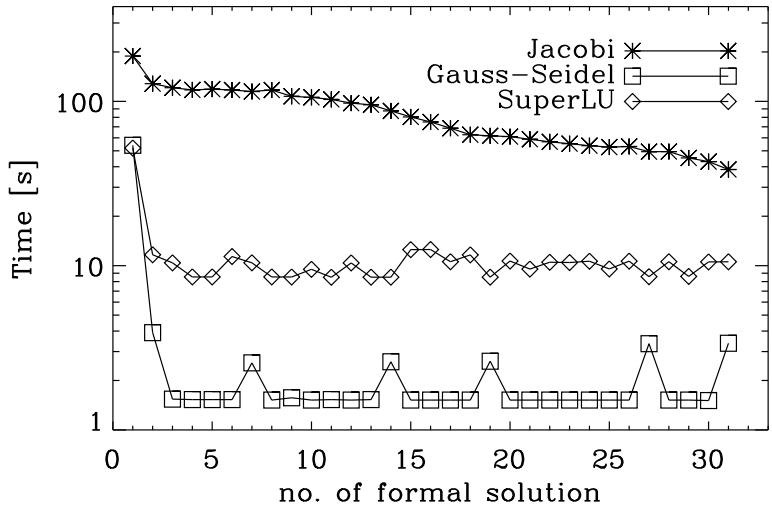

Figure 7.12: The time needed for a formal solution is plotted over the number of formal solutions performed between ALI steps.

true for the improved Gauss-Seidel method. SuperLU is only able to outperform this solver in the first solution where its performance suffers from the unrefined starting conditions. From the second iteration on the Gauss-Seidel method is three to four times faster than SuperLU.
Further there are is no evidence that the Gauss-Seidel method will perform worse for larger systems. A test model with 64 layers and 19276 wavelength points was calculated with the refined Gauss-Seidel method. The timing result is compared to the Gauss-Seidel and SuperLU results from the smaller test case in Figure 7.13. The plot starts at the second formal solution in order to clarify the results by reducing the plot range.
The average time for a formal solution in the large test case is $\approx 5 - 6\,\mathrm{s}$. By tripling the number of wavelength points the computing time was just doubled and the Gauss-Seidel method still performs faster than SuperLU in the smaller test case.
From this follows that the implemented Gauss-Seidel method can replace the SuperLU package. Not only the issue of the large systems is resolved, but in addition this method is faster, appears to be very robust, and uses less memory.

The previous part of this Section dealt with the speedup of the calculation of the formal solution. This has been motivated by the fact that the formal solution is the most often invoked numerical operation during an ALI step as it is used $n_{\mathrm{ray}} \times n_{\mathrm{ALI}}$ times. In order to save computational time also the number of calls can be reduced. Since the number of rays is a fixed number only the number of ALI steps can be reduced.
According to [Auer, L., 1987] a combination of an ALI with a Ng acceleration is well suited to reduce the number of iteration steps.
An iteration is treated as converged if the changes of the mean intensities are below the

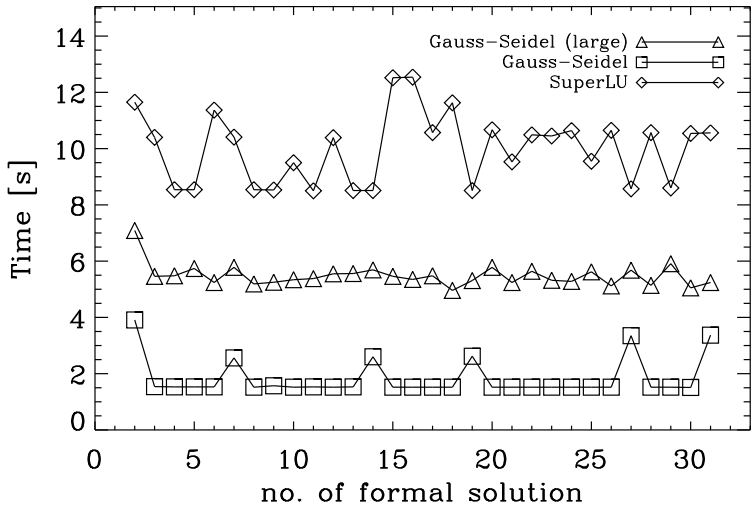

Figure 7.13: The time needed for a formal solution is plotted over the number of formal solutions between ALI steps. The first formal solution was omitted for a cleaner comparison of the times

desired accuracy. In case of PHOENIX these changes are defined as the ratio

$$s_\lambda = \left\langle 2\frac{J_\lambda^{i+1} - J_\lambda^i}{J_\lambda^{i+1} + J_\lambda^i} \right\rangle \tag{7.2}$$

The upper index i indicates the according iteration whereas the brackets indicate an average of the ratio over all layers in the atmosphere. The quantity s which is tested versus the prescribed accuracy is the maximum of all the s_λ.

The convergence rates s for a radiative iteration with and without Ng acceleration in the ALI step are shown in Figure 7.14. The results for Ng accelerated iterations are shown for two different starting points, after the 10th and after the 20th iteration. Indeed the Ng accelerated iterations outperform the normal ALI. The Ng acceleration which started at the tenth ALI step needs three iterations less than the unaccelerated ALI. The Ng accelerated iteration that started at the 20th ALI step outperforms the other Ng iteration by one further iteration.

It must be noted that the Ng acceleration fails to accelerate the iteration if it is already started at the fourth iteration. In this case the number of iterations has been equal to the unaccelerated case. It appears that the data in the first iterations is not suited to be extrapolated by the Ng method. A further delay of the starting point of the acceleration resulted in no further speed up. It is expected that the optimal starting point of the Ng acceleration depends on the given problem.

Although the efforts made to improve the performance of the general radiative transfer were successful the new solution is no alternative to the default method used in PHOENIX.

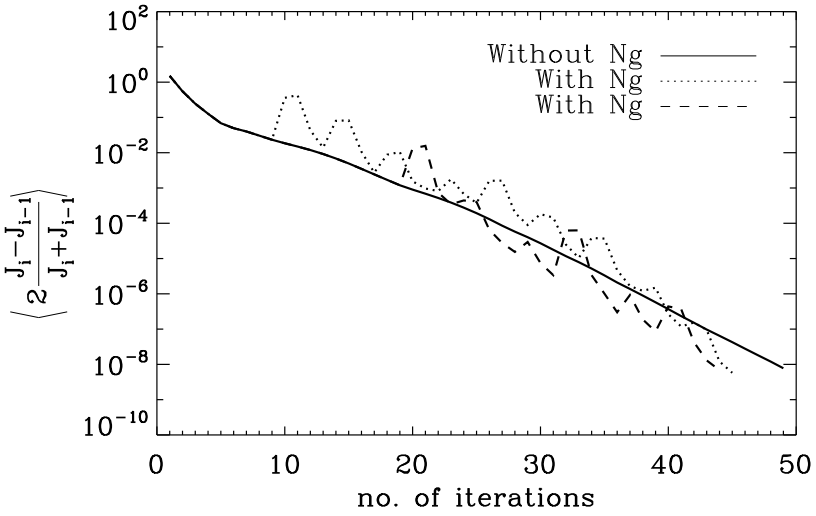

Figure 7.14: The ratio from Equation (7.2) is plotted over the number of iterations for Ng accelerated and normal ALI iterations.

The ratio of the computational time costs of both methods varies slightly with the size of the numerical system, but as a rule of thumb the general method takes about 15 times longer. In the case of a NLTE calculation it even takes about 20 times longer due to the need of the second wavelength loop.
But only the new general solution is capable of describing arbitrarily in wavelength coupled radiative transfer problems. Its use is not limited to the solution of general relativistic radiative transfer, but also applies to arbitrary radial velocity fields. Due to the generality of the method and the formulation developed in Section 3.4 it is also possible to solve the radiative transfer in arbitrary velocity fields in a curved background spacetime within the PHOENIX framework.

Chapter 8

Conclusion and Outlook

The equation of radiative transfer has been formulated in Chapter 3 in terms of the specific intensity. Although this description is physically equivalent to the commonly used description via the distribution function, it offers a new ansatz. The equation of transfer then assumes its characteristic form which is commonly used in special relativistic calculations of radiative transfer. This form is suited for the use of the powerful ALI formalism which is a state of the art method of solution for classical radiative transfer.
The main difference of the developed ansatz to the established solutions of general relativistic radiative transfer is the wavelength parameterization. In general radiative transfer the wavelength is customarily parameterized along the null geodesic with the help of constants of motions. This causes the discrete wavelength grid of the radiative transfer to be dependent on the spatial position along the characteristic.
The ansatz developed in this work keeps the wavelength grid fixed for all spatial points of the atmosphere. This requires that the changes of the momentum coordinates along the characteristics in the equation of transfer are tracked. Since the parameterization of the specific intensity also does not change, the gravitational shift of wavelength is described by a wavelength derivative. The properties of the derivative are contained within the coupling parameter a_λ which in general changes its sign along the null geodesics of the underlying spacetime. This requires a general solution of the radiative transfer problem such as the formal solution described in Section 5.1.
The resulting description of the radiative transfer is more complex and harder to solve but is indispensable for the calculation of radiative line transfer. Because of the fixed wavelength grid, any spectral line can be resolved by the same set of sampling wavelength points throughout the atmosphere. In the case of a varying wavelength grid, the number of wavelength points needed to achieve the same resolution would be much larger and prohibitively large for detailed spectra.
This argument also holds for relativistic flows in flat as well as curved spacetimes where the wavelengths are coupled due to the Doppler effect by the differentially moving flow. The ansatz for radiative transfer within flows in curved spacetimes has been developed in Section 3.4. It applies the same explicit tracking to the momentum variables as in the static case and is therefore suited to describe radiative line transfer in flows in a curved background spacetime.

The ansatz of this work is general enough so that it can also be applied to the Kerr metric. In the absence of a flow, the equation of radiative transfer is given in Section 3.3.4. Although the inclusion of a flow in the radiative transfer in the Kerr metric can proceed in the way described in Section 3.4, the corresponding calculation is an arduous task. The coefficients of the differential operator for the momentum variables in the case of static radiative transfer in the Kerr metric (see Equation (3.55)) are already very complex as can be seen from the according Ricci-rotation coefficients in Appendix B.2. In the case of an additional velocity field, this ansatz results in an unwieldly complicated description. This is due to the fact that the coefficients must describe the turning and twisting of the base vectors for the photon momentum which are complicated functions of the base coordinates of the metric.

In order to resolve this problem, another ansatz is better suited. In case of isotropic emissivities and opacities, the ansatz described in [Chen *et al.*, 2006] can be used. Here, the explicit knowledge of the photon momentum in terms of the local base coordinate system is not necessary in order to describe the radiative transfer. In addition, the local observer frames can be assumed to be constructed in such a way that all the components of the photon momentum but the wavelength are constant. This strategy follows [Schinder and Bludman, 1989], but explicitly avoids the parameterization of the wavelength in terms of the coordinates of the metric.

The distance traveled by the photons in the local instantaneous rest frames can be related to an affine parameterization of the null geodesic. Since the calculation of the null geodesic can be solved independently from the radiative transfer, the effective path length along the characteristic can be calculated without explicitly integrating the system (4.5). The integration of the comoving solid angle can be performed in the inertial frame if the comoving solid angle is related to the inertial solid angle.

This ansatz is also the better choice if the radiative transfer is extended to multiple dimensions as described in [Hauschildt and Baron, 2006]. Then the explicit solution of an ordinary differential equation for each of the numerous characteristics is superfluous and the rays are described analytically. In the extension of the general relativistic radiative transfer to multiple dimension, this new ansatz should be employed. The formal solution can remain unaltered and must only be adopted to the multidimensional description.

The theoretical framework for general relativistic radiative transfer is complemented by a numerical implementation for the one-dimensional Schwarzschild case. The test calculations have been presented in Chapter 6. The radiative transfer has been calculated in a testing environment with a two-level atom spectral line within a flat continuum. The conditions for compact and extended atmospheres as well as relativistic flows have been simulated for a number of different combinations of scattering albedos. It has been found, that the emerging line profiles depend strongly on the structure of the atmosphere. Furthermore, continuous scattering has been found to be important for the detailed shape of the emerging line profiles. The detailed line formation of a NLTE line in the context of general radiative transfer has not been described in the literature before.

In addition to the calculations in static atmospheres, the radiative transfer has been calculated for an accretion like flow in a Schwarzschild spacetime. With the direction of the

velocity field pointing inwards, the classical result shows an reversed P-Cygni profile with an extended emission feature towards shorter wavelengths. In the general relativistic case, the extent of the blue emission feature to shorter wavelengths is reduced, whereas the red emission feature is extended. Since the blueshifting effect of the velocity field is partially compensated by the gravitational redshift in the line forming process, the influence on the line profiles from accretion flows is especially pronounced.

Another application of the test environment has been the calculation of radiative continuum transfer in gray atmospheres. It has been found that for the case of scattering atmospheres the effective temperatures derived from blackbody fits to observed spectra are too high. Consequently, sophisticated modeling of neutron stars must include the treatment of scattering in the context of general relativity.

After testing the radiative transfer code in a controlled environment, it has been implemented into the atmosphere modeling code package PHOENIX. The general radiative transfer has been implemented in a serial as well as a parallelized version and utilizes the already implemented NLTE framework.

Because the new radiative solver is far more costly computationally, the formal solution and the ALI have been optimized. An iterative Gauss-Seidel method with storage of prior results as starting conditions offers excellent performance in the formal solution. Further the ALI has been optimized with a Ng acceleration which resulted only in a slight reduction of ALI steps. With all optimizations in place, the general radiative transfer solver still needs about 20 times longer for a NLTE calculation than the default PHOENIX transfer. This must not be attributed to a poor implementation, but is due to the different method of solution.

There is still room for improvement of the code. This includes the addition of the parabolic interpolation of the wavelength derivative. The according coefficients have been introduced in Chapter 5. However, the explicit construction of the Λ^*-operator uses a linearly interpolated wavelength derivative. Since the Λ^*-operator is ideally constructed with exact elements the formal solution also uses linear interpolation in the wavelength derivative. In order to use a parabolic interpolated formal solution, the construction of Λ^* must be performed with the help of a formal solution for every layer in the model atmosphere. This strategy will only be effective if the convergence rate of the ALI is dramatically improved.

A bottleneck for the numerical performance is the solution of the ALI itself. The numerical system is suited for the same Gauss-Seidel iteration with improved initial conditions which has been introduced for the formal solution. A substantial speedup of the ALI step would greatly improve the overall performance of the general solver.

In terms of performance the new general radiative transfer solver is not a viable option to replace the old transfer for simple models. It offers the unique possibility to solve the radiative transfer in systems for which it could not be solved before. These include arbitrary velocity fields in flat or curved spacetimes. In the future, one is in the position to construct new models within the framework of PHOENIX. A possible application are model atmospheres of neutron stars. In order to construct the atmosphere structure of these compact objects the general relativistic hydrostatic equations – the Tolman-Oppenheimer-Volkoff equations – must be integrated. In a further step the inclusion of magneto-optical

transfer should be added to increase the realism of the model, because strong magnetic fields are associated with neutron stars.
Another option is the construction of models which describe accretion to neutron stars as well as black holes. In this context a formulation of the radiative transfer in the Kerr metric may be appropriate. Physically realistic models will need a multidimensional description. Therefore, the migration of the general radiative transfer solver to a multidimensional framework would be a prerequisite.
The general relativistic solver can also be applied to general relativistic neutrino transport in core collapse calculations. Due to its generality it can also be applied to non general relativistic atmospheres. Possible applications encompass such diverse atmospheres like pulsating giant stars or shocked radiative flows.

Appendix A

The Ricci-Rotation-Coefficients

The change of the momentum vector of a photon along a null geodesic is subject to a covariant derivative. To calculate the derivative $\frac{\partial p^{(a)}}{\partial \xi}$ in tetrad components one starts off the geodesic equation (4.1) and uses the properties of the tetrad fields

$$\frac{\partial^2 x^\alpha}{\partial \xi^2} + \Gamma^\alpha{}_{\beta\gamma} \frac{\partial x^\beta}{\partial \xi} \frac{\partial x^\gamma}{\partial \xi} = 0 \tag{A.1}$$

$$\frac{\partial p^\alpha}{\partial \xi} + \Gamma^\alpha{}_{\beta\gamma} \frac{\partial x^\beta}{\partial \xi} \frac{\partial x^\gamma}{\partial \xi} = 0 \tag{A.2}$$

$$\frac{\partial e_{(c)}{}^\alpha p^{(c)}}{\partial \xi} + \Gamma^\alpha{}_{\beta\gamma} p^\beta p^\gamma = 0 \tag{A.3}$$

$$\rightarrow \quad p^{(c)} \frac{\partial e_{(c)}{}^\alpha}{\partial \xi} + e_{(c)}{}^\alpha \frac{\partial p^{(c)}}{\partial \xi} = -\Gamma^\alpha{}_{\beta\gamma} p^\beta p^\gamma \tag{A.4}$$

$$p^{(c)} \frac{\partial e_{(c)}{}^\alpha}{\partial x^\beta} p^\beta + e_{(c)}{}^\alpha \frac{\partial p^{(c)}}{\partial \xi} = -\Gamma^\alpha{}_{\beta\gamma} p^\beta p^\gamma \tag{A.5}$$

From this follows:

$$e_{(c)}{}^\alpha \frac{\partial p^{(c)}}{\partial \xi} = -p^{(c)} \frac{\partial e_{(c)}{}^\alpha}{\partial x^\beta} p^\beta - \Gamma^\alpha{}_{\beta\gamma} p^\beta p^\gamma$$

and hence follows for the derivative with $e^{(a)}{}_\alpha e_{(c)}{}^\alpha \frac{\partial p^{(c)}}{\partial \xi} = \frac{\partial p^{(a)}}{\partial \xi}$

$$\frac{\partial p^{(a)}}{\partial \xi} = -e^{(a)}{}_\alpha \left(p^{(c)} \frac{\partial e_{(c)}{}^\alpha}{\partial x^\beta} p^\beta + \Gamma^\alpha{}_{\beta\gamma} p^\beta p^\gamma \right) \tag{A.6}$$

$$= -e^{(a)}{}_\alpha \left(p^{(c)} p^{(d)}\ e_{(d)}{}^\beta \frac{\partial e_{(c)}{}^\alpha}{\partial x^\beta} + p^{(c)} p^{(d)}\ e_{(c)}{}^\gamma\, e_{(d)}{}^\beta\, \Gamma^\alpha{}_{\beta\gamma} \right) \tag{A.7}$$

$$= -e^{(a)}{}_{\alpha}\, e_{(d)}{}^{\beta}\, p^{(c)} p^{(d)} \underbrace{\left(\frac{\partial e_{(c)}{}^{\alpha}}{\partial x^{\beta}} + e_{(c)}{}^{\gamma}\, \Gamma^{\alpha}{}_{\beta\gamma} \right)}_{e_{(c)}{}^{\alpha}{}_{;\beta}} \tag{A.8}$$

$$\frac{\partial p^{(a)}}{\partial \xi} = -e^{(a)}{}_{\alpha}\, e_{(d)}{}^{\beta}\, e_{(c)}{}^{\alpha}{}_{;\beta}\, p^{(c)} p^{(d)} \tag{A.9}$$

This motivates the definition of the Ricci-Rotation coefficients

$$\gamma^{(a)}{}_{(d)(c)} = e^{(a)}{}_{\alpha}\, e_{(d)}{}^{\beta}\, e_{(c)}{}^{\alpha}{}_{;\beta} \tag{A.10}$$

and hence

$$\frac{\partial p^{(a)}}{\partial \xi} = -\gamma^{(a)}{}_{(d)(c)}\, p^{(c)} p^{(d)} \tag{A.11}$$

It is noteworthy that the definition employed here differs from most text books. However, there is just a formal difference as the order of the indices is different and there is one upper tetrad index instead of none.

Appendix B

Connection Coefficients

B.1 Spherically Symmetric Metric

The connection coefficients are given from the components of the metric tensors [Frankel, 2004]

$$\Gamma^{\alpha}{}_{\beta\gamma} = \frac{1}{2} g^{\alpha\sigma} \left(\frac{\partial g_{\sigma\beta}}{\partial x^{\gamma}} + \frac{\partial g_{\sigma\gamma}}{\partial x^{\beta}} - \frac{\partial g_{\beta\gamma}}{\partial x^{\sigma}} \right) \tag{B.1}$$

The connection coefficients for the spherically symmetric metric (3.37) are then given by

$$\Gamma^{0}{}_{00} = \frac{\partial \Psi}{\partial \tau} \tag{B.2}$$

$$\Gamma^{0}{}_{11} = \exp\left(2(\Lambda - \Psi)\right) \frac{\partial \Lambda}{\partial \tau} \tag{B.3}$$

$$\Gamma^{0}{}_{22} = \exp\left(-2\Psi\right) R \frac{\partial R}{\partial \tau} \tag{B.4}$$

$$\Gamma^{0}{}_{33} = \exp\left(-2\Psi\right) R \frac{\partial R}{\partial \tau} \sin^2\Theta \tag{B.5}$$

$$\Gamma^{0}{}_{10} = \Gamma^{0}{}_{01} = \frac{\partial \Psi}{\partial r} \tag{B.6}$$

$$\Gamma^{1}{}_{00} = \exp\left(2(\Lambda - \Psi)\right) \frac{\partial \Psi}{\partial r} \tag{B.7}$$

$$\Gamma^{1}{}_{11} = \frac{\partial \Lambda}{\partial r} \tag{B.8}$$

$$\Gamma^{1}{}_{22} = -\exp\left(-2\Lambda\right) R \frac{\partial R}{\partial r} \tag{B.9}$$

$$\Gamma^{1}{}_{33} = -\exp\left(-2\Lambda\right) R \frac{\partial R}{\partial r} \sin^2\Theta \tag{B.10}$$

$$\Gamma^{1}{}_{10} = \Gamma^{1}{}_{01} = \frac{\partial \Lambda}{\partial \tau} \tag{B.11}$$

$$\Gamma^{2}{}_{33} = -\sin\Theta\cos\Theta \tag{B.12}$$

$$\Gamma^2{}_{20} = \Gamma^2{}_{02} = \frac{1}{R}\frac{\partial R}{\partial \tau} \tag{B.13}$$

$$\Gamma^2{}_{21} = \Gamma^2{}_{12} = \frac{1}{R}\frac{\partial R}{\partial r} \tag{B.14}$$

$$\Gamma^3{}_{30} = \Gamma^3{}_{03} = \frac{1}{R}\frac{\partial R}{\partial \tau} \tag{B.15}$$

$$\Gamma^3{}_{31} = \Gamma^3{}_{13} = \frac{1}{R}\frac{\partial R}{\partial r} \tag{B.16}$$

$$\Gamma^3{}_{32} = \Gamma^3{}_{23} = \cot\Theta \tag{B.17}$$

The Ricci-rotation coefficients are repeated here for completeness

$$\gamma^{(1)}{}_{(0)(0)} = \exp(-\Psi)\frac{\partial \Psi}{\partial r} \tag{B.18}$$

$$\gamma^{(1)}{}_{(1)(0)} = \exp(-\Psi)\frac{\partial \Lambda}{\partial \tau} \tag{B.19}$$

$$\gamma^{(1)}{}_{(2)(2)} = -\frac{\exp(-\Lambda)}{R}\frac{\partial R}{\partial r} \tag{B.20}$$

$$\gamma^{(1)}{}_{(3)(3)} = -\frac{\exp(-\Lambda)}{R}\frac{\partial R}{\partial r} \tag{B.21}$$

$$\gamma^{(2)}{}_{(2)(0)} = \frac{\exp(-\Psi)}{R}\frac{\partial R}{\partial \tau} \tag{B.22}$$

$$\gamma^{(2)}{}_{(2)(1)} = \frac{\exp(-\Lambda)}{R}\frac{\partial R}{\partial r} \tag{B.23}$$

$$\gamma^{(2)}{}_{(3)(3)} = -\frac{\cot\Theta}{R} \tag{B.24}$$

$$\gamma^{(3)}{}_{(3)(0)} = \frac{\exp(-\Psi)}{R}\frac{\partial R}{\partial \tau} \tag{B.25}$$

$$\gamma^{(3)}{}_{(3)(1)} = \frac{\exp(-\Lambda)}{R}\frac{\partial R}{\partial r} \tag{B.26}$$

$$\gamma^{(3)}{}_{(3)(2)} = \frac{\cot\Theta}{R} \tag{B.27}$$

The Ricci-rotation coefficients for the tetrads comoving with a purely radial flow are reproduced for completeness

$$\gamma^{(1)}{}_{(0)(0)} = \gamma^3\frac{\partial \beta}{\partial \tau}\exp(-\Psi) + \gamma^3\beta\frac{\partial \beta}{\partial r}\exp(-\Lambda) + \gamma\beta\frac{\partial \Lambda}{\partial \tau}\exp(-\Psi) + \gamma\frac{\partial \Psi}{\partial r}\exp(-\Lambda) \tag{B.28}$$

$$\gamma^{(1)}{}_{(1)(0)} = \gamma^3\beta\frac{\partial \beta}{\partial \tau}\exp(-\Psi) + \gamma^3\frac{\partial \beta}{\partial r}\exp(-\Lambda) + \gamma\frac{\partial \Lambda}{\partial \tau}\exp(-\Psi) + \gamma\beta\frac{\partial \Psi}{\partial r}\exp(-\Lambda) \tag{B.29}$$

$$\gamma^{(1)}{}_{(2)(2)} = -\frac{\gamma}{R}\left\{\beta\exp(-\Psi)\frac{\partial R}{\partial \tau} + \exp(-\Lambda)\frac{\partial R}{\partial r}\right\} \tag{B.30}$$

$$\gamma^{(1)}{}_{(3)(3)} = \gamma^{(1)}{}_{(2)(2)} \tag{B.31}$$

$$\gamma^{(2)}{}_{(2)(0)} = \frac{\gamma}{R}\left\{\exp(-\Psi)\frac{\partial R}{\partial \tau} + \beta\exp(-\Lambda)\frac{\partial R}{\partial r}\right\} \tag{B.32}$$

$$\gamma^{(2)}{}_{(2)(1)} = \frac{\gamma}{R}\left\{\beta\exp(-\Psi)\frac{\partial R}{\partial \tau} + \exp(-\Lambda)\frac{\partial R}{\partial r}\right\} \tag{B.33}$$

$$\gamma^{(2)}{}_{(3)(3)} = -\frac{\cot\Theta}{R} \tag{B.34}$$

$$\gamma^{(3)}{}_{(3)(0)} = \gamma^{(2)}{}_{(2)(0)} \tag{B.35}$$

$$\gamma^{(3)}{}_{(3)(1)} = \gamma^{(2)}{}_{(2)(1)} \tag{B.36}$$

$$\gamma^{(3)}{}_{(3)(2)} = -\gamma^{(2)}{}_{(3)(3)} \tag{B.37}$$

B.2 Kerr Metric

In the following the units of mass are redefined – such that $G = c = 1$ holds – to reduce the complexity of the following relations.

Using Boyer-Lindquist coordinates (τ, r, Θ, Φ) the non vanishing connection coefficients are

$$\Gamma^1{}_{00} = -\frac{\Delta M(\rho^2 - 2r^2)}{\rho^6} \tag{B.38}$$

$$\Gamma^1{}_{03} = \Gamma^1{}_{30} = \frac{a\Delta M(\rho^2 - 2r^2)\sin^2\Theta}{\rho^6} \tag{B.39}$$

$$\Gamma^1{}_{11} = \frac{M - r}{\Delta} + \frac{r}{\rho^2} \tag{B.40}$$

$$\Gamma^1{}_{12} = \Gamma^1{}_{21} = -\frac{a^2\cos\Theta\sin\Theta}{\rho^2} \tag{B.41}$$

$$\Gamma^1{}_{22} = -\frac{\Delta r}{\rho^2} \tag{B.42}$$

$$\Gamma^1{}_{33} = -\frac{\Delta\sin^2\Theta}{\rho^6}\Big(r(a^2 + r^2)(r^2 + a^2\cos 2\Theta) \\ -a^2\sin^2\Theta(r(Mr - a^2)a^2\cos^2\Theta(r - M))\Big) \tag{B.43}$$

$$\Gamma^2{}_{00} = -\frac{a^2 Mr\sin 2\Theta}{\rho^6} \tag{B.44}$$

$$\Gamma^2{}_{03} = \Gamma^2{}_{30} = \frac{aMr(a^2 + r^2)\sin 2\Theta}{\rho^6} \tag{B.45}$$

$$\Gamma^2{}_{11} = \frac{a^2\cos\Theta\sin\Theta}{\Delta\rho^2} \tag{B.46}$$

$$\Gamma^2{}_{12} = \Gamma^2{}_{21} = \frac{r}{\rho^2} \tag{B.47}$$

$$\Gamma^2{}_{22} = -\frac{a^2\cos\Theta\sin\Theta}{\rho^2} \tag{B.48}$$

$$\Gamma^2{}_{33} = -\frac{2Mr(a^2 + r^2)^2 + \Delta\rho^4}{\rho^6}\sin\Theta\cos\Theta \tag{B.49}$$

$$\Gamma^3{}_{01} = \Gamma^3{}_{10} = -\frac{aM(\rho^2 - 2r^2)}{\Delta\rho^4} \tag{B.50}$$

$$\Gamma^3{}_{02} = \Gamma^3{}_{20} = -\frac{2aMr\cot\Theta}{\rho^4} \tag{B.51}$$

$$\Gamma^3{}_{13} = \Gamma^3{}_{31} = \frac{1}{8\Delta\rho^4}\left(8r^4(r-2M) + 4a^2r^2(2r-3M) + a^4(3r+M)\right. \tag{B.52}$$

$$\left. +4a^2r(a^2+2r^2-rM)\cos 2\Theta + a^4(r-M)\cos 4\Theta\right) \tag{B.53}$$

$$\Gamma^3{}_{23} = \Gamma^3{}_{32} = \cot\Theta + \frac{a^2Mr\sin 2\Theta}{\rho^4} \tag{B.54}$$

$$\Gamma^0{}_{01} = \Gamma^0{}_{10} = -\frac{M(r^2+a^2)(\rho^2-2r^2)}{\Delta\rho^4} \tag{B.55}$$

$$\Gamma^0{}_{13} = \Gamma^0{}_{31} = \frac{aM\sin^2\Theta(a^4-3a^2r^2-6r^4+a^2(a^2-r^2)\cos 2\Theta)}{2\Delta\rho^4} \tag{B.56}$$

$$\Gamma^0{}_{02} = \Gamma^0{}_{20} = -\frac{a^2Mr\sin 2\Theta}{\rho^4} \tag{B.57}$$

$$\Gamma^0{}_{23} = \Gamma^0{}_{32} = \frac{2a^3Mr\cos\Theta\sin^3\Theta}{\rho^4} \tag{B.58}$$

During the simplification of the results quite excessive expanding of the terms is needed sometimes. The occurences of multiples of the Θ argument are a result from the compactification of trigonometric expressions.

Using the defintion (3.19) and the tetrad fields for the Kerr metric (3.53) and (3.53) the resulting nonvanishing Ricci-Rotation-coefficients read

$$\begin{aligned}\gamma^{(1)}{}_{(0)(0)} &= -\frac{M}{\sqrt{\Delta}\rho^3\left(a^4+2r^4+a^2r(2M+3r)+a^2\Delta\cos 2\Theta\right)}\times \\ &\left(a^6+a^2(4M-3r)r^3-2r^6+a^2(a^4+2a^2r^2+r^3(r-4M)\cos 2\Theta)\right)\end{aligned} \tag{B.59}$$

$$\begin{aligned}\gamma^{(1)}{}_{(3)(0)} &= \frac{aM\sin\Theta}{8\rho^5\Sigma^2}\left(3(a^6-a^4r^2-8a^2r^4-8r^6)\right. \\ &\left. +4a^2(a^4-a^2r^2-4r^4)\cos 2\Theta + a^4(a^2-r^2)\cos 4\Theta\right)\end{aligned} \tag{B.60}$$

$$\gamma^{(1)}{}_{(0)(3)} = \gamma^{(1)}{}_{(3)(0)} \tag{B.61}$$

$$\gamma^{(1)}{}_{(1)(2)} = -\frac{a^2\cos\Theta\sin\Theta}{\rho^3} \tag{B.62}$$

$$\gamma^{(1)}{}_{(2)(2)} = -\frac{\sqrt{\Delta}r}{\rho^3} \tag{B.63}$$

$$\gamma^{(1)}{}_{(3)(3)} = -\frac{r^3(a^2+r^2)+a^2r(a^2+r^2)\cos 2\Theta + a^2r(a^2-Mr)\cos^2\Theta}{\rho^3\Sigma^2\Delta^{-1/2}} \tag{B.64}$$

$$\gamma^{(2)}{}_{(0)(0)} = -\frac{2a^2Mr(a^2+r^2)\sin 2\Theta}{\rho^3\left(a^4+2r^4+a^2r(2M+3r)+a^2\Delta\cos 2\Theta\right)} \tag{B.65}$$

$$\gamma^{(2)}{}_{(3)(0)} = \frac{a\sqrt{\Delta}\sin\Theta}{a^2+r^2}\gamma^{(2)}{}_{(0)(0)} \tag{B.66}$$

$$\gamma^{(2)}{}_{(0)(3)} = \gamma^{(2)}{}_{(3)(0)} \tag{B.67}$$

$$\gamma^{(2)}{}_{(1)(1)} = \frac{a^2\cos\Theta\sin\theta}{\rho^3} \tag{B.68}$$

$$\gamma^{(2)}{}_{(2)(1)} = \frac{\sqrt{\Delta}r}{\rho^3} \tag{B.69}$$

$$\gamma^{(2)}{}_{(3)(3)} = -\frac{(2Mr(a^2+r^2)^2+\Delta\rho^4)\cot\Theta}{\rho^3\Sigma^2} \tag{B.70}$$

$$\gamma^{(3)}{}_{(1)(0)} = aM\sin\Theta\frac{a^4-3a^2r^2-6r^4+a^2(a^2-r^2)\cos 2\Theta}{2\rho^3\Sigma^2} \tag{B.71}$$

$$\gamma^{(3)}{}_{(0)(1)} = -\gamma^{(3)}{}_{(1)(0)} \tag{B.72}$$

$$\gamma^{(3)}{}_{(2)(0)} = \frac{4a^3\sqrt{\Delta}Mr\cos\Theta\sin^2\Theta}{\rho^3\left(a^4+2r^4+a^2r(2M+3r)+a^2\Delta\cos 2\Theta\right)} \tag{B.73}$$

$$\gamma^{(3)}{}_{(0)(2)} = -\gamma^{(3)}{}_{(2)(0)} \tag{B.74}$$

$$\begin{aligned}\gamma^{(3)}{}_{(3)(1)} = {} & \frac{\sqrt{\Delta}}{4\rho^3\left(a^4+2r^4+a^2r(2M+3r)+a^2\Delta\cos 2\Theta\right)}\times \\ & \left(a^4M+3a^4r-4a^2Mr^2+8a^2r^3+8r^5\right. \\ & \left.+4a^2r(a^2+2r^2+rM)\cos 2\Theta-a^4(M-r)\cos 4\Theta\right)\end{aligned} \tag{B.75}$$

$$\gamma^{(3)}{}_{(3)(2)} = \frac{\cot\Theta}{\rho^2}+\frac{a^2Mr(a^2+r^2)\sin 2\Theta}{\rho^4\Sigma^2} \tag{B.76}$$

It should be kept in mind that the nomenclature of the coefficients is different from most standard textbooks. The definition used here is the same as in (A.10).

Bibliography

[Anderson and Spiegel, 1972] Anderson, J. L. and Spiegel, E. A. 1972, ApJ, 171, 127–+

[Anile and Breuer, 1974] Anile, A. M. and Breuer, R. A. 1974, ApJ, 189, 39–50

[Auer, L., 1987] Auer, L. 1987, Acceleration of Convergence, pages 101–109, In [Kalkofen, 1987]

[Avrett, 1965] Avrett, E. H. 1965, SAO Special Report, 174, 101–+

[Baron and Hauschildt, 1998] Baron, E. and Hauschildt, P. H. 1998, ApJ, 495, 370–+

[Baron and Hauschildt, 2004] Baron, E. and Hauschildt, P. H. 2004, A&A, 427, 987–994

[Baron *et al.*, 1989] Baron, E., Myra, E. S., Cooperstein, J., and van den Horn, L. J. 1989, ApJ, 339, 978–986

[Broderick, 2006] Broderick, A. E. 2006, MNRAS, 366, L10–L12

[Bruenn, 1985] Bruenn, S. W. 1985, ApJS, 58, 771–841

[Bruenn *et al.*, 2001] Bruenn, S. W., De Nisco, K. R., and Mezzacappa, A. 2001, ApJ, 560, 326–338

[Cannon, 1973] Cannon, C. J. 1973, Journal of Quantitative Spectroscopy and Radiative Transfer, 13, 627

[Castor, 1972] Castor, J. I. 1972, ApJ, 178, 779–792

[Chandrasekhar, 1950] Chandrasekhar, S. 1950, Radiative transfer., Oxford, Clarendon Press, 1950.

[Chandrasekhar, 1992] Chandrasekhar, S. 1992, The mathematical theory of black holes, New York : Oxford University Press, 1992.

[Chen *et al.*, 2006] Chen, B., Kantowski, R., Baron, E., Knop, S., and Hauschildt, P. H. 2006, MNRAS, in press,

[Connors *et al.*, 1980] Connors, P. A., Stark, R. F., and Piran, T. 1980, ApJ, 235, 224–244

[Cunningham, 1975] Cunningham, C. T. 1975, ApJ, 202, 788–802

[Demmel *et al.*, 1999] Demmel, J. W., Eisenstat, S. C., Gilbert, J. R., Li, X. S., and Liu, J. W. H. 1999, SIAM J. Matrix Analysis and Applications, 20, 720–755

[Dewitt and Dewitt, 1973] Dewitt, C. and Dewitt, B. S. 1973, Black holes, Black holes, by C. DeWitt and B.S. DeWitt. New York: Gordon and Breach, 1973.

[Ehlers, 1971] Ehlers, J. 1971, General Relativity and Kinetic Theory, pages 1–70, In [Sachs, 1971]

[Frankel, 2004] Frankel, T. 2004, The geometry of physics : an introduction, The geometry of physics : an introduction, 2nd ed. By Theodore Frankel. Cambridge, UK: Cambridge University Press, 2004.

[Gebbie and Thomas, 1968] Gebbie, K. B. and Thomas, R. N. 1968, ApJ, 154, 285–+

[Golub and Van Loan, 1989] Golub, G. H. and Van Loan, C. F. 1989, Matrix computations, Johns Hopkins University Press, Baltimore

[Hauschildt, 1992] Hauschildt, P. H. 1992, Journal of Quantitative Spectroscopy and Radiative Transfer, 47, 433–453

[Hauschildt, 1993] Hauschildt, P. H. 1993, Journal of Quantitative Spectroscopy and Radiative Transfer, 50, 301–318

[Hauschildt *et al.*, 2003] Hauschildt, P. H., Barman, T. S., Baron, E., and Allard, F. 2003, Temperature Correction Methods, In [Hubeny *et al.*, 2003], pages 227–238

[Hauschildt and Baron, 1999] Hauschildt, P. H. and Baron, E. 1999, Journal of Computational and Applied Mathematics, 109, 41–63

[Hauschildt and Baron, 2004] Hauschildt, P. H. and Baron, E. 2004, A&A, 417, 317–324

[Hauschildt and Baron, 2006] Hauschildt, P. H. and Baron, E. 2006, A&A, 451, 273–284

[Hauschildt *et al.*, 1997] Hauschildt, P. H., Baron, E., and Allard, F. 1997, ApJ, 483, 390–+

[Hauschildt *et al.*, 2001] Hauschildt, P. H., Lowenthal, D. K., and Baron, E. 2001, ApJS, 134, 323–329

[Hauschildt *et al.*, 1995] Hauschildt, P. H., Starrfield, S., Shore, S. N., Allard, F., and Baron, E. 1995, ApJ, 447, 829

[Hauschildt *et al.*, 1994] Hauschildt, P. H., Strözer, H., and Baron, E. 1994, Journal of Quantitative Spectroscopy and Radiative Transfer, 51, 875–891

[Hubeny, 2003] Hubeny, I. 2003, Accelerated Lambda Iteration: An Overview, In [Hubeny *et al.*, 2003], pages 17–+

[Hubeny *et al.*, 2003] Hubeny, I., Mihalas, D., and Werner, K., editors 2003, Stellar Atmosphere Modeling

[Jackson, 1975] Jackson, J. D. 1975, Classical electrodynamics, 92/12/31, New York: Wiley, 1975, 2nd ed.

[Kalkofen, 1987] Kalkofen, W. 1987, Numerical radiative transfer, Numerical Radiative Transfer

[Knop *et al.*, 2007] Knop, S., Hauschildt, P. H., and Baron, E. 2007, A&A, 463, 315–320

[Landau and Lifschitz, 1979] Landau, L. and Lifschitz, E. 1979, Lehrbuch der theoretischen Physik, in Teil 3, Quantenmechanik, Akademie Verlag Berlin, neunte Edition

[Landau and Lifschitz, 1987] Landau, L. and Lifschitz, E. 1987, Lehrbuch der theoretischen Physik, in Teil 5, Statistische Physik, Teil 1, Akademie Verlag Berlin, achte Edition

[Landau and Lifschitz, 1997] Landau, L. and Lifschitz, E. 1997, Lehrbuch der theoretischen Physik, in Teil 2, Klassische Feldtheorie, Harry Deutsch, zwölfte Edition

[Landi Degl'Innocenti, 1983] Landi Degl'Innocenti, E. 1983, Solar Phys., 85, 3–31

[Lindquist, 1966] Lindquist, R. 1966, Annals of Physics, 37, 487

[Madej, 1974] Madej, J. 1974, Acta Astronomica, 24, 327–336

[Messiah, 1962] Messiah, A. 1962, Quantum mechanics, Amsterdam: North-Holland Publication, 1961-1962

[Mihalas, 1970] Mihalas, D. 1970, Stellar atmospheres, Series of Books in Astronomy and Astrophysics, San Francisco: Freeman, |c1970

[Mihalas, 1978] Mihalas, D. 1978, Stellar atmospheres /2nd edition/, San Francisco, W. H. Freeman and Co., 1978. 650 p.

[Mihalas, 1980] Mihalas, D. 1980, ApJ, 237, 574–589

[Mihalas *et al.*, 1975] Mihalas, D., Kunasz, P. B., and Hummer, D. G. 1975, ApJ, 202, 465–489

[Mihalas and Weibel-Mihalas, 1984] Mihalas, D. and Weibel-Mihalas, B. 1984, Foundations of radiation hydrodynamics, New York: Oxford University Press, 1984

[Mihalas, D., 2003] Mihalas, D. 2003, Los Alamos National Laboratory, LA-14062-MS

[Misner *et al.*, 1973] Misner, C. W., Thorne, K. S., and Wheeler, J. A. 1973, Gravitation, San Francisco: W.H. Freeman and Co., 1973

[Morita and Kaneko, 1986] Morita, K. and Kaneko, N. 1986, Ap&SS, 121, 105–125

[Narayan and Yi, 1994] Narayan, R. and Yi, I. 1994, ApJ, 428, L13–L16

[Ng, 1974] Ng, K. C. 1974, J. Chem. Phys., 61, 2680

[Novikov and Thorne, 1973] Novikov, I. D. and Thorne, K. S. 1973, Astrophysics of Black Holes, pages 345–405, In [Dewitt and Dewitt, 1973]

[Olson and Kunasz, 1987] Olson, G. and Kunasz, P. 1987, Journal of Quantitative Spectroscopy and Radiative Transfer, 38, 325

[Olson *et al.*, 1986] Olson, G. L., Auer, L. H., and Buchler, J. R. 1986, Journal of Quantitative Spectroscopy and Radiative Transfer, 35, 431–442

[Oxenius, 1986] Oxenius, J. 1986, Kinetic theory of particles and photons. theoretical foundations of Non-LTE plasma spectroscopy, Springer Series in Electrophysics, Berlin: Springer, 1986

[Press *et al.*, 1992] Press, W. H., Flannery, B. P., Teukolsky, S. A., and Vetterling, W. T. 1992, Numerical Recipes: The Art of Scientific Computing, Cambridge University Press, Cambridge (UK) and New York, 2nd edition

[Rutten, 2003] Rutten, R. J. 2003, Radiative transfer in stellar stmospheres

[Sachs, 1971] Sachs, R. K. 1971, General relativity and cosmology., General relativity and cosmology by R.K. Sachs. New York: Academic Press, 1971.

[Schinder, 1988] Schinder, P. J. 1988, Phys.Rev.D, 38, 1673–1683

[Schinder and Bludman, 1989] Schinder, P. J. and Bludman, S. A. 1989, ApJ, 346, 350–365

[Schmid-Burgk, 1978] Schmid-Burgk, J. 1978, Ap&SS, 56, 191–218

[Schuster, 1905] Schuster, A. 1905, ApJ, 21, 1–+

[Shakura and Sunyaev, 1973] Shakura, N. I. and Sunyaev, R. A. 1973, A&A, 24, 337–355

[Shapiro, 1996] Shapiro, S. L. 1996, ApJ, 472, 308–+

[Thomas, 1930] Thomas, L. H. 1930, Quart. J. Math. (Oxford), 1, 239–251

[van Kampen, 1969] van Kampen, N. 1969, Physica, 43, 244–262

[Viergutz, 1993] Viergutz, S. U. 1993, A&A, 272, 355–+

[Wilson, 1971] Wilson, J. R. 1971, ApJ, 163, 209–+

[Yakovlev *et al.*, 2002] Yakovlev, D. G., Gnedin, O. Y., Kaminker, A. D., and Potekhin, A. Y. 2002, Cooling of Superfluid Neutron Stars, in Neutron Stars, Pulsars, and Supernova Remnants, edited by Becker, W., Lesch, H., and Trümper, J., pages 287–+

[Zane *et al.*, 1996] Zane, S., Turolla, R., Nobili, L., and Erna, M. 1996, ApJ, 466, 871–+

[Zavlin and Pavlov, 2002] Zavlin, V. E. and Pavlov, G. G. 2002, Modeling Neutron Star Atmospheres, in Neutron Stars, Pulsars, and Supernova Remnants, edited by Becker, W., Lesch, H., and Trümper, J., pages 263–+

[Zurmühl and Falk, 1986] Zurmühl, R. and Falk, S. 1986, Matrizen und ihre Anwendungen, volume 2, Springer-Verlag, Berlin, 5th edition

Danksagung

Mein Dank gebührt Prof. Dr. P. H. Hauschildt für die Vergabe einer Aufgabenstellung, die genau meinen Wünschen entsprach, sowie für die ausgezeichnete Betreuung als Doktorvater. Dies gilt im gleichen Maße für Prof. Dr. E. Baron, der sich nicht nur als Zweitgutachter zur Verfügung gestellt hat, sondern mich auch an die University of Oklahoma eingeladen hat, um mich bei meiner Arbeit zu betreuen und zu unterstützen und mir jederzeit Gehör geschenkt hat. Des Weiteren geht mein Dank an Bin Chen und Ron Kantowski, die mit ihren Ausführungen über Relativität zu meinem Verständnis der Materie enorm beigetragen haben.
Ich danke allen Mitarbeitern der Hamburger Sternwarte, die einem ein angenehmes und reibungsloses tägliches Arbeiten ermöglicht haben. Dies gilt vor allem für meine Arbeitsgruppe und insbesondere für meine Büronachbarn Chris und Daan, die sowohl mit mir eine harmonische Bürogemeinschaft gegründet haben, als auch essentiell dazu beigetragen haben, dass wir einen frühen Arbeitsbeginn in unserer Haushälfte etablieren konnten.
Dank für eine hervorragende Aufnahme in die Bürogemeinschaft gebührt auch den gradstudents der Nielsen Hall von OU – »gumball«.
Chris und Andreas sollen hier nicht im Zusammenhang mit ihren Verdiensten um das Ausmerzen von Fehlern bei ihrer Lektüre dieser Arbeit unerwähnt bleiben.

Mareike danke ich dafür, dass es sie gibt und sie in der teilweise stressige Zeit des Schreibens mich immer unter- und gestützt hat.

Diese Arbeit wäre nicht ohne die Unterstützung meiner Eltern möglich gewesen, die mir nicht nur während des Studiums, sondern im gesamten Leben eine unersetzliche Hilfe gewesen sind. Daher gebührt ihnen auch der größte Dank.

Danke!